The design of a closed orbit correction system for the EUTERPE Ring

Bresser, J.

Award date:
1997

The Design of a Closed Orbit Correction System for the EUTERPE Ring

VDF/NK 95-22

J. Bresser

August 1995

Report of a graduation study under supervision of Dr. J.I.M. Botman & Dr.Ir.C.J.Timmermans in the group Nuclear Physics Techniques at the Eindhoven University of Technology

Abstract

For the successful operation of the electron storage ring EUTERPE a closed orbit correction system is required. In this graduation report the closed orbit distortion has been determined and a correction system has been designed. This includes the design of the magnets used for the correction: the sextupoles and the so-called window frame magnets.

As a result of displacements of and field errors in the magnetic elements, the electron orbit is distorted. The position errors are mainly determined by the finite measurement precision during alignment. The position errors due to other effects, e.g. thermal expansion, are negligible. The distortion of the electron beam due to all errors equals $x_{rms} = 4 \pm 2$ mm and $y_{rms} = 1.0 \pm 0.4$ mm in the most sensitive mode of operation, the High Brilliance Small Beam mode. These distortions have been calculated with the use of the computer code Methodical Accelerator Design (MAD).

The closed orbit distortions have been reduced with a factor 26 in the horizontal and a factor 6 in the vertical direction with the use of a correction system. After correction the distortion equals $x_{rms} = 0.14 \pm 0.02$ mm in the horizontal and $y_{rms} = 0.16 \pm 0.02$ mm in the vertical direction. The size of the distortions approximates the amplitude of the position and read errors of the monitors ($\sigma_x = \sigma_y = 0.1$mm for both errors). Without the monitor errors, the distortions can be further reduced with a factor 2.

The number of monitors and correctors in the correction system has been minimized to 24 monitors and 24 correctors. This number corresponds to four monitors and correctors per betatron wavelength. Eight sextupoles included in the main lattice are used as corrector magnets in order to save lattice space.

The sextupoles are used as corrector magnets with the generation of additional dipole fields. Simulations show that very uniform dipole fields can be produced in the sextupoles. Additional corrector magnets are required for the correction in the long straight sections of the ring. These corrector magnets are of the window-frame type. Uniform dipole fields can be generated in both directions. The measured field strengths in the prototype window-frame magnet are in perfect agreement with the calculated strengths.

Contents

4 Design of a closed orbit correction system

5 Hardware regarding the closed orbit correction system

6 Conclusions and Recommendations

Chapter1

Introduction

The storage ring EUTERPE is under construction by the group Particle Accelerators in the Cyclotron laboratory at the technical University of Eindhoven. The storage ring will mainly be used for the storage of 400 MeV electrons. The EUTERPE-project is set up for the production of synchrotron radiation and for studies of charged particle dynamics and applications of synchrotron radiation.

The EUTERPE-ring has a circumference of 40 meters. Before entering the ring the electrons

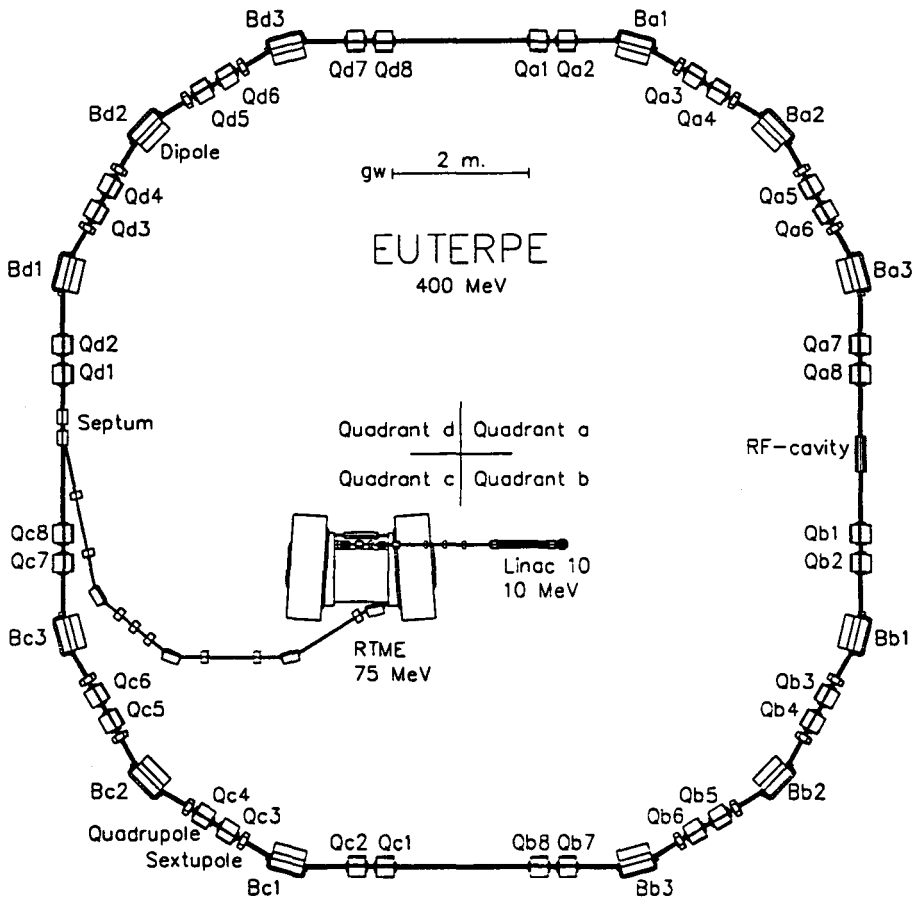

Fig. 1.1 A schematic view of the EUTERPE ring.

are pre-accelerated in a linear accelerator up to 10 MeV, then they are injected in a microtron, where their kinetic energy is increased to 75 MeV. These 75 MeV electrons are injected in the EUTERPE-ring where they can be accelerated to a maximum energy of 400 MeV. This report concerns the EUTERPE-ring, which is depicted in figure 1.1.

When electrons are accelerated they produce synchrotron radiation (or Brehmstralung). The EUTERPE-ring contains twelve dipoles in which the electron trajectory is bent. In each dipole synchrotron radiation is produced. This synchrotron radiation can be coupled out by special ports constructed in the vacuum chamber. The radiation has some exceptional properties, which makes it very useful for the studies of materials: e.g. it has a low divergence, it is a continuous radiation source over a wide wavelength range, from the infra-red up to soft x-rays and has a well-defined polarisation.

As mentioned the EUTERPE ring is still under construction. At the beginning of this study the design of the EUTERPE lattice was finished [Xi 95]. The locations of all magnetic elements is determined. Furthermore the field strengths in all elements have been calculated for three different modes of operation. The behaviour of the particles in an ideal lattice is known. However due to lattice imperfections the electron orbit is distorted: the particle trajectories will deviate from the designed orbit.

The aim of this study is to design a correction system in order to reduce these distortions as much as possible. After the study the design of the correction system in the storage ring must be fully prepared. This includes the determination of the locations of all correction elements - the beam position monitors and corrector magnets - and a method to calculate the corrector settings, but it also includes the design of the hardware regarding the closed orbit correction system.

1.2 The EUTERPE-lattice

The EUTERPE-lattice consists of four identical sections or superperiods. Each superperiod contains dipole, quadrupole and sextupole magnets separated by drift spaces. As mentioned in the introduction, the electron trajectory is bent in the dipoles. The quadrupoles are used for the focusing of the beam. The sextupoles in turn are used for the correction of the chromatic aberrations (the so-called chromaticity) introduced by the quadrupoles (the chromaticity and all other beam parameters used in this report are discussed in chapter 2). A schematic view of the EUTERPE lattice [Xi 95] is shown in fig. 1.2. The element types and sizes are given in table

1.1.

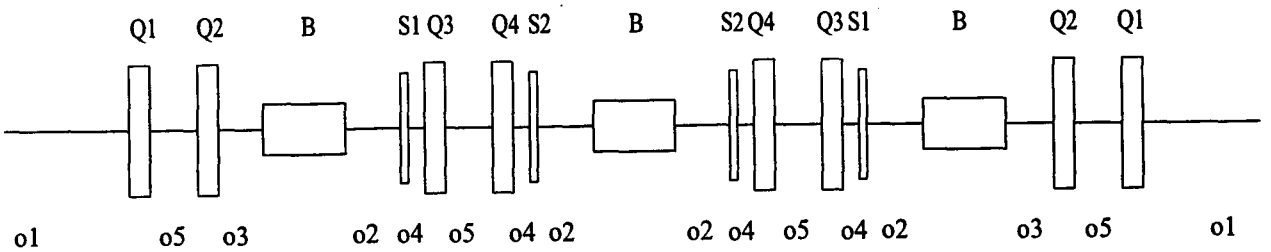

Fig. 1.2 The basic structure of the EUTERPE ring for one superperiod.

Table 1.1: Sizes of the different elements in the ring.

Name	Elementtype	Length (in meters)
O1	Driftspace	1.000
O2	Driftspace	0.450
O3	Driftspace	0.600
O4	Driftspace	0.100
O5	Driftspace	0.165
B	Dipoles	0.516 *
Q1,Q2,Q3 and Q4	Quadrupoles	0.274 *
S1 and S2	Sextupoles	0.05 **

* This is the effective length of the magnets.

** The sextupoles have been designed during this study; this the expected length of the sextupoles according to [Xi 95].

Apart from the normal magnetic elements each superperiod contains several corrector magnets and beam position monitors. The corrector magnets and position monitors are part of the correction system for the closed orbit distortion. These distortion are a result of lattice imperfections (see chapter3). The deviations of the beam are measured at the locations of the monitors; the electron trajectory is adjusted by introducing a magnetic induction in the corrector magnets. The locations of the beam position monitors and corrector magnets are determined in this project and are not included in figure 1.2.

At the entrance and exit of each superperiod there is a long straight section; the total length of the long straight section between two successive quadrupole doublets is two meters. As a result of the dipole configuration in the lattice all four straight sections are dispersion free; a small energy-deviation of an electron will not influence its dispersion or position in the straight sections. The straight sections are used for the insertion of special elements whose operations require the absence of dispersion.

One of these special elements is the rf-cavity, which is placed in one of the dispersion-free sections in order to prevent synchro-betatron coupling. The rf-cavity is used for the acceleration of the electrons in order to compensate for energy-losses in the ring due to synchrotron radiation. Another straight section is reserved for the injection system of the 75 MeV electrons coming from the microtron. The remaining two sections will be used in future for devices like undulators and wigglers. These are special devices in which multiple electron deflection results in intense synchrotron radiation.

1.3 Modes of operation

The design of the EUTERPE-lattice has a high flexibility: it allows for changing the character of the electron beam by adjusting the focussing strengths of groups of quadrupoles. So far three different modes of operation have been investigated [Xi 95]: the High Brilliance Small Beam mode (HBSB), the High Light Flux mode (HLF) and the Small Bunch Length (SBL) mode. The characteristics of the different modes are summarised below.

- In the HBSB mode the beam size in the dipoles will be very small, which results in a very high brilliance. A small beam size requires strong focussing which gives rise to a large natural chromaticity; therefore strong sextupole magnets are required.
- In the HLF mode the main interest is a high light flux. The beam size is of less importance. The comparatively weak focussing of the quadrupoles makes the mode the least error-sensitive. Therefore the HLF-mode is very useful for the first phase of the commissioning of the ring.

- The SBL mode is an optical mode in which the bunch length is minimised. The bunch length is in the order of several millimetres corresponding to a pulse length of several picoseconds.

The most important beam parameters in the three different modes have been calculated by B.Xi [Xi 95] and are listed in table 1.2. The parameters are explained in chapter 2.

Table 1.2: Beam parameters of EUTERPE

Mode		HLF	HBSB	SBL
Tune	ν_x	2.57	5.128682	3.37
	ν_y	1.63	2.47	2.41
Betatron and Dispersion functions (m)	$\beta_{x\,max}$	10.335	23.835	8.241
	$\beta_{z\,max}$	8.060	11.114	9.113
	D_{max}	0.854	0.494	1.040
	$<\beta_x>$	5.673	7.694	0.760
	$<\beta_y>$	4.809	6.636	0.584
	<D>	0.269	0.137	-0.211
Natural chromaticity	ξ_x	-2.917	-15.859	-3.729
	ξ_y	-5.755	-11.039	-8.376
Emittance (nm.rad)	ϵ	184.5	5.776	155.2
Energy spread	σ_E/E	3.47×10^{-4}	3.47×10^{-4}	3.47×10^{-4}
Coupling coefficient	κ	0.1	0.1	0.1
Beam size (mm) *	σ_{x1}, σ_{x3}	0.89	0.058	0.56
	σ_{y1}, σ_{y3}	0.36	0.076	0.35
	σ_{x2}	0.38	0.079	0.45
	σ_{y2}	0.20	0.063	0.11
	σ_{x0}	1.31	0.349	1.14
	σ_{y0}	0.25	0.014	0.19

* At the positions represented by:
0 - middle of long straight section
1 - dipole B1,
2 - dipole B2,
3 - dipole B3.

1.4 The contents of this report

In this report the design of a correction system for the closed orbit distortion in the EUTERPE ring is described. In the first part of this chapter a general description of the EUTERPE-ring, its lattice structure and the different modes of operation has been given.

The particle dynamics of the electrons in the storage ring is discussed in chapter 2. Beam parameters used in this report will be explained. Furthermore a description of the closed orbit distortion and correction will be given. In addition some general aspects concerning the design of the sextupoles and the corrector magnets are discussed.

The sources for the closed orbit distortion - the deviations of the electron trajectories from their ideal, designed path - are weighted in chapter 3. The closed orbit distortions due to single and multiple errors are determined with numerical simulations.

The design of a correction system for these closed orbit distortions is discussed in chapter 4. The influence of the positions of the beam position monitors and corrector magnets is discussed. In addition a comparison of the closed orbit distortion before and after correction is made.

The sextupoles already included in the main lattice, can be used as corrector magnets. In chapter 5 the design of the sextupoles and the generation of the additional horizontal and vertical dipole fields for the correction are discussed. Furthermore additional corrector magnets are designed, which are of the so-called "window-frame" type. The first measurements of the magnetic induction in the prototype window-frame corrector are compared with simulations. Finally two types of beam position monitors are compared.

Concluding remarks are given in chapter 6.

Chapter 2

Particle Dynamics and Control

First some general concepts of particle motion in an electron storage ring will be discussed. Important beam parameters such as the emittance, tune, chromaticity and closed orbit distortion are treated. Finally a general description of the closed orbit correction is given.

2.1 The coordinate system

The description of the non-linear particle trajectory in a storage ring is in Cartesian coordinates rather complex. The trajectory equations are simplified by using a curvilinear coordinate system. The coordinate system used throughout this report is schematically shown in figure 2.1. The *s*-axis is defined to be tangent to the ideal particle trajectory at every position. The *x*-axis points in the radial and the *y*-axis in the vertical direction. Furthermore the rotational directions φ, θ and ψ are defined for rotations around respectively the *x*-, *y*- and *s*-axis.

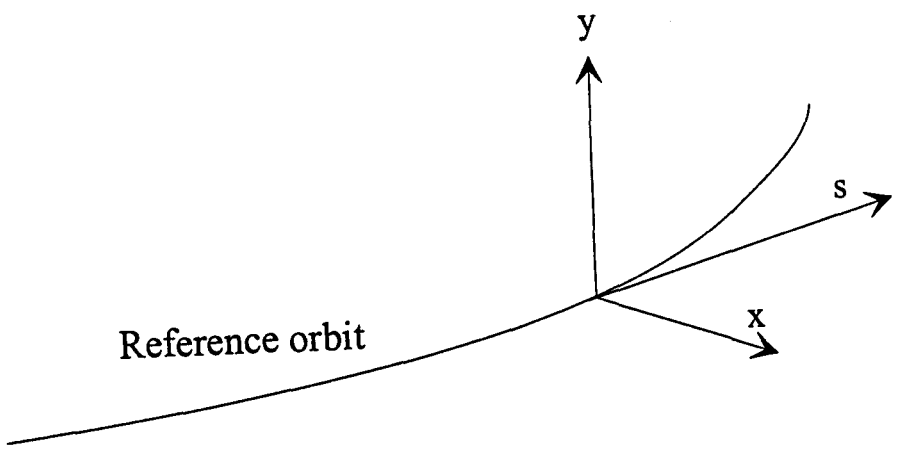

Fig. 2.1 The curvilinear coordinate system.

In the new reference frame an ideal particle with the design energy E_0 moves along the *s*-axis, which is the design trajectory. The trajectory of an arbitrary particle will differ slightly from the

design trajectory. The trajectory equations for such a particle are derived in the following paragraphs.

2.2 The Hill-equations

An electron passing through an electromagnetic field will experience a Lorentz force. Neglecting all non-linear terms the trajectory equations in the curvilinear coordinate system become

$$\frac{d^2x}{ds^2} + [\frac{1}{\rho^2(s)} - K_x(s)]x = \frac{1}{\rho(s)}\frac{\Delta p}{p} \tag{2.1a}$$

and

$$\frac{d^2y}{ds^2} + K_y(s)\, y = 0. \tag{2.1b}$$

In this formula $\rho(s)$ is the local radius of curvature of the particle trajectory; $\Delta p/p$ is the relative momentum shift and $K(s)$ is the focusing or defocusing strength, dependent on the direction. In the case of a mono-energetic beam, the two equations in formula 2.1 are similar and can be expressed as

$$\frac{d^2u}{ds^2} + K(s)u = 0, \qquad with\ u = x,\ y, \tag{2.2}$$

$$and \qquad K(s) = \begin{cases} 1/\rho^2(s) - K_x(s) \\ K_y(s) \end{cases}.$$

All distortions from the central orbit are small; therefore only linear terms are non-negligible. The transfer matrix between the divergence and position at a location s_2 can be expressed as the position and divergence at an initial position s_1,

$$U(s_2) = R \cdot U(s_1) \tag{2.3}$$

$$with \qquad U(s) = \begin{pmatrix} u(s) \\ u'(s) \end{pmatrix}.$$

R is the transfer matrix. Every magnetic element in the ring (e.g. dipoles, drift spaces etc.) can be easily expressed in an elementary matrix-form. A sequence of elements can be represented by a single transfer matrix R, which is a multiplication of the elementary matrices. Numerical calculations are simplified with the use of the matrix formalism. Many computer programs use this formalism, e.g. Methodical Accelerator Design (MAD), which is used throughout this report.

2.3 Betatron oscillations

In a circular machine $K(s)$ is a periodic function along the circumference L; as a result of the periodicity eq. 2.2 is of the Hill-type. The solution of the Hill-equation is given by Flocquet's theorem [Cas94]

$$u(s) = \sqrt{\epsilon_0}\sqrt{\beta(s)}\cos(\psi(s) + \phi_0). \tag{2.4}$$

In here $\beta(s)$ and $\psi(s)$, are respectively the betatron function and the betatron phase; ϵ_0 is a constant, which is particle dependent. Eq. 2.4 describes the oscillation of a particle around the central particle trajectory, which is called the betatron oscillation. The oscillation amplitude, $\sqrt{\epsilon_0}\sqrt{\beta}$, and the betatron phase are particle dependent; as a result the electron beam has a certain width, which continuously changes with the betatron function β.

The emittance, ϵ, is a measure for the maximum amplitude of the betatron oscillations. The emittance is defined as the volume, which encloses all particles in the ring (with a deviation of 2 σ) in 6 dimensional phase space. The area enclosing all particles in 2 dimensional phase space at a certain position s is graphically shown in figure 2.2. The shape of the emittance continuously changes due to the contraction and divergence of the beam in the focusing and defocusing elements in the lattice. However according to Liouville's Theorem, the emittance remains constant if the energy of the particles remains constant. Magnetic forces are non-dissipative and therefore only change the shape of the beam, not the emittance.

Due to the emission of synchrotron radiation the particles lose a fraction of their energy; the energy-loss is compensated in the rf-cavity in which the particles are accelerated. Synchrotron radiation is emitted in the direction tangential to the particle's velocity; so part of the particle's transversal momentum is lost. The energy-gain in the rf-cavity is only in the s-direction; the particle's transversal oscillations are damped. Similar arguments prove that the synchrotron oscillation - the oscillation in the longitudinal direction - is also damped due to the emission of synchrotron radiation. As a consequence of quantum excitation - the

synchrotron radiation is emitted in quanta - the amplitude of the betatron oscillations is increased. The resulting amplitude is an equilibrium between the radiation damping and quantum excitation.

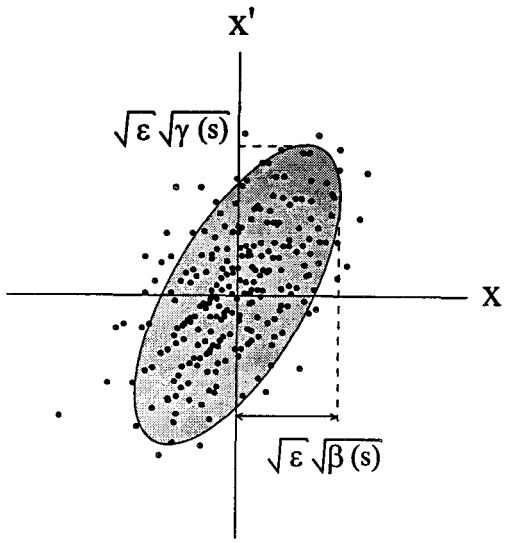

Fig. 2.2 The phase space in two dimensions at a certain position s.

The parameter γ in figure 2.2 is a Twiss parameter, which is not further discussed here.

2.4 Resonances

The betatron number or tune ν is defined as the number of betatron oscillations per turn. It depends on the strengths of the focusing elements in the ring. The main contribution to the focusing comes from the quadrupoles; for quadrupoles *K(s)* is equal to:

$$K_u(s) = \frac{1}{B\rho}\frac{\delta B}{\delta u} \qquad (u=x,\ y). \tag{2.5}$$

Small lattice imperfections will distort the beam; as a result the amplitude and phase of the betatron oscillation is slightly changed. If the value of the betatron tune equals an integer value the excitations are resonantly amplified; the resonance will result in an unstable orbit and a loss of the particles. In general resonances occur when the horizontal and vertical tune satisfy:

$$m\nu_x + n\nu_y = r, \tag{2.6}$$

with m, n and r integers. It is stated that dipole errors lead to integer resonances, quadrupole errors to resonances at half-integer ν-values and sextupole errors excite third-integer resonances [Cas94]. Combinations of horizontal and vertical tunes can result in resonances due to coupling between horizontal and vertical betatron oscillation, mainly in the sextupoles. Low order resonances (m,n < 3) generally result in a loss of the beam and should be avoided. Higher order resonances have a less severe effect on the beam.

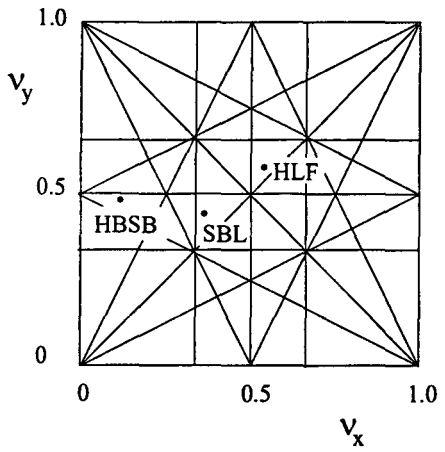

Betatron tunes for the different modes of operation in the EUTERPE ring:

HBSB: $\nu_x = 5.13$ $\nu_y = 2.47$,
HLF: $\nu_x = 2.57$ $\nu_y = 1.63$,
SBL: $\nu_x = 3.37$ $\nu_y = 2.41$.

Fig. 2.3 Resonance diagram

The working point for a storage-ring is defined by its betatron numbers ν_x and ν_y. The working points for the HBSB, HLF and SBL mode are depicted in the resonance diagram, see fig. 2.3. In the resonance diagram the tune values are reduced to their values between 0 and 1. The working point in the HBSB-mode is near a semi-integer resonance in the vertical direction. A small tune-shift, $\Delta\nu_y = +0.03$ results in an unstable orbit.

2.5 Dispersion and chromaticity

So far, only mono-energetic bunches are considered. In reality not all particles will have the same energy (or momentum). Particles with a larger momentum $p > p_0$ are bent less in the dipoles, as a result their orbit is shifted. However, the focusing quadrupoles do not permit the particles to deviate too much from the design orbit and bend the particles towards the centre of the beam. The defocusing quadrupoles in turn bend the particles away from this centre. The resulting orbit of the off-momentum particles differs from the reference particles.

The dispersion function $D(s)$ is defined as the particular solution of the Hill equation, $\Delta p \neq 0$,

$$x\ (s,\ \frac{dp}{p}) = D(s).\ \frac{dp}{p_0}. \tag{2.7}$$

With the use of the dispersion function the particle trajectory is described with

$$x(s,\ \Delta p/p) = x(s) + D(s)\ \Delta p/p, \tag{2.8}$$

which is a simple superposition of the homogeneous and particular solution of the Hill equation. The dispersion function will be largest in the focusing quadrupoles and smallest in the defocusing quadrupoles. Due to dipole and quadrupole configuration in the EUTERPE ring the long straight sections in the EUTERPE ring are dispersion free.

Another consequence of the momentum shift is that the tune of the off-momentum particles changes. In the quadrupoles the particles with a higher momentum experience a weaker focusing. The chromaticity ξ is a measure for the dependence of the tune as a function of the dispersion,

$$\xi_y = \frac{\Delta \nu_y}{\Delta p/p}. \tag{2.9}$$

The chromaticity produced by all linear magnetic elements in the lattice is called the natural chromaticity.

Chromaticity must be avoided for two reasons: the tune-shift due to chromaticity can cause off-momentum particles to cross resonance lines; as a result their orbits become unstable. Secondly the chromaticity can result in head-tail instabilities [Tur91]. The wake field generated by the leading part of a bunch excites an oscillation in the following part. Due to longitudinal oscillations (synchrotron oscillations) the electrons in a bunch interchange their positions. As a result the oscillations can be anti-damped, which may cause a beam loss. It appears that the oscillations are damped for zero chromaticity.

The natural chromaticity can be corrected with the use of sextupoles. The particles with a larger orbit distortion x due to a larger momentum p are extra focused in the sextupoles ($B \sim r^2$), which results in an increase in the betatron tune. The chromaticity in a sextupole is given by [Cas85]

$$\xi = \frac{1}{4\pi} \oint \beta(s)\, k_2(s)\, D(s)\, ds, \tag{2.10}$$

with $\beta(s)$ the betatron function, $D(s)$ the dispersion function and k_2 the sextupole strength. A disadvantage of the chromaticity correction is that with the use of sextupoles third-order resonances are excited and as a result the boundary of stable motion - the dynamic aperture - is decreased.

2.6 Closed Orbit Distortions

The lattice of a real machine is never perfect. Small imperfections, such as misalignments and field errors, lead to a distortion of the beam. As a result the particles in a bunch will not oscillate around the designed orbit, but will perform their betatron oscillation around a new closed orbit. In this paragraph the physics concerning the closed orbit distortion is treated.

In linear theory all perturbations can be seen as small angular kicks, originating from small additional dipoles. This similarity is used to calculate the closed orbit distortion. The field error is the difference between the real field strength $(\int B.dl)_{real}$ and the designed field strength $(\int B.dl)_{ideal}$

$$\delta(\int B.dl) = (\int B.dl)_{real} - (\int B.dl)_{ideal}. \tag{2.11}$$

The field error results in an additional deflection

$$\Delta u' = \frac{\delta \int B dl}{(B\rho)}, \quad with\ u = x,\ y. \tag{2.12}$$

As mentioned above a particle in a bunch will oscillate around the design orbit. Because the betatron function β is dependent on the longitudinal position (s), the particle will not oscillate harmonically, see eq. (2.4). However, new coordinates η and ϕ can be chosen with which the Hill-equation is transformed into that of a harmonic oscillator [Cas85]. Both η and ϕ are normalised with respect to β. Furthermore ϕ is normalised with respect to the tune. This results in the new coordinates, which are defined as:

$$\eta = \beta^{-1/2} u \quad and \quad \phi = \int \frac{ds}{\nu\beta}. \tag{2.13}$$

With the use of these coordinates the Hill-equation is transformed into

$$\frac{d^2\eta}{d\phi^2} + \nu^2\eta = g(\phi). \tag{2.14}$$

In this formula $g(\phi)$ expresses the perturbation and is a function of $F(s)$, which represents the field error introduced at position s, according to:

$$g(\phi) = \nu^2\beta^{3/2} F(s), \quad with \quad F(s) = \frac{\Delta B(s)}{B\rho}. \tag{2.15}$$

If the lattice is perfect except for a small angular kick at position s_1, then $g(\phi)$ will be zero throughout the ring except for position s_1. In that case equation (2.14) describes a harmonic oscillation with a small deflection at position s_1. We are free to choose the origin of the coordinate ϕ; with ϕ equal to π at position s_1 we find the closed orbit which is visualised in figure 2.4. Note that the figure is symmetrical in $\phi = \pi$.

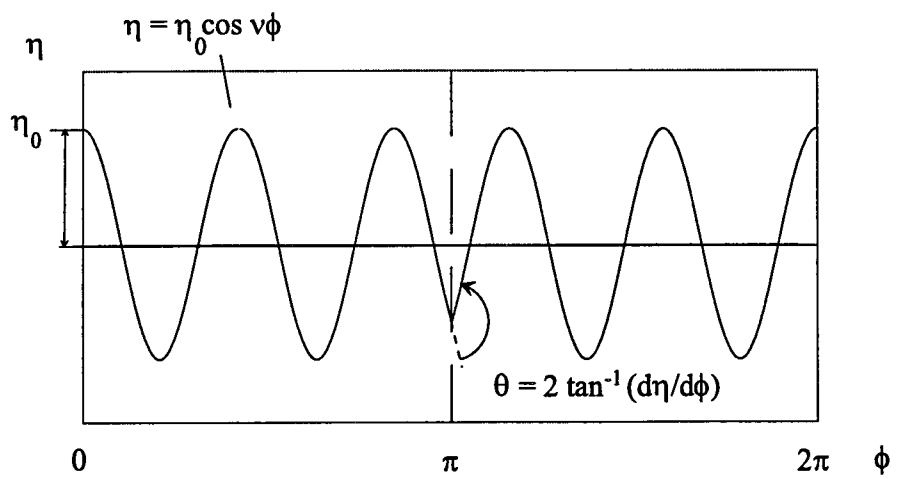

Fig. 2.4 Closed orbit in a perfect lattice with one imperfection

The oscillation of the particles is in the homogeneous area can described by

$$\eta = \eta_0 \cos\nu\phi. \tag{2.16}$$

At the location of the imperfection, the deflection is equal to $\Delta(d\eta/d\phi) = 2\,(d\eta/d\phi)$ (see figure 2.4); the deflection as a function of the field error is given in equation (2.11). Combining these two equations and using the definitions of the parameters η and ϕ, results in the orbit equation [Cas85]

$$x = \sqrt{\beta(s)}\eta_0 \cos\nu\phi(s) = [\frac{\sqrt{\beta(s)\beta_k}}{2\sin\pi\nu} \cdot \frac{\delta(Bl)}{B\rho}] \cos\nu\phi(s), \qquad (2.17)$$

with β_k the betatron function at the position of the imperfection. The equation shows that the closed orbit is most sensitive for imperfections at locations where the betatron functions β is large. It also expresses the fact that the distortion becomes infinite if the tune is equal to an integer.

The expression in square brackets is the maximum amplitude of the perturbation at the location *s*. If there are more perturbations around the ring, the closed orbit distortion is the sum of these partial distortions.

2.7 Closed orbit correction

Deviations of the electrons from the design orbit are not wanted. The distortions can cause part of the beam to hit the walls of the vacuum chamber, especially in special insertion devices such as undulators and wigglers in which the aperture is very small. The distortion of the electron beam can be reduced with the use of a correction system.
The electron orbit can be measured using Beam Position Monitors (BPM's). If the position of the beam is known the closed orbit can be adjusted by deflecting the beam with corrector magnets. Several methods are developed to calculate the corrector settings, which minimise the position errors. In this report the MICADO method is used. The method is discussed in this paragraph.

2.7.1 Determining the number and position of the corrector magnets and monitors

The predominant harmonic in the uncorrected orbit is close to the tune ν. In order to establish its amplitude and phase one needs four monitors per wavelength [Cas94], [Kuo93] in both the horizontal and vertical plane. Furthermore one needs four correctors per wavelength for the correction.

Less correctors are needed if only the two harmonics nearest to the tunes are corrected; studies show that the closed orbit distortion is already reduced to ca 30% of it's initial value with this simple harmonic correction.

The positioning of the monitors and correctors determines largely the effectiveness of the closed orbit correction system. The horizontal position is most accurately measured near a F-quadrupole (a quad focusing in the horizontal direction), where β_x is large and the closed orbit distortion will reach its maximum. The vertical position is best measured near a D-quadrupole (defocusing horizontally and focusing vertically), where β_y is large. Therefore horizontal monitors are best placed near the F-quadrupoles and the vertical monitors near the D-quadrupoles. The best position of the correctors is near the sources of the distortion or 180° in betatron phase shifted [Cas94].

The monitors should not be placed equidistantly; in that case distortions with a wave-length twice the monitor distance are not measured. If the monitor distance is variable more harmonics of the closed orbit distortion are measured. The positioning of the monitors and corrector magnets is of course restricted by the free space available after the insertion of the other elements in the storage ring, such as dipoles, quadrupoles, etc.

2.7.2 Closed orbit correction methods

If the position and number of monitors is roughly determined a closed orbit correction method has to be chosen, with which the correction settings can be determined. Most correction methods are based on a Least Squares approximation; the square errors at the position of beam monitors are minimised. The number of correctors is not necessarily equal to the number of beam position monitors. It is customary to use the smallest set of correctors necessary to obtain a given orbit quality.

There are different strategies to minimise the orbit deviations using the smallest set of correctors [Kou89]:

- The brute force method. For all possible combinations of correctors the least-squares problem is solved, the combination with the smallest residue being the most effective configuration.
- Most effective corrector. The most effective configuration of correctors is quicker found if iteratively the most effective corrector is added to the subset of correctors. The most effective corrector is selected by calculating the least squares error for the subset of correctors plus every possible new corrector. The iteration is repeated until the squared error is below a certain threshold value.

- MICADO. The MICADO-algorithm [Aut73] basically follows the selective approach of the most effective corrector. However in this algorithm the most effective corrector is not determined by solving a least squares problem. Instead the response of each corrector at the position of each monitor is determined. The cross-correlation between this response and the residue distortion is calculated. The corrector with the highest cross-correlation is considered to be the next most effective corrector. Only for this new subset of correctors the least-squares problem is solved. The settings of all correctors previously selected remains unchanged.

The least-squares norm is very sensitive to large measurement errors, which must somehow be removed beforehand. The MICADO-method is implemented in the software packet 'Methodical Accelerator Design (MAD)', see [Mad91], which will be used throughout this report.

Other norms are also implemented in correction techniques, e.g. the l_1-norm penalises errors independently of their magnitude and thus wrong measurements have less weight. The l_1-norm is implemented in Simplex [Kou89]. The harmonic analysis method mentioned in the previous paragraph is another method, which is more immune to noise. This noise can be caused by for example, radiation striking the position monitor.

The differences in the quality from the different correction techniques and methods is small. According to [Kou89] all methods are approximately equivalent from the point of view of the final orbit residues.

Chapter 3

The closed orbit distortion in the EUTERPE ring

A synchrotron with a perfect lattice has an ideal reference orbit. In a real machine the orbit is distorted as a consequence of lattice imperfections. The reference particle will deviate from the designed, ideal orbit. All particles will perform their betatron oscillations around this new closed orbit. In this chapter the closed orbit distortions due to different error sources are estimated. In § 3.1 the sources of the closed orbit distortion are discussed; the amplitudes of the most important error sources are estimated. The effects of these errors on the closed orbit distortions are simulated in the computer group of codes "MAD" (Methodical Accelerator Design). The resulting closed orbit distortions are discussed in § 3.2.

3.1 Sources of closed orbit distortion

The trajectory of the electrons in a storage ring is mainly affected by magnetic forces. The distortion of the closed orbit is therefore normally a result of local field errors. These local field errors are in turn a consequence of position errors of the magnets or of magnet imperfections. The sizes of the position errors and magnet imperfections are estimated in this paragraph.

The position errors originate from different error sources; the contributions of these error sources to the total position errors are estimated separately. In §3.1.1 to §3.1.3 respectively the displacement errors due to misalignments, thermal expansion and vibrations are estimated. The field errors are determined in §3.1.4. The total position and field errors used for the simulations are given in §3.1.5.

3.1.1 Alignment errors

The position of the magnetic elements in the ring can only be measured with a finite precision. Displacements with a smaller amplitude than the measurement error can not be eliminated. A

special alignment lattice has been designed [Stei94]; with this lattice the amplitude of the misalignments is reduced to $\sigma_x = \sigma_y = \sigma_z = 0.1$ mm and $\sigma_\phi = \sigma_\theta = \sigma_\psi = 0.1$ mrad; all errors having a Gaussian distribution.

The magnets are aligned with the use of three reference points on top of the magnets. These reference points on the magnets are aligned with respect to 8 reference points located outside the ring. As a consequence of the overdetermination of the magnet location the position error can be reduced.

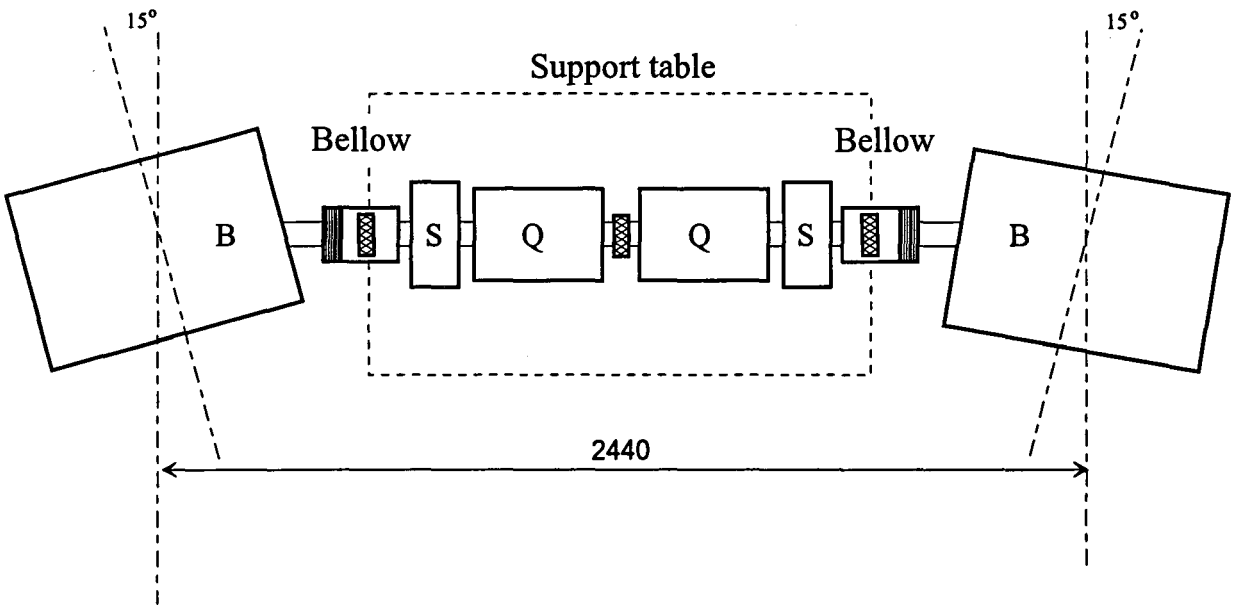

Fig. 3.1 Subsection containing a quadrupole doublet and two sextupoles.

Each quadrupole doublet and set of sextupoles in a short straight section of the ring is placed on a large table, see figure 3.1. The position errors of the quadrupoles and sextupoles are a superposition of two errors: the errors in the positioning of the quadrupoles on the tables and of alignment errors of the tables in the ring. It is expected that the rms-values of the position errors of the quadrupoles can be reduced to 0.1 mm [Tim95] in all directions.

The sextupoles can be aligned with the same accuracy. However the closed orbit is less sensitive to sextupole displacements, therefore the alignment of the sextupoles is not necessarily as accurate as the alignment of the dipoles or quadrupoles. With less effort the sextupoles could be aligned with an error equal to 0.2 mm.

Table 3.1 Expected alignment errors in the EUTERPE ring

Alignment error	Dipole	Quadrupole	Sextupole
$\sigma_x = \sigma_y = \sigma_s$ (mm)	0.1	0.1	0.2
$\sigma_\phi = \sigma_\theta = \sigma_\psi$ (mrad)	0.1	0.1	0.2

3.1.2 Thermal effects

The temperature in the hall in which the EUTERPE ring is placed is not conditioned. As a consequence the temperature in the hall will change during operation and in-between experiments. The temperature change will result in a heating or cooling of the storage ring floor. The thermal expansion or contraction of the storage ring floor results in a displacement of the ring elements. The amplitudes of the displacements are estimated in this paragraph. A differentiation has been made between local and global thermal expansion.

3.1.2.1 Global thermal expansion

The global temperature in the storage ring hall changes with the temperature outside. The temperature in the hall varies from about 10 °C in winter to circa 30°C in summer: a temperature-variation of 20 K. Moreover the temperature changes on a daily basis due to the heating of the hall by the sun.

The temperature of the storage ring floor will change only in the surface layer of the concrete. An upper limit to the global expansion is found assuming the temperature in the concrete is homogeneously changed with 20 K ($\Delta T = \pm 10K$). In that case the storage ring floor will expand linearly

$$\Delta x = r.\epsilon.\Delta T \approx \pm 0.8 \; mm, \qquad (3.1)$$

r is the radius of the ring ($r = 6.4$ m) and ϵ the linear expansion factor of concrete ($\epsilon = 1.2.10^{-5}/K$). The displacement of all elements is approximately equal and is for all elements in the radial direction.

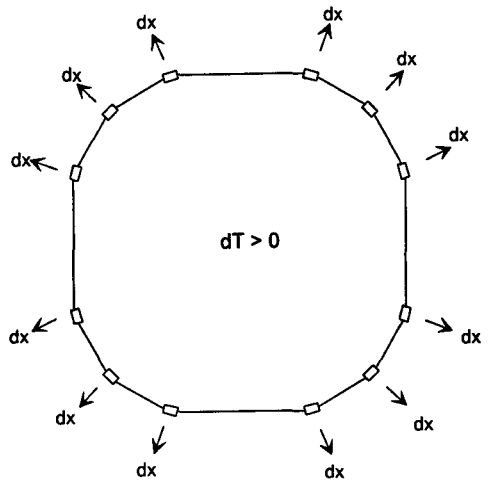

Fig. 3.2 Displacements due to global heating of the storage ring floor.

In reality the concrete floor of the hall is not homogeneously heated and due to stress in the concrete the thermal expansion of the storage ring floor is reduced. An indication of the difference between the thermal expansion of a homogeneously heated floor and the real thermal expansion can be deduced from experiments at the Photon Factory in Japan. The thermal expansion of the storage ring was measured [KAT93] as a function of the temperature of the storage ring floor and of other parts of the storage ring hall. The main contribution to the displacements was the temperature change in the storage ring floor; $\Delta x = 3.2\ 10^{-6}/K$. This measured thermal expansion is 3 to 4 times smaller than the expansion calculated with eq. 3.1, which holds for a homogeneous heated concrete layer.

Based on the experience in Japan it is expected that the thermal expansion calculated with eq. 3.1 (Δx =0.8 mm) is several times larger than the real thermal expansion. However the displacements due to global thermal expansion are expected to be at least of the same order as the alignment errors, viz. $\sigma = 0.1$ mm.

3.1.2.2 Local temperature effects.

Not only the global, but also the local temperature in the storage ring hall will vary in-between and during experiments. Due to local heating and the absence of ventilation the temperature in the storage ring will vary locally. Local thermal expansion of the storage ring floor causes local displacements; the direction of the local displacements is uncorrelated. However the local temperature changes in the storage ring floor are small (the floor is slowly heated) and the

domains over which the temperature changes are small. Assuming the temperature variation is 2 K over a length of 2 m (the length of a short straight section) an upper limit to the thermal expansion is calculated with eq. 3.1; $\sigma_x = \sigma_s < 0.05$ mm. The displacements are expected to be several times smaller than this upper limit. The displacements due to local thermal expansion of the storage ring floor are several times smaller than the alignment errors; their contribution to the total displacement errors are therefore negligible.

Not only the storage ring floor is heated locally; the metal frames on which the dipoles are placed can be heated by sunlight. The temperature difference between the dipole-frame is possibly $\Delta T = \pm 5$K.The temperature in a frame is homogeneous due the good thermal conduction of the steel. In the case of linear expansion, which can be expected for a homogeneously heated dipole, the vertical displacement of the dipole is equal to $\Delta y \approx \pm 0.06$ mm ($\Delta T = \pm 5$ K and h=1.20m).

Local thermal expansion does have an influence on the vertical dipole position, but the total amplitude of the vertical displacements is hardly increased. Furthermore local thermal expansion is easily prevented with shielding.The effects of global and local thermal expansion are summarised in table 3.2.

Table 3.2 The effects of thermal expansion

Cause	Direction	ΔT (K)	Displacement
Local heating of a dipole-frame	vertical direction	±5	$\Delta y < 0.06$ mm
Local temperature differences	All directions	±2	$\sigma_x, \sigma_y, \sigma_z < 0.05$ mm
Global heating of storage ring floor	horizontal direction	±10	$\Delta x < 0.8$ mm

3.1.3 Vibrations and other sources affecting the element positions.

The position of the magnetic elements is influenced by position errors originating from other effects. In this paragraph the effects of vibrations of the storage ring floor and the dipole-supports is estimated. Furthermore the influence of the rebuilding of the concrete bunker inside the ring after alignment will be estimated.

Vibrations in the storage ring floor can be excited due to external sources, such as trucks or trains passing by. These vibrations in the storage ring floor in turn excite the vibrations in the supports of the magnetic elements; as a result the positions of these elements are continuously displaced.

Several experiments have been done to determine the amplitudes and resonance frequencies of the dipole-frames. The oscillation amplitudes of the dipole-frame in 3 dimensions were measured as a function of the kick on the frames, see table 3.3. Furthermore the maximum displacements of the dipole-frame have been measured during a small interval of time (about 1 minute). During these experiments the water cooling system through the dipole was switched on; also the storage ring floor was excited as much as possible. The maximum displacements remained smaller than 300 nm. The experiments are described in [Bres95].

Table 3.3 Parameters concerning the vibrations in the support of the first EUTERPE dipole

Parameter	x-direction	y-direction	s-direction
Maximum displacement	$\Delta x < 300$ nm	$\Delta y < 300$ nm	$\Delta z < 30$ nm
Resonance frequency	f = 9.5 Hz	f = 11.5 Hz	f = 9.5 Hz
Response	dx= 28 ± 1 μm/N	dy= 22 ± 4 μm/N	dz < 4 μm/N

During the alignment of the dipoles, part of the bunker inside the storage ring (see figure 1.1) may have to be removed; after alignment the bunker shall be rebuild again. The large mass-concentration (150 ton per bunker) might cause the concrete floor to bend a little between the piles. The size of the tilt-angle has been estimated. In the situation that all mass of the bunker would be concentrated in the middle of one floor segment (5 metre by 5 metre), the tilt-angle would still be smaller than 0.02 mrad. The effects of the rebuilding of the bunker are therefore negligible.

3.1.4 Field errors due to magnet imperfections

Imperfections in the geometry of the magnets result in field errors. These field errors are measured in the integrated field strengths along the electron trajectory.

At the start of this study only one dipole was completely manufactured. The quadrupoles were still under construction and the sextupoles were designed during this study. The magnetic field in the first dipole has been measured [Der93]. The fieldstrength along the electron trajectory (the

field integral) is a function of the radial position of the dipole. The field integral changes more than 0.05% if the dipole is 10 mm displaced in the radial direction; this corresponds to a deflection of the beam with 0.015°. The dependency of the field strength on the magnet position is described by higher order field components. The sizes of the higher field components according to[Der93] are given in table 3.4. The relative difference in the field integral between different dipoles is in the order of 10^{-4}. The extra deflection in a dipole with a relative error $\Delta_{\int B.dl} / \int B.dl = 10^{-4}$ is ca 0.05 mrad, which has a negligible effect on the total closed orbit distortion.

Relative errors in the fieldstrengths in the quadrupoles mainly affect the betatron tunes. The relative quadrupole errors are expected to have an amplitude equal to $\sigma_{\int k1.dl} / \int k_1.dl = 1.10^{-3}$, which result in relative tune shifts of the same order. The higher order field errors in the quadrupoles and sextupoles are expected to have a negligible influence on the closed orbit.

Table 3.4 Expected field errors in the EUTERPE dipoles and quadrupoles

Elements	Error	Magnitude
Dipoles	relative field strength	$\sigma_{\int B.dl} / \int B.dl = 1.10^{-4}$
Dipoles	sextupole field strength	$\int k_2' \, dl \approx 2.10^{-1}\ m^{-3}$
Quadrupoles	relative field strength	$\sigma_{\int k1.dl} / \int k_1.dl = 1.10^{-3}$

3.1.5 Resulting displacement and field errors

In the previous paragraphs an extensive study of the displacements and field errors of the magnetic elements in the EUTERPE ring has been made. Only the errors with the largest amplitudes will be simulated in MAD in order to get an impression of the closed orbit distortion in the storage ring (see next paragraph). The largest displacement errors are a result of the finite measurement precision during the alignment. Apart from these alignment errors only the displacements due to global thermal expansion are non-negligible. The amplitudes of the displacement errors used for the simulations are summarised in table 3.5.

Note that the alignment errors and the displacements due to thermal expansion are fundamentally different. The alignment errors are constant, while the errors due to thermal expansion vary continuously. These errors cause the closed orbit to change during and in-between the experiments.

The field errors in the magnetic elements are expected to have little effect on the total distortions. The relative field errors in the dipoles are $\sigma_{\int B.dl} / \int B.dl = 1.10^{-4}$, which result in deflections in the order of $\Delta x'$=0.05mm per dipole. The relative field errors in the quadrupoles are expected to have a larger effect, mainly on the tunes. Only the higher order field components in the dipoles have been measured; their effect on the closed orbit distortions will be determined with simulations, see table 3.5.

Table 3.5 Total displacements and field errors

Source	Displacement	Elements involved
Misalignments	$\sigma_x = \sigma_y = \sigma_z = 0.1$ mm and $\sigma_\phi = \sigma_\theta = \sigma_\psi = 0.1$ mrad	All dipoles and quadrupoles.
Misalignments	$\sigma_x = \sigma_y = \sigma_z = 0.2$ mm and $\sigma_\phi = \sigma_\theta = \sigma_\psi = 0.2$ mrad	All sextupoles
Thermal expansion due to global heating	$\Delta x \approx$ 1mm	All elements
Magnet imperfections	$\int k_2' \, dl \approx 17$ m^{-3} $\sigma_{\int k1 dl} / \int k_1 dl \approx 1.10^{-4}$	Dipoles Quadrupoles

3.2 Resulting closed orbit distortions

The size of the displacement and field errors in the magnetic elements has been estimated in the previous paragraph. The effects of these errors on the closed orbit of the electrons are examined by simulating them with the program MAD. The effects of both the displacement of a single element in one direction as well as the effect of the displacements of multiple elements in all directions have been determined.

3.2.1 Simulations in MAD

The principle concern of this report is the closed orbit distortion. In this paragraph the closed orbit distortions and tune shifts are calculated for many different error configurations. The software packet Methodical Accelerator Design (MAD) is used for the calculations. MAD has been

developed at CERN as a tool for charged particle optics in accelerators. Many features are included in the program [Mad85]; among these features are the calculation of the closed orbit distortion and the closed orbit correction. More information about the program is given in appendix A.

Many other beam parameters are calculated with MAD. During the simulations in this report the chromaticity ξ, the dispersion D, the betatron amplitudes β, the momentum compaction factor α, and the increase of the closed orbit length Δs are calculated. Only the values of the parameters affecting the closed orbit (the tunes and closed orbit distortions) are given in the different tables.

Each element in the EUTERPE ring will have a random displacement error with an rms-value as mentioned in §3.1.5. In MAD random displacement errors are assigned to each element using a Gaussian table. All displacement errors used in the simulations are defined as the relative displacements at the entrance of the magnetic elements[1]. For one possible error-configuration the closed orbit distortion is determined. The statistical error introduced by this error-assignment is reduced by averaging the results over 10 runs.

3.3.2 The effects of single misalignments

The effects of all possible single misalignments - a perfect lattice containing only a specified displacement of one element in one direction - have been calculated with MAD in order to get a first impression of the sensitivity for different displacements. The displacements with the largest effects on the amplitudes of the closed orbit distortions or tunes are given in table 3.6. The effects of all possible misalignments are given in appendix B. The effects of single misalignments of the other dipoles (D2) and quadrupoles (Q2, Q3 and Q4) were comparable with the effects of the displacements of the first dipoles and quadrupoles. An example of the closed orbit distortion due to a single displacement is given in figure 3.3.

The closed orbit is very sensitive to displacements of the quadrupoles in the x-direction, see table 3.6. The displacement of the first quadrupole in the x-direction results is 34 times amplified in the closed orbit distortion! The sensitivity of the distortion for the quadrupole displacements are a consequence of comparatively large values of both the induction and the betatron function.

[1] This definition of the displacement errors differs from the definition of misplacements at the centre of each element, see appendix B.

Table 3.6 *The effects of single displacements on the closed orbit (D1=dipole 1, Q1=quadrupole 1), mode HBSB*

Element	Displacement	x_{max} (mm)	y_{max} (mm)	$\Delta \nu_x$ $*10^{-4}$	$\Delta \nu_y$ $*10^{-4}$
Q1	dx=0.1mm	3	0	25	1
Q1	dy=0.1mm	0.004	0.4	0.5	0.2
Q1	dθ=0.1mrad	0.5	0	4	1
D1	dx=0.1mm	0.2	0	0.1	2
D1	dy=0.1mm	0.002	0.3	0.04	0.02
D1	ds=0.1mm	0.7	0	0.2	8
D1	dψ=0.1mm	0.002	0.3	0.04	0.02

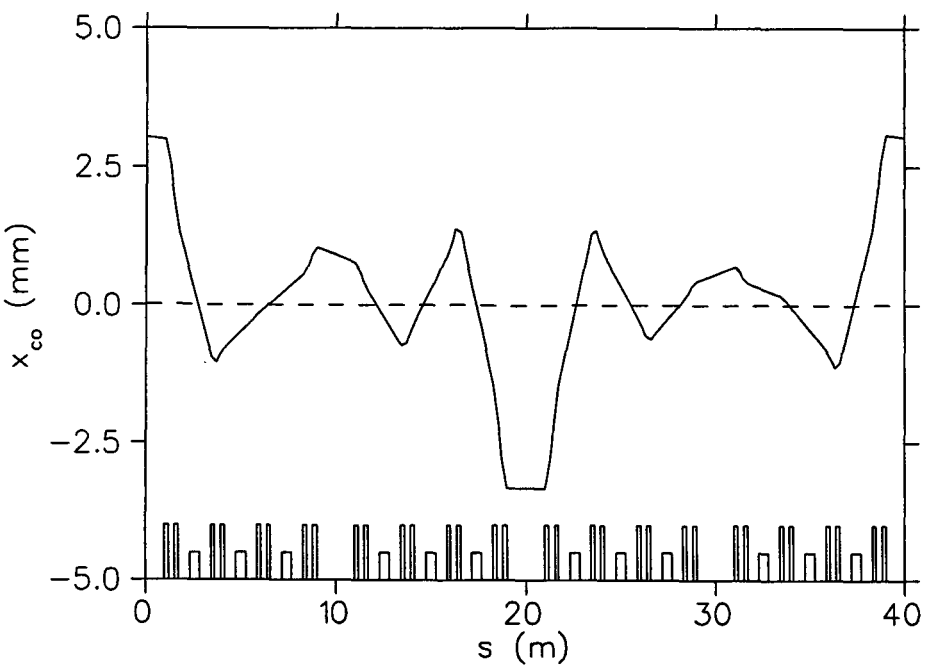

Fig. 3.3 *The closed orbit distortion in the HBSB-mode due to a displacement dx=0.1mm of the first quadrupole (Q1).*

It must be noted that in practice the displacements of an element in a certain direction may have a significant influence on the closed orbit, while a single misalignment in the specific direction does not affect the closed orbit. E.g. a single misalignment of a quadrupole in the s-direction does not distort the closed orbit, because the beam is not deflected in the quadrupole. In a real lattice however the closed orbit is already distorted due to other lattice errors and the closed orbit does not coincide with the magnet axis of the quadrupole. As a consequence the particles are deflected and a displacement of a quadrupole in the longitudinal direction does have an effect on the closed orbit.

The effects of single misalignments have also been examined in the HLF-mode; for this mode the effects of single misalignments on both the closed orbit distortions and the tunes were about 10 times smaller. This is a result of a difference in the focusing strength of the quadrupoles.

3.3.2 The effects of multiple misalignments and field errors

The consequences of misalignments in all directions of all dipoles, quadrupoles and/or sextupoles have been examined. The results are summarised in table 3.7 for the HBSB-mode. All results are averaged over 10 runs with different random displacements. The deviations of the closed orbit distortions are about 50 %; the deviations of the tune-shifts are even larger. These uncertainties are not a result of the limited number of simulations; the deviations are not reduced if their value is averaged over more runs.The rms-value of the closed orbit distortion in the horizontal and vertical plane is calculated for 50 error-configurations and is equal to $x_{rms}\,(co) = 0.7\pm0.3$ mm and $y_{rms}\,(co) = 0.4\pm0.2$ mm. These results differ little from the values in table 3.7.

The displacements of the quadrupoles are the main sources of the closed orbit distortions. The influence of the displacements of all dipoles is several times smaller; this is partly due to a smaller amount of dipoles (12 dipoles and 32 quadrupoles) but also a consequence of a bigger sensitivity for quadrupole-displacements. The sextupole-displacements have little effect on the distortion, due to their comparatively weak magnetic field. However the sextupole displacements have a significant effect on the betatron tunes, as a consequence of their additional focusing.

Table 3.7 *Effects of multiple displacements (σ=0.1mm and σ=0.1mrad) and field errors on the closed orbit distortion (mode HBSB)*

Displacement	x_{rms} (mm)	y_{rms} (mm)	$\Delta\ \nu_x$ $*10^{-2}$	$\Delta\ \nu_y$ $*10^{-2}$	$N_{unstable}$ (*)
All dipoles	0.7 ±0.2	0.5 ±0.2	0.07 ± 0.03	0.1 ± 0.1	0
All quadrupoles	4 ±2	1.1 ±0.3	0.4 ± 0.3	--- (*)	8
All sextupoles	0.007 ±0.004	0.006 ±0.003	0.02 ± 0.01	0.2 ±0.1	1
All elements	3 ±1	1.4 ±0.5	0.9 ± 0.8	--- (*)	7
All elements + field errors	3 ±1	1.4 ±0.5	0.9 ± 0.8	--- (*)	8

(*) The betatron oscillations in the vertical plane were unstable for several error-configurations as a consequence of the tune shifts caused by the lattice imperfections. For errors which resulted in a high number of unstable runs $N_{unstable}$ the tune shifts in the vertical direction are not given.

The closed orbit distortions are within a few percent a linear function of the amplitude of the misalignments. The distortions are proportional to the error fields. Moreover the resulting error fields in both the dipoles and quadrupoles are proportional to the displacement of the elements. The error fields due to sextupole misalignments are a quadratic function of the displacement errors, as a consequence of the proportionality of the sextupole field to r^2. However the effects of the sextupole misalignments on the total distortion are negligible. The closed orbit distortions due to misalignments with a different amplitude are easily calculated with the values listed in table 3.7 as a result of this linearity.

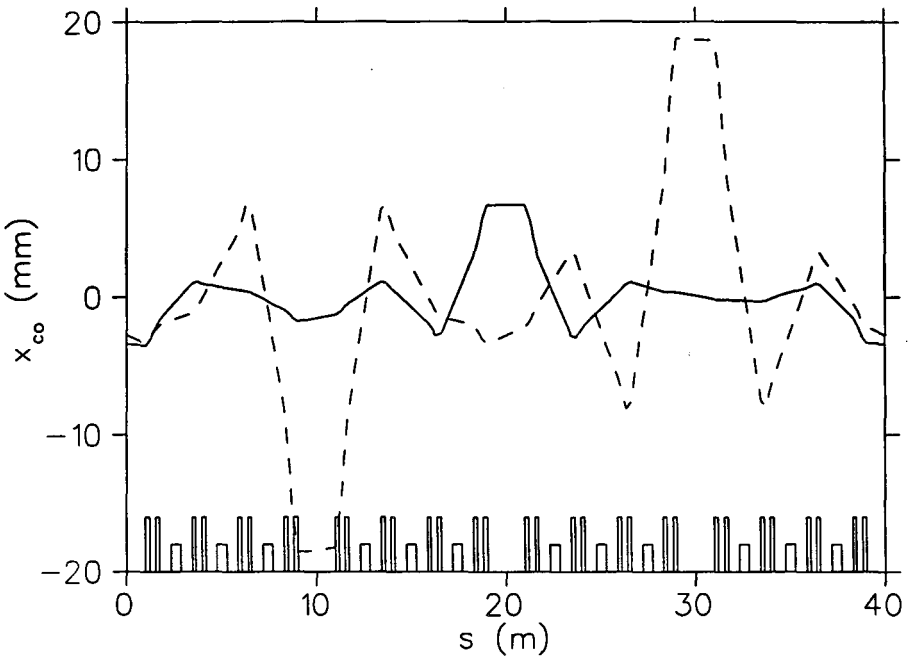

Fig. 3.4 *The closed orbit due to the random displacements of all dipoles, quadrupoles and sextupoles for two different error-configurations.*

The closed orbit distortion due to the misalignments of all dipoles, quadrupoles and sextupoles gives a good impression of the real closed orbit. An example is given in figure 3.4.

If the maximum values of the closed orbit distortions exceed the dimensions of the vacuum chamber the beam is instantly lost. The maximum value of the lattice with all elements misaligned and with field errors in the dipoles is for ten different error-configurations equal to:

$x_{max} \approx 18$ mm,

and $y_{max} \approx 5$ mm.

These values are still smaller than the inner radius of the vacuum chamber, which is 22.5 mm. The distortions reach their maximum value in the long straight sections for all error-configurations. Due to the absence of focusing elements the betatron values and the distortions are maximum in these sections. The maximum closed orbit distortions are listed in appendix B.

The closed orbit distortions are calculated in the HLF mode using the same displacement errors as in the HBSB mode. The distortions in the HLF mode are 10 times smaller in the horizontal and 2 times smaller in the vertical direction than in the HBSB mode. Moreover the tune shifts in the HLF mode are smaller, $\Delta \nu_x$, $\Delta \nu_y < 2.10^{-3}$. As a result the betatron oscillations in the vertical plane are stable for all error configurations.

Finally the effects of global thermal expansion and the energy spread are calculated. The effects of global thermal expansion are illustrated in fig. 3.5. All elements are displaced in the radial direction. The closed orbit is shifted with the elements.

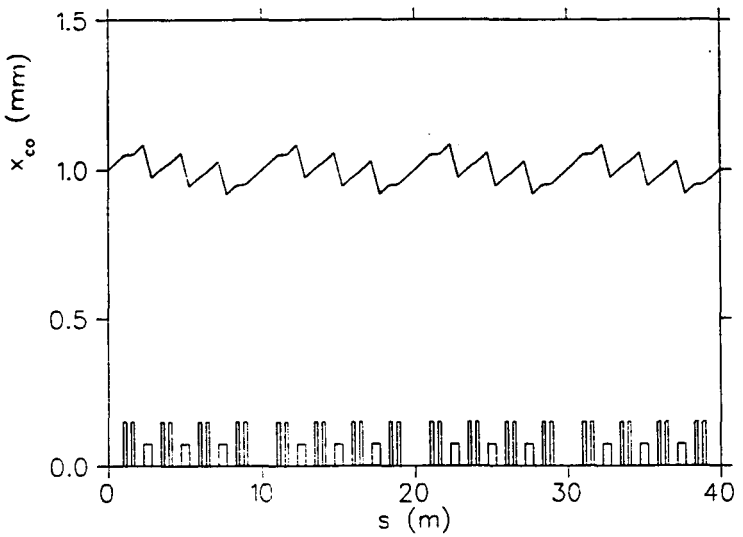

Fig. 3.5 *The closed orbit distortion due to global heating; all elements are displaced in the radial direction, Δx=1mm, in the HBSB mode.*

The influence of momentum deviations (or energy spread) on the orbits is described by the dispersion function. The dispersion function for the EUTERPE ring is depicted in appendix C. The maximum value of the dispersion function is $D = \partial x / \partial(\Delta p/p)$ = 0.5 mm in-between the dipoles. The momentum spread of the particles in the EUTERPE ring is given by [Xi 95]

by the injection of the beam: $\Delta p/p = 0.5\ \%$, *which gives* $\Delta x_{max} = 2.6mm$
during operation for a 400 MeV beam $\Delta p/p = 0.04\ \%$, *which gives* $\Delta x_{max} = 0.2mm$.

The effects of the dispersion on the total distortion of the electrons is limited. However the dispersion increases the beam width significantly. According to table 1.2 the beam width is less than 0.1 mm in the HBSB mode. At the injection the local broadening of the beam due to the dispersion is several times larger than this value. During operation the momentum spread is damped; as a consequence the dispersion is reduced.

3.3 Summary

Due to position and field errors of the magnetic elements in the EUTERPE ring the closed orbit of the electrons is distorted. In this chapter the closed orbit distortion has been calculated as a function of the estimated position and field errors.

A study of the error sources resulting in the displacements of the magnetic elements showed that the finite measurement precision during alignment is the main source of the position errors. The resulting displacements and tilt angles of the elements have a Gaussian distribution with $\sigma_x=\sigma_y=\sigma_s=0.1$ mm and $\sigma_\phi=\sigma_\theta=\sigma_\psi=0.1$ mrad. The influence of other effects, such as thermal expansion, and vibrations, are several times smaller and therefore negligible for the total displacements.

The closed orbit is most affected by displacements of the quadrupoles in the horizontal direction. The sensitivity of the closed orbit for the displacements of the different elements has been determined with simulations of single displacements: simulations of a perfect lattice containing only a displacement of a single element in one direction. A single displacement of a quadrupole in the horizontal direction results in a 34 times larger closed orbit distortion. The largest distortions are in the long straight sections, between two focusing quadrupoles.

The closed orbit distortion due to the misalignment of all elements in all directions is equal to x_{rms} = 3±1mm in the horizontal and y_{rms} = 1.4±0.5 mm in the vertical direction. The distortion has been determined with simulations in MAD; random displacement errors have been assigned to all elements. For statistical reasons the results have been averaged over 10 error-configurations. The closed orbit distortions in the horizontal plane are more error-sensitive due to the higher tune-values in the horizontal direction. The higher order field components in the dipoles have a negligible influence on the total distortion.

The displacements of the elements and the field errors resulted in shifts of the betatron tune. The vertical tune in the HBSB-mode is near a semi-integer resonance. The tune shift due to the displacements of the elements resulted for 8 out of 10 error configurations in a resonance of the vertical betatron oscillation, which in practise results in a loss of the beam. With a small adjustment of the working point, away from the semi-integer resonance line, this resonance can be prevented.

All results mentioned above are calculated for the High Brilliance Small Beam mode, which is the mode of operation with the strongest focusing and as a result most sensitive for lattice imperfections. The closed orbit distortions in the High Light Flux mode, which has the weakest

focusing, are about ten times smaller than in the HBSB mode. Furthermore the tune shifts in the HLF mode are about 10 times smaller. As a result the betatron oscillations in the vertical plane were stable for all simulated error-configurations. The results confirm the stability of the HLF mode; this same stability is the reason why the mode will be used for the first phase of the commissioning of the machine.

Chapter 4

Design of a closed orbit correction system

In this chapter a closed orbit correction system is described, which has been designed in order to reduce the closed orbit distortion. The locations available for the insertion of the corrector magnets and beam position monitors are determined in §4.1. With the use of the available locations different correction lattices have been designed. In §4.2 the lattices are given and compared. The maximum reduction of the distortion is determined. In §4.3 the number of monitors and correctors required for the correction is minimised. The results are summarised in §4.4.

4.1 Introduction

The uncorrected closed orbit distortions in the High Brilliance Small Beam mode are large in comparison to the inner radius of the vacuum chamber. The stability of the beam is improved if the distortion is reduced. Therefore a closed orbit correction system is necessary. The aim of the correction system for the EUTERPE ring is to reduce the distortion as much as possible, while using as little space as possible for the insertion of the correction elements.

The calculations of the closed orbit distortion in the previous chapter showed that the horizontal closed orbit distortions in the HBSB mode are the largest. Therefore the reduction of the horizontal closed orbit distortion in this mode will be the main purpose here. The resulting distortions in the HLF mode will be checked after correction with the final lattice.

Only a few locations are available for the insertion of the correction system, which consists of beam position monitors and corrector magnets. The major part of the ring is reserved for the 'normal' lattice elements, such as the dipoles, quadrupoles and sextupoles. The available locations are marked in fig. 4.1. The long straight sections between the quadrupole doublets of two successive superperiods are reserved for special elements, such as the rf-cavity and the injection elements. The available locations in these sections are still unknown.

Different correction lattices have been compared. A standard lattice is composed in §4.2.1.

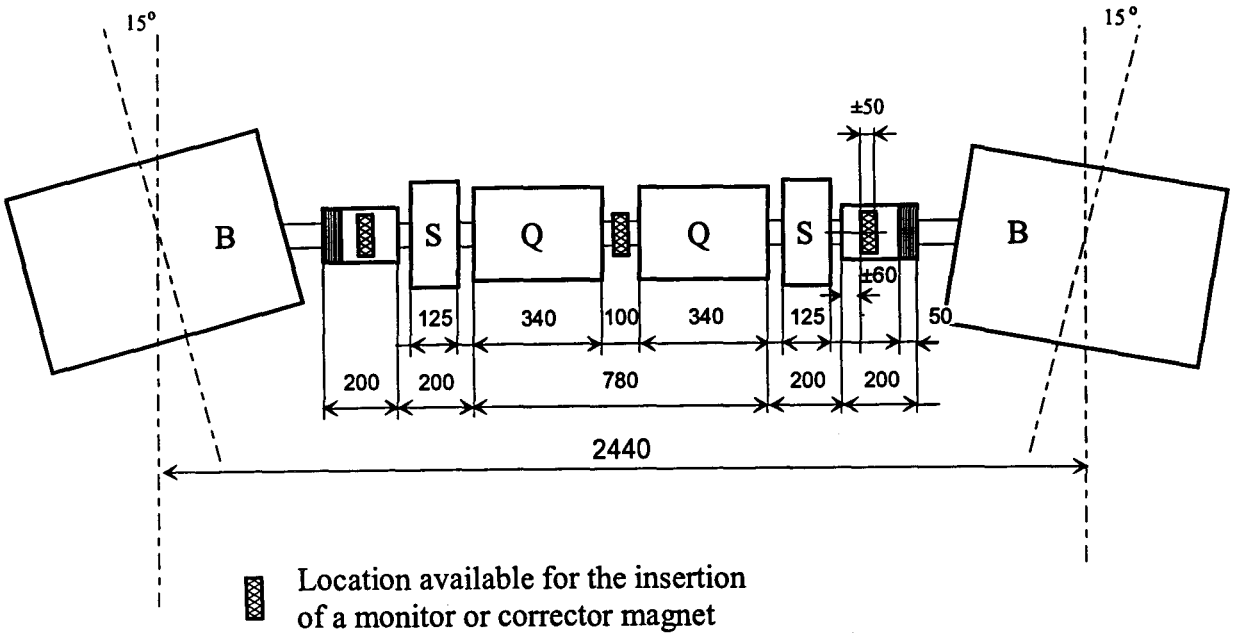

Fig. 4.1 Available locations for the insertion of the correction elements.

The monitors in this lattice are placed near the focusing quadrupoles. The total number of monitors and correctors used in the lattice is equal to 20. Both the correctors and monitors function in both the horizontal and vertical direction. The positions of the elements of the correction systems are at the available locations mentioned above. The long straight sections are considered to be available for the insertion of the corrector magnets and beam position monitors; the effect of the displacement or removal of these correctors and monitors is determined later.

The dipoles and sextupoles in the ring can be used as corrector magnets with the generation of additional dipole fields. With the use of the sextupoles and dipoles as corrector magnets the total number of monitors and correctors can be enlarged without increasing the space required for the correction system. In §4.1.2 both the sextupoles and dipoles are used as corrector magnets. Even with the use of both the sextupoles and dipoles, additional corrector magnets are required in the long straight sections. Extra monitors are included at the locations of the corrector magnets in the standard lattice; the total number of monitors is increased to 36.

In order to reduce the number of different elements used as corrector magnets, only the sextupoles are used as additional corrector magnets. The distortions after correction with these lattices are given in §4.1.3. The influence of monitor misalignments and monitor read errors on

the resulting distortions are discussed.

Finally the space occupied by the correction system will be minimised. The distortions after correction with the lattices with more monitors will serve as a reference.

4.2 A comparison of different correction lattices

The reduction of the closed orbit distortions due to the closed orbit correction is determined with simulations in the computer code Methodical Accelerator Design [Mad91]. First the uncorrected closed orbit distortions have been calculated after giving all elements (dipole, quadrupole and sextupole) misalignment errors, with $\sigma_x=\sigma_y=\sigma_s=0.1$mm and $\sigma_\phi=\sigma_\theta=\sigma_\psi=0.1$mrad. Then the distortions after correction with the different correction lattices are determined; the elements of the correction system are given the same misalignments. The monitor readings have a deviation equal to $\sigma_x=\sigma_y=0.1$mm. For statistical reasons this procedure is repeated 10 times and the results are averaged.

4.2.1 The standard correction lattice

In correction lattice, *A*, the monitors are placed near the focusing quadrupoles. In between every quadrupole doublet a monitor is placed; an extra monitor is inserted in the long straight sections. The corrector magnets are evenly distributed at the available locations in the ring. The total number of monitors and correctors equals N_{mon}= 20 and N_{corr} =20. This correction lattice will be used as a reference for the following correction lattices and is referred to as the standard lattice.

The best correction is obtained if the monitors are included at the locations with the largest electron beam distortions. The maximum orbit distortions are reached at the locations with the largest betatron function, $\beta_x(s)$ and $\beta_y(s)$. The betatron functions are depicted in figure 4.2. Of course, the maximum values of the betatron functions are in the focusing quadrupoles. In the long straight sections between the focusing quadrupoles, the betatron function reaches a very high constant value. The monitors are placed at the locations with the highest horizontal betatron values. The standard lattice *A* is shown in fig. 4.3.

Quadrupoles focusing horizontally are defocusing vertically. As a consequence the maxima and minima of the betatron functions β_x (s) and β (s) are reversed. A second lattice has been simulated in which the locations of the monitors and correctors is reversed. Because the monitors in this second lattice are placed at the locations with the largest values of $\beta_y(s)$, the

vertical correction is expected to improve with this lattice. The horizontal correction is expected to deteriorate.

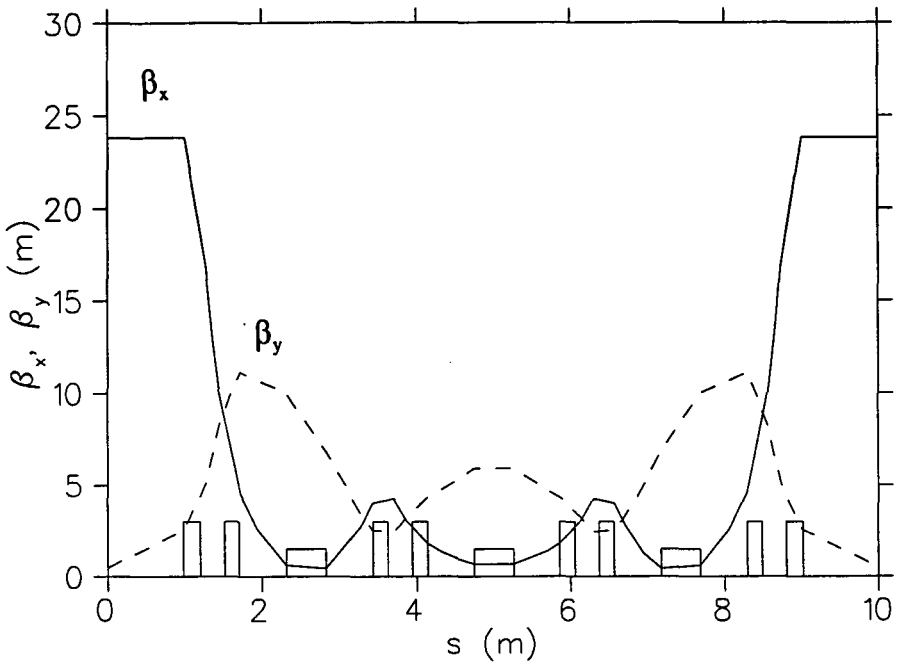

Fig. 4.2 The betatron amplitudes in the horizontal and vertical direction (β_x and β_y) for one superperiod for the HBSB-mode.

The number of monitors and correctors used in the standard lattice approximate the number of four correctors and monitors per betatron wavelength. This number of monitors is required for the full establishment of the amplitude and phase of the distortion. The highest tune-values in the EUTERPE-ring are $\nu_x = 5.13$ and $\nu_y = 2.47$, both for the HBSB-mode, which corresponds to 20 to 24 horizontal and 8 to 12 vertical beam position monitors required for the correction system.The number of both the monitors and correctors in the standard lattice are within these limits.

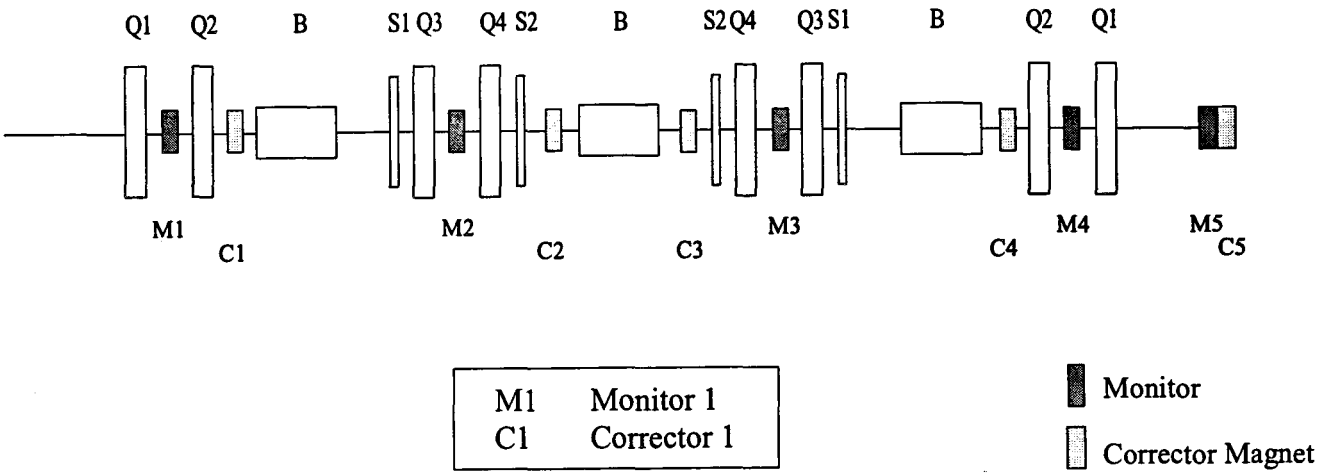

Fig. 4.3 Schematic view of the standard lattice, A.

The closed orbit correction with the standard lattice is very successful. The rms-values of the closed orbit distortions are reduced with a factor 22 in the horizontal and a factor 5 in the vertical direction.

The beam position errors in the monitors have been reduced to $x_{rms} = 0.01$ mm and $y_{rms} = 0.01$ mm. The resulting distortions are therefore a consequence of the limited number of monitors and the position and read errors of the monitors. The vertical closed orbit distortions are shown in appendix C.

Table 4.1 The closed orbit distortions after correction with the standard lattice.

Correction lattice.	x_{max} (mm)	x_{rms} (mm)	y_{max} (mm)	y_{rms} (mm)
No correction	10±5	4±2	2.7±0.8	1.0 ± 0.4
Standard lattice A	0.44±0.09	0.16±0.06	0.6±0.1	0.19±0.03
Locations of monitors and correctors reversed	0.5±0.1	0.23±0.06	0.4±0.1	0.16±0.03

With the locations of the monitors and correctors reversed, the horizontal distortion after correction is ±40 % larger. On the contrary the vertical distortion is ±20% extra reduced. The

results confirm the expectation that the monitors should be placed at the locations with the highest values of the betatron functions. The reduction of the distortion after correction is much smaller in the vertical than in the horizontal plane, which is a result of the smaller vertical distortions before correction. The maximum reduction is limited by the size of the monitor displacements and read errors (both with $\sigma_x=\sigma_x=0.1$ mm).

The vertical tune shifts are reduced due to correction with about a factor 3 for most lattices. As a result, the number of error configurations resulting in resonance of the vertical betatron oscillation is reduced. The beam deflections in the correctors and the tune shifts are given in the table below.

Table 4.2 The tune shifts and orbit deflections for the standard correction lattice.

Correction lattice.	$\Delta\nu_x$	$\Delta\nu_y$	$N_{unstable}$ (*)	$\Delta x'_{rms}$ (mrad)	$\Delta y'_{rms}$ (mrad)
No correction	0.01 ±0.01	---(*)	6	0	0
Standard lattice (A)	0.008 ±0.004	0.02 ±0.01	3	0.5±0.1	0.42 ±0.08
Locations of monitors and correctors reversed	0.005 ±0.003	0.01 ±0.01	1	0.8±0.2	0.40 ±0.06

(*) The betatron oscillations in the vertical plane were unstable for several error-configurations as a consequence of the tune shifts caused by the lattice imperfections. For errors which resulted in a high number of unstable runs $N_{unstable}$ the tune shifts in the vertical direction are not given.

4.2.2 The use of the dipoles and sextupoles as additional corrector magnets

The dipoles and sextupoles included in the main lattice of the ring can be used as corrector magnets with the generation of additional dipole fields. E.g. the dipoles can be used as horizontal corrector magnets if extra currents are injected in the coils around the poles; this way an additional correction field can be added to the common dipole-field. Additional dipole-fields can be generated in the sextupoles with the injection of currents in the coils around opposite poles (see chapter 5).

Using this idea, a second lattice *B* has been designed, in which all sextupoles and dipoles in the

ring serve as corrector magnets. With the use of as corrector magnets the total number of correctors and monitors can be increased without increasing the space occupied by the correction system.

The number of monitors in lattice *B* is increased with respect to the standard lattice, while the number of corrector magnets is the same. This is done, because an increase in the number of position monitors is expected to result in the largest reduction of the orbit distortion. There are no sextupoles or dipoles included in the long straight sections, therefore an additional corrector magnet is used in the middle of every long straight section. The extra monitors are inserted at the positions, which have been occupied by the corrector magnets in the standard lattice.

The total number of monitors in lattice *B* equals $M_{mon} = 36$; the number of horizontal correctors is equal to N_{corr} $(x) = 32$ and the number of vertical correctors N_{corr} $(y) = 20$. The number of horizontal and vertical correctors is different, because the dipoles can only be used as horizontal correctors.

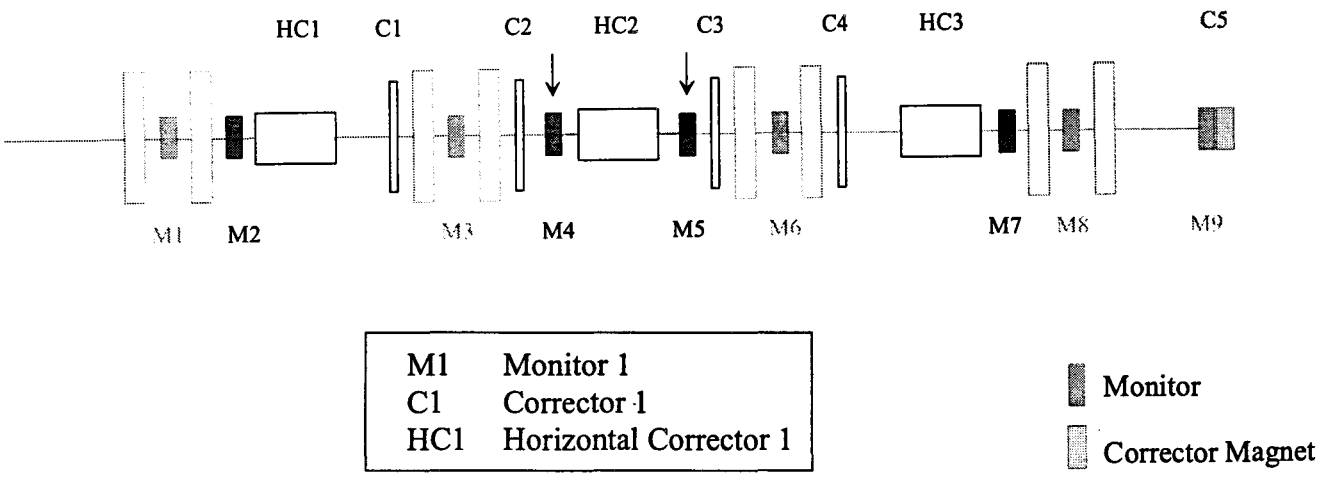

Fig. 4.4 *Schematic view of correction lattice B, in which both sextupoles and dipoles are used as corrector magnets.*

Simulations show that the horizontal distortion after correction (see table 4.3) is not further decreased with the use of all dipoles and sextupoles as additional horizontal correctors. On the contrary, the distortion after correction is larger than the distortion after correction with the standard lattice.

This is a consequence of the number of correctors, which is locally too large. Several monitors

in the lattice are placed directly in-between two corrector magnets (these are the monitors indicated in fig. 4.4). The readings in these monitors can always be minimised with a large deflection in the first corrector and a compensating large deflection in the second. Position and read errors of the monitors result in amplified distortions as a consequence of the large amplitude of the divergence, $\Delta x'$. The horizontal deflections in the lattice, with all sextupoles and dipoles used for the correction, are an order of magnitude larger than the horizontal deflections in the standard lattice, the maximum deflections are respectively $\Delta x'_{rms}$ = 15 mrad and $\Delta x'_{rms}$ = 1.2 mrad.

The correction system is significantly improved if the use one of the two correctors near the monitors is discarded. In fact the horizontal distortions after correction are 20% smaller than after correction with the standard lattice. The vertical distortions are nearly 40 % smaller. Furthermore the number of error-configurations in which the betatron oscillations were unstable is reduced to 1 out of 10 (for the standard lattice: 3 out of 10).

The use of the dipoles and sextupoles as additional corrector magnets can be considered an improvement for the closed orbit correction. Because the closed orbit distortions after correction are even smaller than after correction with the standard lattice, without occupying more space in the ring.

Table 4.3 The closed orbit distortions in the HBSB mode after correction with lattice B

Correction lattice.	x_{max} (mm)	x_{rms} (mm)	y_{max} (mm)	y_{rms} (mm)
Standard lattice, *A*	0.44±0.09	0.16±0.06	0.6±0.1	0.19±0.03
All dipoles and sextupoles used as additional correctors.	0.8±0.3	0.23±0.06	0.4±0.1	0.13±0.01
8 sextupoles and all dipoles used as additional correctors.	0.41±0.08	0.13±0.01	0.3±0.1	0.12±0.02

4.2.3 A correction system containing only sextupoles as additional correctors

Sextupoles, dipoles and additional magnets have been used as corrector magnets in the previous paragraph. Because a uniform correction lattice is desired, it is examined here if the use of the sextupoles as additional correctors is sufficient for the correction.

In lattice *C* differs all sextupoles are used as additional correctors; the only difference with the previous lattice B is that the dipoles are not used for the correction. The monitor locations are the same.

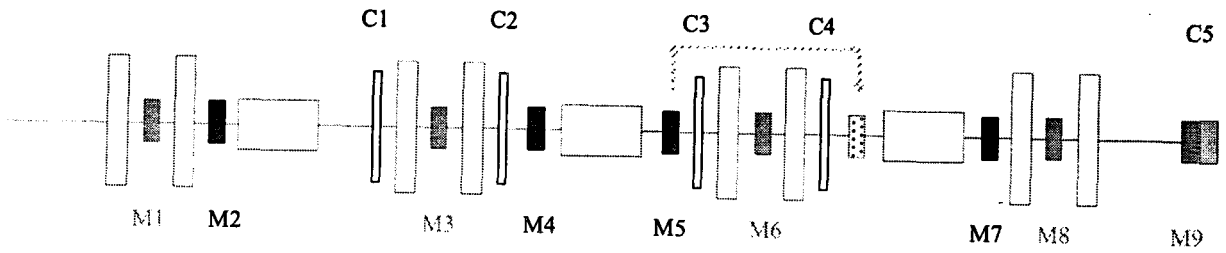

Fig. 4.5 *The representation of correction lattice C, in which only the sextupoles are used as additional correctors.*

Table 4.4 The closed orbit distortions in the HBSB mode after correction with lattice C

Correction lattice.	x_{max} (mm)	x_{rms} (mm)	y_{max} (mm)	y_{rms} (mm)
Standard lattice, *A*	0.44±0.09	0.16±0.06	0.6±0.1	0.19±0.03
Lattice *C*, all sextupoles used as additional correctors.	0.40±0.07	0.13±0.02	0.4±0.1	0.13±0.02
Four monitors relocated	0.4±0.2	0.15±0.02	0.5±0.1	0.15±0.05

With the relocating of one of the monitors the dependency of the correction on the monitor positions is examined. The new location of the monitor is given in fig. 4.7. The monitor is shifted from a place between defocusing elements to a place near defocusing elements. Therefore it might be expected that the correction is slightly improved.

However, due to the displacement of the monitor, the monitor near the central dipole is placed between two correction elements, with no strong focusing elements in between. This resulted in large deflections in the previous paragraph. Because the distance between the correctors is increased, the effects are smaller.

The closed orbit distortion after correction equals the distortion after correction with lattice B

(with the dipoles used as additional correctors) and is an improvement over the standard lattice. With the use of only sextupoles as additional correctors the number of correctors is smaller than lattice B; furthermore only two types of corrector magnets are used in lattice C (the dipoles are not used as additional horizontal correctors). Therefore the use of only the sextupoles as corrector magnets can be considered an improvement.

The closed orbit distortions in the HLF mode have after correction with lattice *C* approximately the same amplitude as the distortions in the HBSB mode: $x_{rms} = 0.13 \pm 0.03$ and $y_{rms} = 0.12 \pm 0.01$.

4.2.4 The influence of position and read errors in the monitors

In this paragraph the contribution of the monitor errors to the orbit distortion will be discussed. The horizontal distortion after correction with a lattice containing only perfectly aligned monitors will be compared with the distortion after correction with the same lattice, but with monitor errors.

Lattice *C*, treated in the previous paragraph, is used for the comparison. In figure 4.4 the closed orbit after correction is shown for a correction lattice with read errors and misalignments and the same correction lattice, but with ideal monitors, perfectly aligned. The closed orbit distortion is more than twice as small for the ideal correction lattice. For the lattice with monitor displacements and misalignments the rms-value of the closed orbit distortion is about equal to the rms-value of the monitor misalignments.

Table 4.5 The influence of the monitor read errors and misalignments on the horizontal distortion, mode HBSB.

Note	$x_{co\ rms}$ (mm)	$\Delta\nu_x$
Ideal lattice	0.06 ±0.02	0.007 ±0.005
Monitors displaced, $\sigma_x=\sigma_y$ =0.1 mm, no read errors	0.11 ±0.02	0.01 ±0.01
Monitors displaced, $\sigma_x=\sigma_y$ =0.1 mm + read errors, $\sigma_x=\sigma_y$ =0.1 mm	0.13 ±0.02	0.01 ±0.01

The closed orbit distortion after correction approximates the amplitude of the position and read errors of the monitors. In order to improve the correction these errors should be reduced.

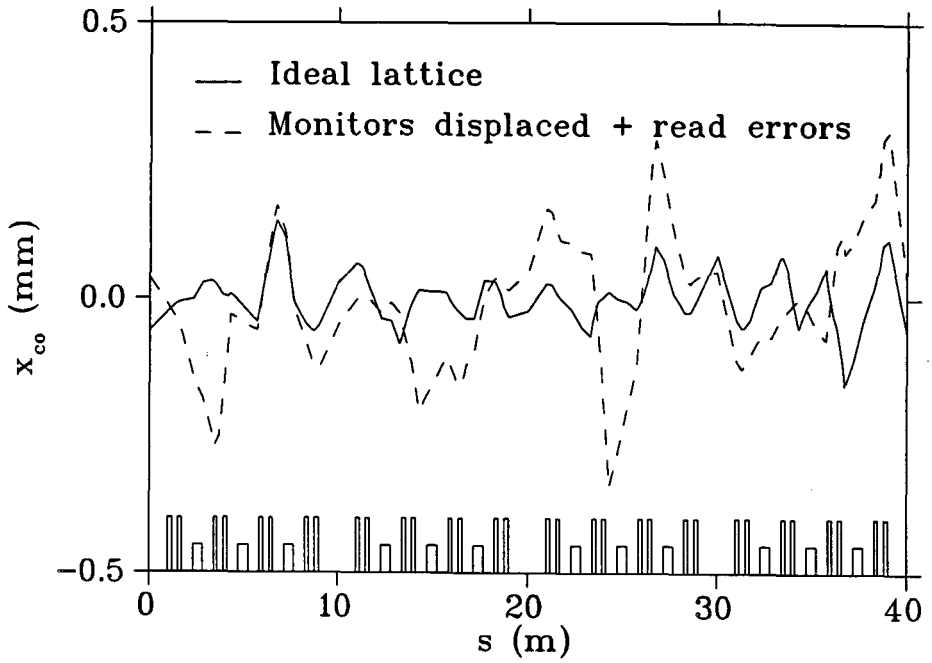

Fig. 4.6 The closed orbit after correction with lattice C; comparison of a perfect correction lattice and a lattice with misaligned monitors and read errors.

The closed orbit distortion after correction with an ideal lattice is equal to x_{rms} = 0.06±0.02 mm, which is smaller than the beam width near the dipoles (see table 1.2).

If the size of the distortion after correction is compared to the distortion due to dispersion, another impression of the size of the distortions is obtained. The momentum spread of the particles in a bunch results in a local increase in the beam width. This increase only depends on the dispersion function *D(s)* and is not a function of the distortion. A momentum spread of 0.04% is expected for the normal operation of the EUTERPE ring. The closed orbits of two particles with different momentum, $\Delta p/p$ = + 0.04% and $\Delta p/p$ = - 0.04%, are compared in fig. 4.7.

The figure shows that the increase of the beam width is of the same order as the closed orbit distortion after correction. This illustrates how small the amplitude of the distortion after

correction is.

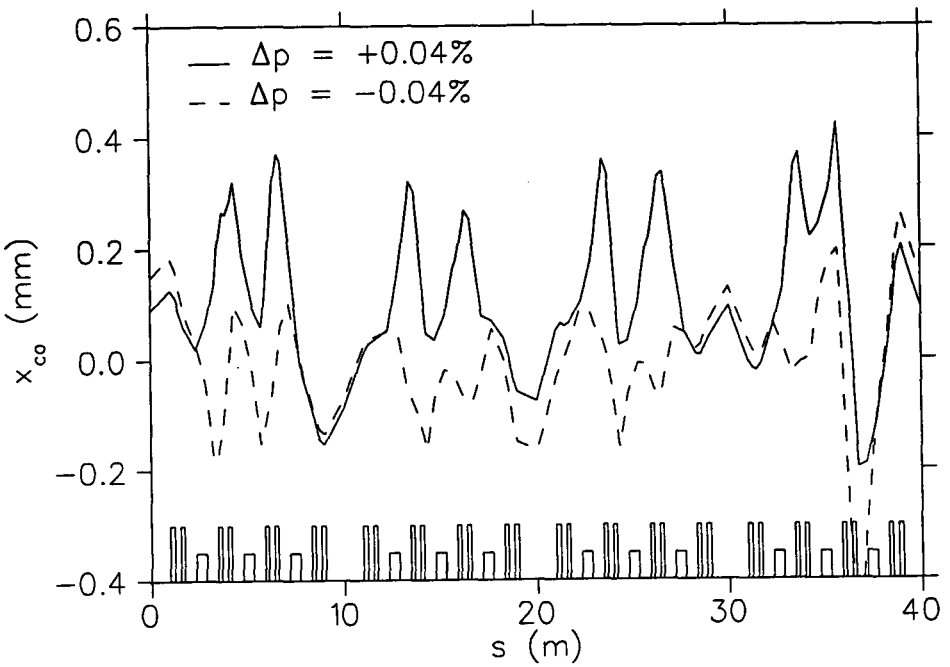

Fig. 4.7 *The closed orbits after correction for a particle with* $\Delta p/p = +0.04\%$ and $\Delta p/p = -0.04\%$

4.3 Reducing the number of monitors and corrector magnets

In the previous paragraph the possible reduction of the closed orbit distortions with the use of a correction system has been determined. However, the correction lattice with the largest reduction factor contained 50% more monitors than is necessary. With four monitors per betatron wavelength it should be possible to obtain a similar reduction (see §2.6). In this paragraph the total number of monitors and correctors and so the space occupied by the correction system is minimised. For this purpose several new correction lattices are compared.

With the standard lattice a reduction of the distortion with a factor 22 has been obtained. This lattice contains 20 monitors and 20 correctors. However, all these elements have to be added to main lattice of the ring. Less elements are necessary if the sextupoles are used as correctors without increasing the number of monitors, the occupied lattice space is reduced.

Simulations show that if only the sextupoles and 4 additional corrector magnets in the long

straight sections are used for the correction, the quality of the correction system is significantly reduced. The resulting closed orbit distortions are x_{rms} = 0.35 ± 0.07 mm and y = 0.35±0.07mm. An example of the closed orbit after correction is shown in fig. 4.5. The correction is deteriorated, because the distance between the corrector in the middle of the long straight section and the next corrector is too large. Correction lattices in which the monitor locations have been adjusted, but with the same corrector configuration, have been simulated and resulted in the same (large) distortions after correction.

The distance between successive correctors is reduced in the second lattice with an extra corrector magnet in front of the first and after the third dipole of a superperiod. The number of corrector magnets used remains constant, while the nearest sextupoles are not used for the correction. The reduction of the distortions is significantly improved as is shown in table 4.6.

However, the lattice two has to be adjusted if the monitors and correctors in the middle of the long straight section have to be removed for the insertion of the special devices in these sections. If the monitor and corrector in the long straight section are removed and no extra monitors are inserted for compensation the distortion will increase. The influence of the removal of these monitors and correctors has been measured for the correction lattice *C* in the previous paragraph and resulted in a 40 % increase of the distortion, see appendix C.

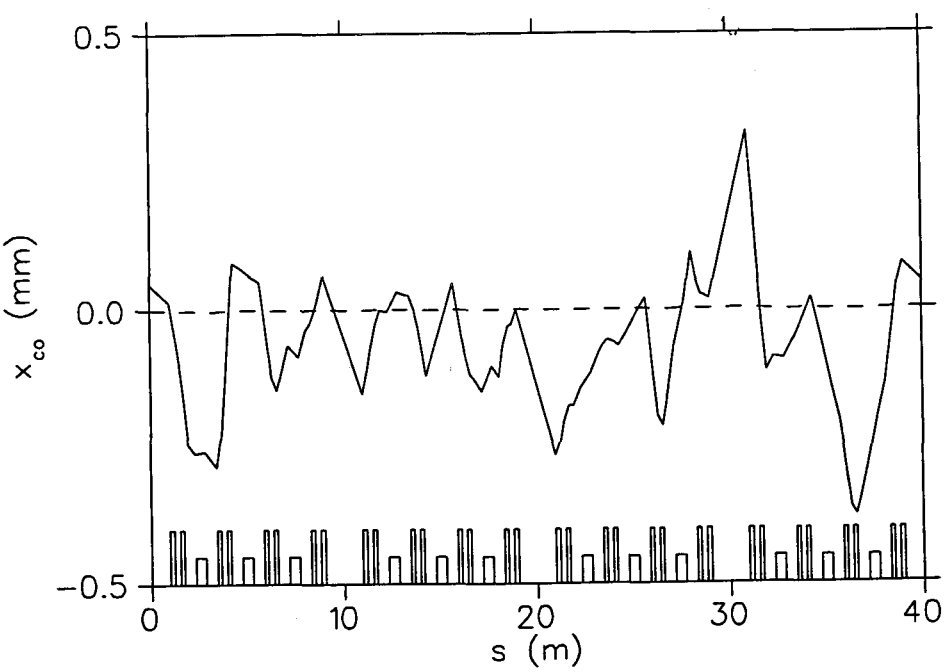

Fig. 4.8 *The closed orbit distortion after correction with the final lattice, containing 24 monitors and 24 correctors.*

Table 4.6 *The closed orbit distortions after correction with the correction systems with a reduced number of monitors and correctors.*

Correctors	x_{max} (mm)	x_{rms} (mm)	y_{max} (mm)	y_{rms} (mm)
16 sextupoles + 4 additional correctors	1.3 ± 0.4	0.35 ± 0.07	0.61 ± 0.07	0.22 ± 0.02
8 sextupoles + 12 additional correctors	0.4 ± 0.1	0.15 ± 0.02	0.49 ± 0.08	0.17 ± 0.03
8 sextupoles + 16 additional correctors	0.38 ± 0.08	0.14 ± 0.02	0.42 ± 0.08	0.16 ± 0.02

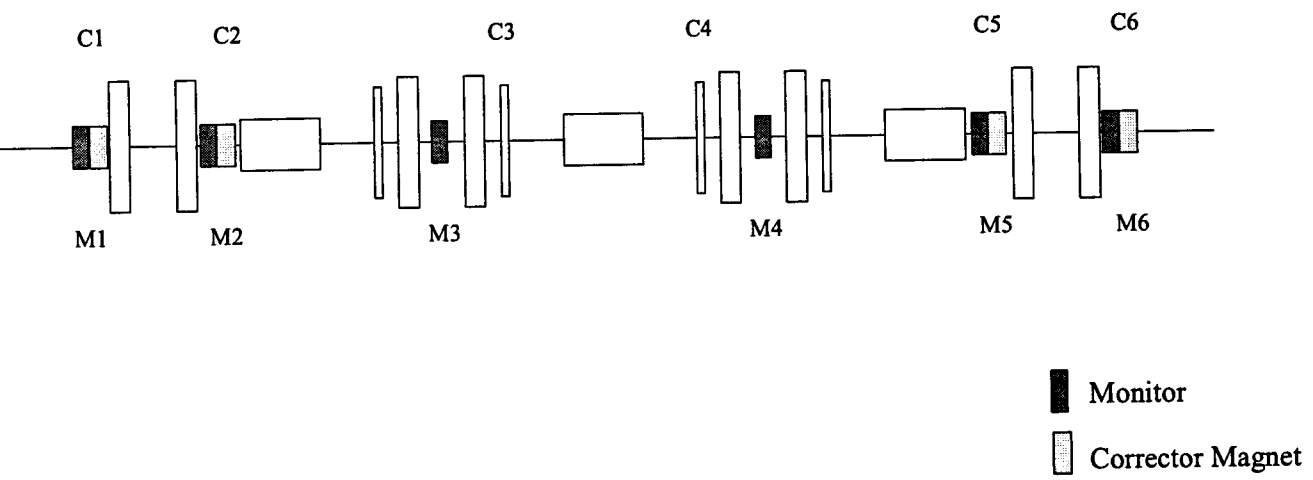

Fig . 4.9 *The lattice of the final correction system, with 24 monitors and 24 corrector magnets*

In the final lattice (*D*) two monitors and correctors are placed on both sides of the long straight sections, next to the quadrupoles, for compensation. This way the space available for the

insertion of the special devices is only slightly reduced. As a consequence of the two monitors on each side of the long straight sections with no focusing or defocusing elements in between, the distortion in these sections is extra reduced. The rms values of the distortions in the whole ring are reduced as well, to x_{rms} = 0.14±0.02 mm and y_{rms} = 0.16±0.02 mm. The number of error-configurations in which the betatron oscillations were unstable is reduced to 1 out of 10. These values approximate the values for the best lattice in the previous paragraph with 36 monitors.

So indeed a reduction of the number of elements in the correction system is possible without a significant loss of the correction quality.

4.4 Summary

A closed orbit correction system has been designed for the EUTERPE ring. Several correction systems have been compared. For all lattices, the closed orbit distortions and tunes after the correction have been determined for ten different error-configurations using the program MAD. The corrector settings are calculated with the MICADO method.

First different correction systems have been compared in which the space occupied by the correction system is kept constant. A standard correction lattice has been composed with monitors in-between the quadrupoles in a doublet and an extra monitor in the long straight section. Furthermore 20 corrector magnets are used. With the standard lattice, the closed orbit distortion is already reduced with a factor 22 in the vertical and a factor 5 in the vertical direction (see table 4.7).

However, the correction system is further improved if more beam position monitors are used. With the use of the sextupoles and dipoles as corrector magnets, the number of monitors can be increased without occupying more lattice space. As a result the distortion is reduced with 20 % in the horizontal and 40% in the vertical direction. In this lattice only 8 sextupoles are used for the correction. Otherwise monitors are placed directly between corrector magnets, which results in large beam deflections in both magnets and as a consequence in large distortions.

If only the sextupoles are used as corrector magnets (plus four additional correctors in the long straight sections) the same correction quality can be achieved. The complexity of the correction system is reduced, because only two instead of three different type of magnets are

straight sections) the same correction quality can be achieved. The complexity of the correction system is reduced, because only two instead of three different type of magnets are used for the correction.

Table 4.7 Summarised results of the correction systems discussed in this chapter.

Lattice	$N_{mon.}$	$N_{corr.}$	x_{rms} (mm)	y_{rms} (mm)	Note
A	20	20	0.16 ± 0.06	0.19 ± 0.03	Standard lattice
B	36	32	0.13 ± 0.01	0.12 ± 0.02	Both the sextupoles (8) and dipoles are used as additional correctors
C	36	20	0.13 ± 0.02	0.13 ± 0.02	All sextupoles (16) are used as additional correctors, no dipoles used.
D	24	24	0.14 ± 0.02	0.16 ± 0.02	Final Lattice Minimisation of the total number of elements and of the space occupied by the correction system.

The number of monitors and corrector magnets has been reduced in the final correction lattice. This lattice contains 24 monitors and 24 corrector magnets, which corresponds to 4 monitors and correctors per betatron wavelength. These are required for the full establishment of the amplitude and phase of the distortion.

The closed orbit after correction is limited by the displacements and read errors of the monitors. Without monitor misalignments and read errors the closed orbit in both the horizontal and vertical plane are further reduced with a factor 2.

Chapter 5

Hardware regarding the closed orbit correction system

The closed orbit correction system contains several corrector magnets and beam position monitors. The design of the sextupoles, which will be used as corrector magnets, is discussed in §5.2, the design of the window-frame corrector magnets in §5.3. Furthermore a brief study of the beam position monitors is represented in §5.4 followed by a summary of the results in §5.5. But first the basic principles used for the magnet design are discussed in §5.1.

5.1 Introduction

The magnetic fields in the magnets will be induced with currents through the coils around the magnet-poles. The current required for a certain induction is found using Ampere's law:

$$\oint H.dl = N.I. \tag{5.1}$$

In this formula $N.I$ is the total current through all the windings in the coil and H is the magnetic field strength. The magnetic field is given by $H = B/\mu_o\mu_r$; with μ_r the relative magnetic permeability.

The effect that a magnet has on the particle trajectory depends completely on the integrated field strengths. E.g. the deflection of the electron beam depends on the field integral $\int B.dl$, and the chromaticity in a sextupole depends on the integrated sextupole strength $\int k_2\, dl$. Based on the requirements on the deflection or chromaticity, the required induction can be calculated if the effective length of the magnet is known.

The effective length of a magnet is defined as:

$$L_{eff} = \frac{\int B.dl}{B_{max}}. \qquad (5.2)$$

The field lines outside the magnet yoke (the fringe fields) give an extra contribution to the field integral. As a consequence the effective length of a magnet is larger than its mechanical length. The effective lengths in a dipole and quadrupole are [Mut95].

$$L_{eff} = L_{yoke} + k.R, \qquad \begin{array}{ll} with & k \approx 2.4 \text{ for a dipole} \\ and & 0.9 < k < 1.1 \text{ for a quadrupole.} \end{array}$$

In this formula L_{yoke} is the length and R the aperture radius of the magnet; k is a constant dependent on the magnet design. The effective length for quadrupole fields is more than twice as small as the effective length for dipole fields.

This decrease in effective length is a consequence of the proportionality of the induction B to the distance w.r.t. the magnetic axis r. Because the induction in a sextupole is proportional to $B \sim r^2$, its effective length will be further decreased. The size of the effective length for a sextupole has not been found in literature, and must therefore be measured for the prototype EUTERPE-sextupole.

In order to estimate the quality of the magnetic field in the designed magnets; the magnetic fields in the magnets will be described as the summation over the multipole components.

$$B = \sum_n \frac{k_n}{n!} r^n. \qquad (5.3)$$

with k_n the harmonic components; e.g. k_0 is the dipole coefficient. In an ideal dipole, no multipole fields are present and all values of k_n with $n \neq 0$ are equal to zero. The description of the error fields in their harmonic components is called harmonic analysis.

5.2 Design of the sextupoles

The sextupoles in the EUTERPE-ring have been designed to generate both sextupole and dipole corrector fields. The sextupole field is produced by sending equal currents through all coils; the direction of the currents through the coils around successive poles is reversed. The

horizontal and vertical corrector fields are generated with additional currents through the coils around opposite poles.

The design of the sextupoles is discussed in this paragraph. The requirements on the sextupoles are determined and listed in § 5.2.1. According to these requirements a prototype sextupole has been designed; the design is discussed in §5.2.2. The field profile in this sextupole has been determined with simulations in the software-packet POISSON; the calculated field profiles are shown in § 5.2.3.

5.2.1 Requirements on the EUTERPE sextupoles

The sextupoles in the EUTERPE ring have to satisfy both mechanical conditions and requirements on the field profiles. These requirements are treated separately below.

The dimensions of the sextupoles are limited by the size of the vacuum chamber and by the space available in the lattice. The aperture of the sextupoles must be several millimetres larger than the size of the vacuum chamber (d = 48 mm). This safety margin required for the positioning of the sextupoles is the equal to the margin required for the positioning of the quadrupoles (3mm).

Unlike the quadrupoles the sextupoles can not pass the ends of the vacuum chamber and have to be assembled around the vacuum chamber. As a consequence the sextupoles must be divisible into two parts.

The length of the sextupoles is limited by the space between the bellows and quadrupoles in between which the sextupoles are placed. The available lattice space is ca 150 mm. In order to avoid excessive synchrotron radiation hitting the sextupoles, the total diameter of the sextupoles must remain smaller than 270 mm.

All mechanical requirements are listed in table 5.1.

Table 5.1 The requirements on the geometry of the sextupoles

Requirement	Cause
$d > 48$ mm	This is the diameter of the vacuum chamber.
$l_{mech} \leq 150$ mm (*)	This is the space reserved for the insertion of the sextupoles.
$d_{total} \leq 270$ mm (**)	To avoid blocking of the synchrotron radiation.
The mantle must be constructed out of two parts	The sextupoles have to be constructed around the vacuum chamber.

(*) l_{mech} is the total mechanical length of the sextupole including the coils.
(**) d_{total} is the outer diameter of the sextupole

The field profiles in the sextupoles have to satisfy certain conditions too. The most important parameter in the sextupoles is the sextupole strength integrated over the electron trajectory

$$\int k_2 \, ds = \int B\rho \, k_2' \, ds = \int \frac{1}{2} \left(\frac{\partial^2 B}{\partial r^2} \right) ds, \qquad (5.4)$$

k_2' is the sextupole strength normalised with respect to $B\rho$, which is a measure for the momentum of the electrons; Bρ=1.33 for the 400 MeV electrons in the EUTERPE ring. The normalised sextupole strength is mentioned, because it is used in MAD. The maximum value of the integrated sextupole strength is $\int k_2 \, ds = 28$ Tm^{-1}, for S1 in the HBSB mode. The required sextupole coefficient (k_2) still depends on the effective length of the sextupole.

The required field integral for the correction ($\int k_0.ds$) is calculated with eq. (2.22)

$$\Delta u' = \frac{\int B.ds}{B\rho}, \qquad with \; u = x, \; y.$$

The maximum deflection in the corrector magnets is $\Delta u'$=1.5 mrad, which gives for the required field integral $\int k_0.ds = 2.10^{-3}$.

During the acceleration of the electrons the strengths of the sextupole fields have to increase proportional to the electron energy. The time constant of the inductance in the coils, has to be smaller than the time required for the acceleration of the electrons from 75 to 400 MeV, which

is ca 3 seconds.

Table 5.2 The requirements on the induction in the sextupoles

Requirement	Reason
$\int k_2.ds \geq 75$ T/m	This equals the required integrated sextupole-strength for S1 (HBSB mode).
$\int k_0.ds \geq 2.10^{-3}$ Tm	The field integral required for a 1.5 mrad deflection of 400 MeV electrons
τ (inductance) < 3 seconds	The sextupole strength is increased proportionally to the electron energy
$\Delta k_2/k_2 \leq 5$ % for $r \leq 10$mm	The relative field error in the beam domain has to be smaller than 5 %

Other aspects taken into account in the design of the sextupoles are construction costs and the power required during operation.

- The construction costs will be minimised by keeping the mechanical design as simple as possible. E.g. a prototype sextupole has been constructed out of solid iron instead of the laminated iron which is used for the quadrupoles and dipoles and which is more difficult to manufacture.

- Furthermore the total size of the sextupole is minimised in order to reserve as much space in the EUTERPE lattice as possible.

5.2.2 The prototype sextupole

Based on the requirements in the previous paragraph a prototype sextupole is designed. The geometry of the sextupole is determined in §5.2.2.1. With the use of 'Poisson' the field profiles in the sextupole are calculated. The generated sextupole field is shown in §5.2.2.3; the corrector fields in §5.2.2.3. The specifications of the coils are given in §5.2.2.3. Finally the field profile in a sextupole in full operation - with additional horizontal and vertical correction - is discussed.

5.2.2.1 The geometry of the sextupole

The geometry of the sextupole depends on the requirements listed in table 5.1. The prototype sextupole is shown in fig. 5.1. It has an aperture diameter of 51mm, which equals the aperture radius of the quadrupoles. The mechanical length of the sextupole is 75 mm. Due to the fringe fields the effective length of the sextupole is estimated to increased $L_{eff} \approx 85 \pm 10$mm, which results in a required sextupole strength of $k_2 \approx 880$ Tm^{-2}. The effective length of the sextupoles has a large uncertainty, because the value has not been found in literature.

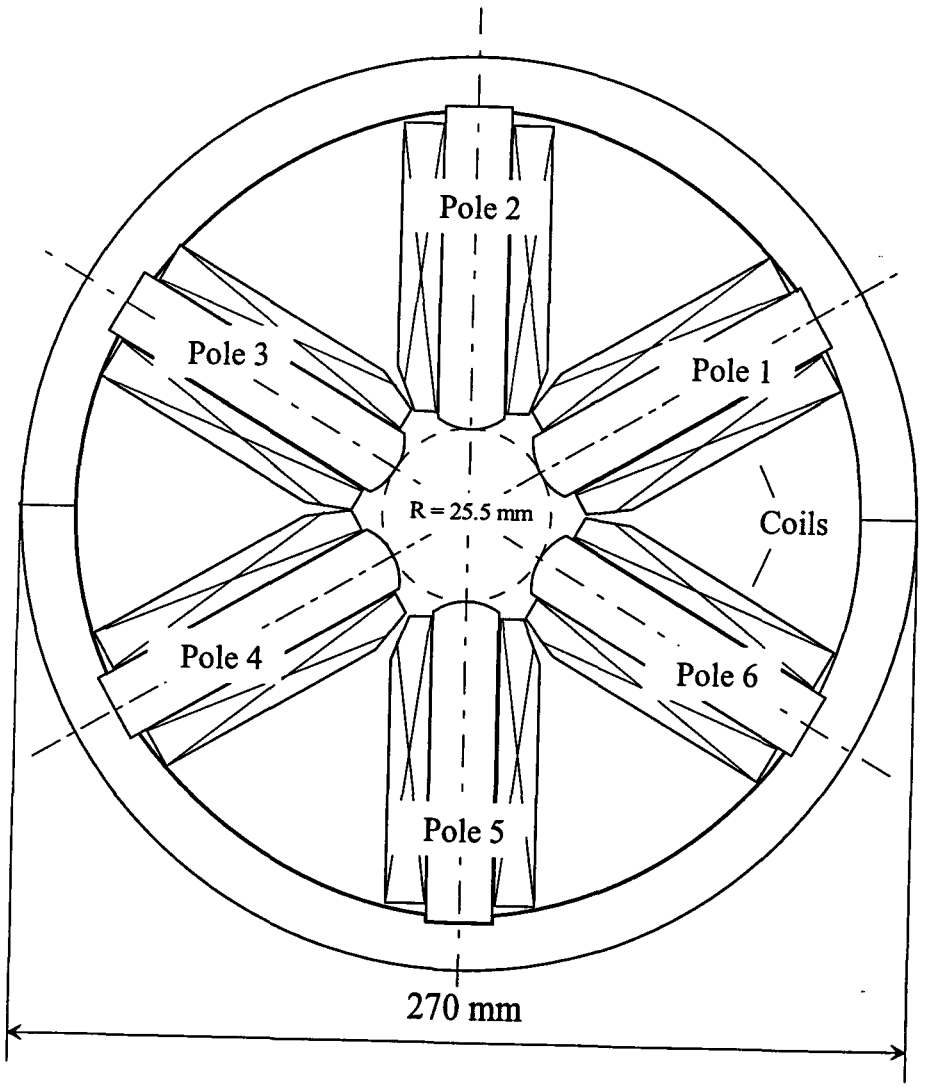

Fig.5.1 The prototype sextupole for the EUTERPE ring

The pole-width of the sextupoles is 20 mm. Due to this finite width of the poles error-fields are introduced. These errors depend on the aperture radius and the pole-width. The relative error in the EUTERPE sextupole with an aperture radius equal to 25.5 mm is less than 2 % in the region with radius r = 10mm around the magnetic axis [Mon85]. These field-errors are several times smaller than the required accuracy.

The ideal pole shape is described by a equipotential surface, due to the fact that the magnetic field is directed perpendicularly to the pole surface. These surfaces are found with the poisson equation derived in appendix F. The ideal pole shape of a sextupole satisfies

$$x^3 + 3xy^2 = R^3. \qquad (5.5)$$

R is the distance between the pole and the magnet axis, which is equal to R=25.5 mm for the EUTERPE sextupole. The ideal pole-shape is approximated by a circle with a radius ρ=17.2 mm, which makes the poles easier to manufacture. The difference between the ideal pole surface and the circle approximation is at every position less than 0.013 mm and can be neglected.

5.2.2.2 The generation of the sextupole field

The sextupole field is generated with currents through all coils. Using Ampere's law, and with $B=1/2.k_2 r^2$ the total required current can be calculated

$$(NI)_{sextupole} = \int_0^R \frac{B}{\mu_0}.dl = \frac{k_2 R^3}{6\mu_0} \approx 1935\ A.turns.$$

The total current NI = 1935 A.turns corresponds to a prototype sextupole with an effective length of L_{eff}=85 mm.

This value is verified with simulations in the program POISSON (see appendix F). With the program the induction in the sextupole is determined as a function of the current through the coils. In Poisson the induction is calculated with the Poisson equation [Poi91]. Only field profiles in planes in which the magnetic induction is symmetric can be calculated.

The field profile in the middle of the sextupole perpendicular to the particle trajectory is shown in fig. 5.2.

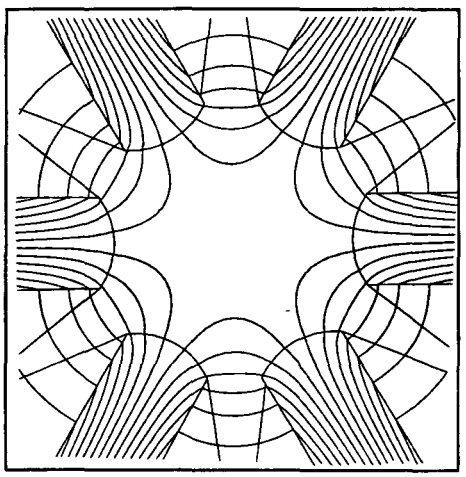

Fig. 5.2 The generated sextupole field

Table 5.3 Harmonic components of the generated field shown in fig. 5.2.

k_0	1 G
k_1	0.1 G/cm
$k_2/(2!)$	440 G/cm^2
$k_3/(3!)$	-0.1 G/cm^3
$k_8/(8!)$	0.04 G/cm^8

with $B = \sum \frac{k_n}{n!} r^n$.

The required sextupole field k_2 = 880 T/m^2 (=880 G/cm^2) is generated with a total current $NI \approx 2040$ A.turns; this is about 5 % larger than the value calculated with Ampere's law above. The extra number of Ampere.turns necessary for the generation of the sextupole field is a consequence of the contribution of the higher order field components to the field integral. In the region of interest, the relative contributions of the higher order field components to the induction are small with respect to the sextupole field (see harmonic components in table 5.3). Even the dodecapole component (k_8), which is a result of the finite pole width, is negligible. Within a radius of 10 mm around the magnetic axis the induction differs less than 3 % in comparison to the induction of an ideal sextupole.

The field components are calculated above in the case of an ideal sextupole. Due to pole misalignments the field profile could be distorted. The distortion of the field profile is expected to be largest if the poles are displaced in the radial direction. In table 5.4 the effect on the harmonic components is shown of the displacement of one pole in the radial direction.

Table 5.4 The effects of the displacement of pole 2 on the field profile.

Displacement	k_0 (G)	k_1 (G/cm)	$k_2/(4!)$ (G/cm^2)	$k_8/(8!)$ (G/cm^8)	$(\Delta k_2/k_2)_{max}$ $r \leq$ 10mm
dy=0.2mm	7	-3	438	0.003	< 1%
dy=1.0mm	30	18	396	3	< 3%

The induction in a sextupole with a pole 1 mm displaced still satisfies the condition that the relative error in the sextupole coefficient is less than 5 %. However the generated dipole and quadrupole fields are large. A field error equal to B = 30 G results in a 0.3mrad deflection, which is not acceptable. In principle the field errors can be corrected with additional currents through the coils, but this is not desirable. With with these currents the uniformity of the sextupoles is broken. If the displacements of the poles remain smaller than Δy = 0.1 mm both the dipole and quadrupole fields are negligible.

As a consequence of the manufacturing technique used for the production of the prototype sextupole all displacement errors and surface errors are reduced to less than 0.05 mm.

5.2.3 Generation of the dipole fields in the sextupole

The sextupoles will be used as both horizontal and vertical correctors. For the correction it is necessary to induce dipole fields in the sextupoles. In this paragraph the generation of the dipole fields in the sextupole is discussed.

The corrector magnets have to be able to deflect the electron with $\Delta u'$ = 1.5 mrad. The effective length of the sextupole used as corrector magnet becomes:

$$L_{eff} \approx L_{yoke} + 2.4\ R = 136\ mm,$$

with R the aperture radius (R=25.5 mm) and $L_{mechanical}$ the pole length (75mm). The field integral needed for the correction are equal to $\int k_0.dl = 2.10^{-3}$, as a consequence the strength of the dipole field in the sextupole must be at least $k_0 \approx 150$G.

The sextupole is used as a horizontal corrector with the generation vertical dipole-field; this dipole-field can be produced if currents are injected through the coils around pole 2 and 5. The field generated with a total current NI=340 A.turns through the coils around these poles is shown in figure 5.4a. In the region of interest a dipole field is generated. The field deteriorates quickly if the distance to the magnet axis is increased; the maximum values of the relative field error ($\Delta B_y/B_y$) and the coupling coefficient (B_x/B_y) are about 25 % within a radius of 10 mm around the magnetic axis, see table 5.5. The sextupole component of the generated field is the main component of the error field.

The homogeneity of the field is increased if additional currents are sent through the coils around pole 1, 3, 4 and 6. Simulations show that the homogeneity of the induction is best if the current through these coils is 50% of the current through coil 2 and 5. The maximum values of the coupling coefficient (B_x/B_y) and the relative field error ($\Delta B_y/B_y$) are reduced to less than 2 % within the region of interest, see table 5.5. The sextupole coefficient in the induction has vanished. With the insertion of additional currents through the coils around pole 1, 3, 4 and 6 the field strength around the magnet axis is ca 50 % increased to B=150G.

The currents needed for the generation of an induction B=150 G can be compared to the required currents calculated with Ampere's law for a dipole with an aperture radius R=25.5 mm: NI =305 A.turns. The extra currents required in the sextupole are a consequence of the divergence of the field in the area around the magnet axis.

Table 5.5 Harmonic components of the generated vertical dipole field

Currents	$(\Delta B_x/B_y)_{max}$ r<10mm	$(\Delta B_y/B_y)_{max}$ r < 10 mm	k_o [G]	k_1 [G/cm]	k_2 /2! [G/cm^2]	k_4 /4! [G/cm^4]
I_1 = 360 A.turns[1] I_2 = 0 [2]	25 %	25 %	101	-1.10^{-2}	26	2
I_1 = 360 A.turns I_2 = 180 A.turns	0.6 %	1.5 %	152	-4.10^{-3}	2.10^{-2}	3

[1] I_1 is the current through the coils around pole 2 and 5

[2] I_2 is the current through the coils around pole 1, 3, 4 and 6.

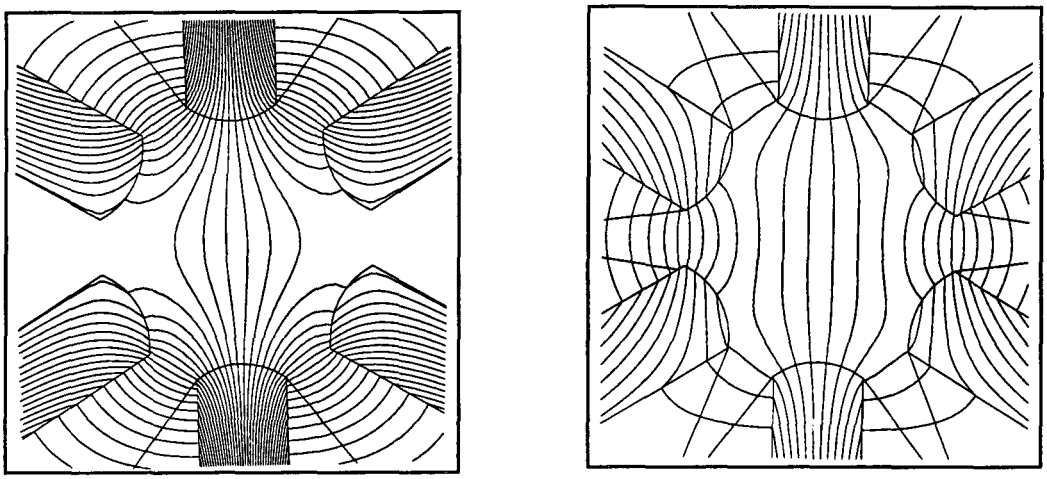

Fig. 5.3 *The sextupole used as a horizontal corrector; fig. a) with currents through the coils around pole 2 and 5 (I_1=500 A.turns) and fig. b) with currents through all coils (I_1 = 500 A.turns, I_2 =250 A.turns).*

With the generation of a vertical dipole field the sextupole can be used as a horizontal corrector. The maximum required field strength is k_0 = 150 G. A dipole field with this strength is produced if a total current I=310 A.turns is injected in each of the coils around pole 1, 3, 4 and 5. Due to the pole symmetry the error fields are very small. The maximum values of B_y/B_x and $\Delta B_x/B_x$ are less than 2 % in the region of interest. A further reduction of the error fields with the use of additional currents through the coils around pole 2 and 5 is not necessary.

Table 5.6 The generation of the horizontal dipole field

Current	$(\Delta B_x/B_x)_{max}$ $r < 10$mm	$(B_y/B_x)_{max}$ $r < 10$mm	k_o [G]	k_1 [G/cm]	k_2 [G/cm^2]	k_4 [G/cm^4]
I = 310 A.turns	1.6 %	0.6 %	150	1.10^{-3}	3.10^{-2}	3

The decapole-component of the magnetic field is comparatively strong. However, the contribution of the decapole-component to the total induction is still very small.

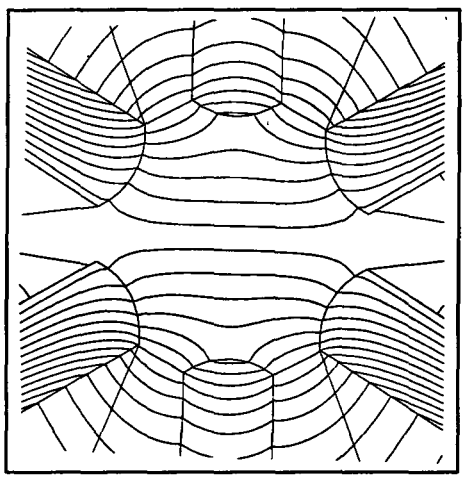

Fig. 5.4 The generated correctorfield in the horizontal direction

5.2.4 Coil specifications

With the currents required for the generation of the different fields known, the specifications of the coils around the poles can be determined.

The total current through the coils must be sufficient for the generation of the maximum sextupole and corrector fields. The maximum current required for the generation of the corrector fields is *NI*=480 turns through coil 1, 3, 4 or 6 in the case of 1.5 mrad deflection of the beam in both directions. The current through coil 2 and 5 never exceeds *NI*=360 A.turns. For reasons of uniformity all coils will be equal.

The coil around each pole will be divided in two parts: one part for the generation of the sextupole field (*NI*=2040A.turns), the other for the generation of both corrector fields (*NI*=480A.turns). In practice these two coils are set in serie, which reduces the number of power supplies.

The currents through the coils around opposite poles are always equal, even if additional corrector fields are generated (see appendix D). The coils around opposite poles are therefore connected, which reduces the number of power supplies per sextupole to 3.

The wires used for the coils have a maximum current *I*=7A, which is the maximum current provided by the original power supplies. The conductive area in the wire is 2.5 x 1.5 mm^2. The

specifications of the coils are summarised in table 5.7.

Table 5.7 Specifications of the coils around the poles of the sextupoles.

Parameter	Size
Maximum current	$I_{max} = 7$ A
Conductive area per winding	$A = 2.5 \times 1.5$ mm^2
Number of turns inserted for the generation of the: - sextupole field - corrector fields Total number of turns	 $N_s = 272$ turns $N_c = 100$ turns $N_{tot} = 372$ turns
Maximum current for the generation of the - sextupole field - corrector fields Total current	 $(Ni_{sextupole})_{max} = 1905$ A.turns $(Ni_{corr})_{max} = 700$ A.turns $(Ni_{tot})_{max} = 2604$ A.turns.
Total size per coil	Thickness: 25 mm Length: 85 mm (in radial direction) Total length: 126 mm (along s-axis)
Time constant for the generation of the sextupole field	$\tau \approx 0.1$ s *

*The time constant of the inductance is calculated in appendix D.

The total number of turns is sufficient for the generation of the fields. The division of the turns has to be adjusted to N_s =302 and N_c= 70.

The coils in the sextupole are winded so that they increase the total length of the sextupoles as little as possible. The coils are therefore not winded in a triangular form, but the top of the coils is flattened. The total length of the sextupoles becomes L_{tot} = 126 mm (see appendix D)

5.2.4 Field profile in a sextupole in full operation

The field profile in a sextupole used both as a horizontal and vertical corrector with maximum correction settings is shown in fig. 5.6. The resulting field profile is just a superposition of the

elementary fields, shown in fig. 5.6b. The harmonic analysis of the field shows that the error-fields are very small. The main contribution to the error field comes from the decapole field, which is introduced with the generation of the correction fields. The decapole component is too small to have a significant effect on the closed orbit.

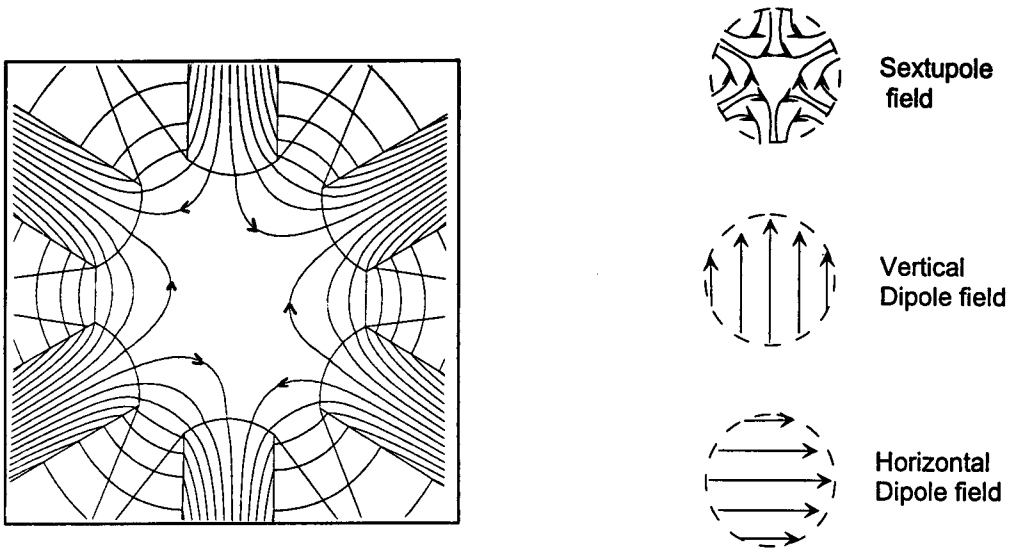

a) field profile in the xy-plane *b) Principle harmonic fields*

Fig. 5.5 The sextupole in full operation, with maximum sextupole and horizontal and vertical dipole strength. The currents through the coils are according to table 5.8.

Table 5.8 The harmonic components in the sextupole with additional hor. and vert. corrector fields.

Currents	B_{ox} [G]	B_{ox} [G]	k_1 [G/cm]	k_2 [G/cm^2]	k_4 [G/cm^8]	k_8 [G/cm^8]
I_{1+4} = 2530 A.turns (*) I_{2+5} = 1680 A.turns I_{3+6} = 1910 A.turns	152	150	0.7	440	4	0.04

(*) The currents through the coils around opposite poles are equal. I_{1+4} is the current through the coils around pole 1 and 4; I_{2+5} the current through the coils around pole 2 and 5 and I_{+6} the current through the coils around pole 3 and 6.

In order to get an impression of the field strengths, the induction is depicted as a function of

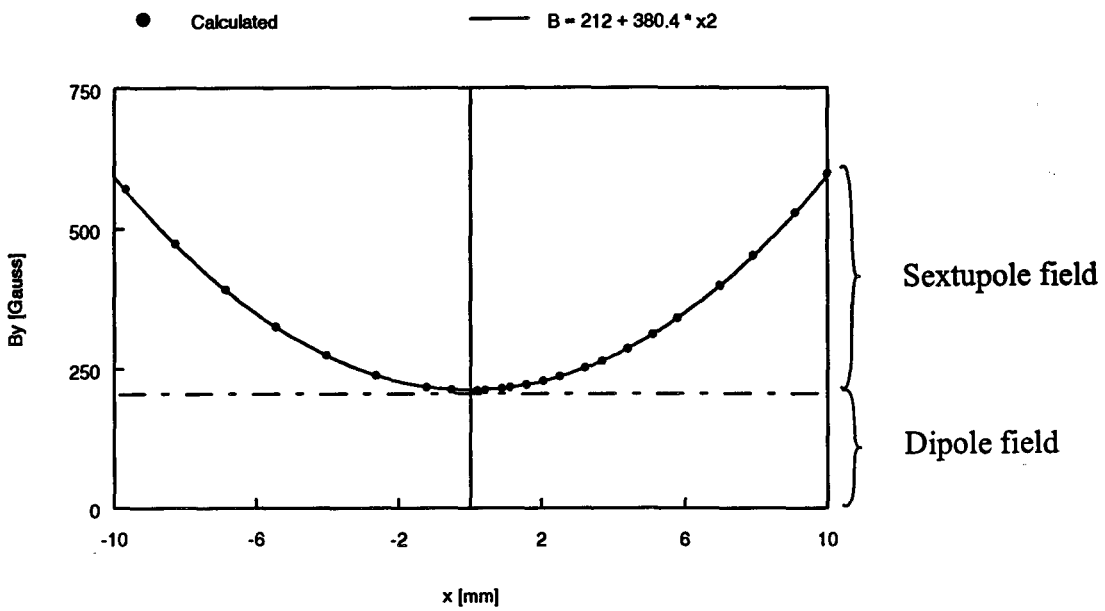

Fig. 5.6 *The induction along the x-axis in the sextupole calculated with Poisson compared to the superposition of an ideal sextupole and dipole field.*

the horizontal position x in fig. 5.7. The figure shows that the approximation of the induction by a superposition of a dipole and a sextupole field is almost perfect. All contributions from higher order fields are negligible, which is expressed in the low values of the harmonic components in table 5.8. There is no danger of saturation of the magnetic field. The maximum induction in air is $B = 0.6$ T near the pole-edge. Within the yoke the flux density is increased; the maximimum induction is $B \approx 1.2$ T, for which there is still no saturation.

5.3 The window frame corrector magnets

The number of sextupoles used as corrector magnets is not sufficient to correct the closed orbit. The closed orbit distortion is further reduced if corrector magnets are inserted between the superperiods. Therefore corrector magnets have been designed. In order to use as little space as possible, the corrector has to deflect the beam in both the horizontal and vertical direction.

In this paragraph the design of a prototype corrector magnet is discussed. The requirements on the corrector magnet are already discussed in §5.2. The design of the prototype corrector

magnet is given in §5.3.1. The field profiles calculated in Poisson are shown in §5.3.2. A prototype corrector magnet has been constructed at the central workshop of the TUE; the measured induction is compared with the field profiles calculated in Poisson.

5.3.1 The design of the window frame corrector magnet

The corrector magnets are of the so called window frame type. The yoke of the magnet has the shape of a window-frame, see fig. 5.8. The window frame shape has the main advantage that perfect dipole fields can be generated in two directions, which is impossible with the conventional dipoles. Furthermore the construction is very simple and easy to manufacture.

The maximum deflections of the electron beam in the window frame magnets are equal to the maximum deflections in the sextupoles, $\Delta x'_{max} = \Delta y'_{max} = 1.5$ mrad. This corresponds to a field integral $\int B.dl = 2.10^{-3}$ Tm. The length of the magnets is a compromise between the length of and the field strength in the magnet. A increase in the required field strength also results in an increase in the coil size and the aperture diameter. The final length of the magnet is $l = 0.05$m and the aperture diameter is d=0.08m.

The large aperture diameter in comparison to the magnet length results in a large extension of the field along the magnet axis.

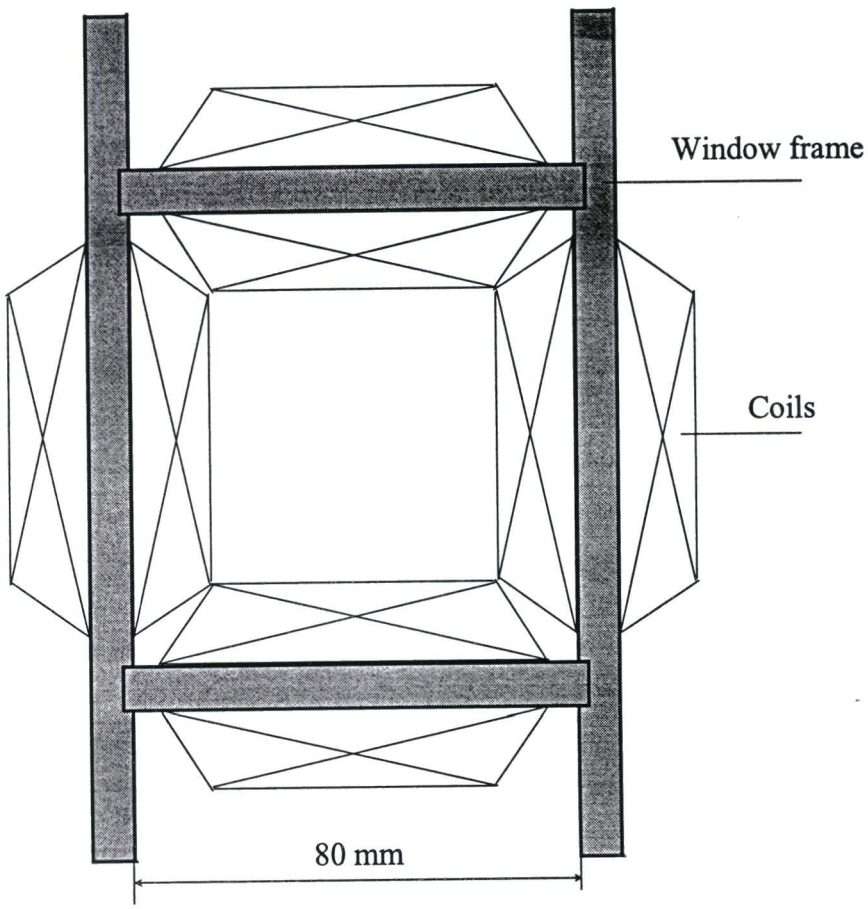

Fig. 5.7 The window frame corrector magnet

5.3.1.2 Field profiles calculated with Poisson

With simulations in Poisson the induction in the window-frame magnets is determined. Firstly the magnetic field profile is calculated in the xy-plane in the middle of the corrector. Secondly the induction in the sy-plane - the induction along the magnetic axis - is determined.

In the horizontal and vertical direction the uniformity of the induction is almost perfect, which is illustrated in fig. 5.8.

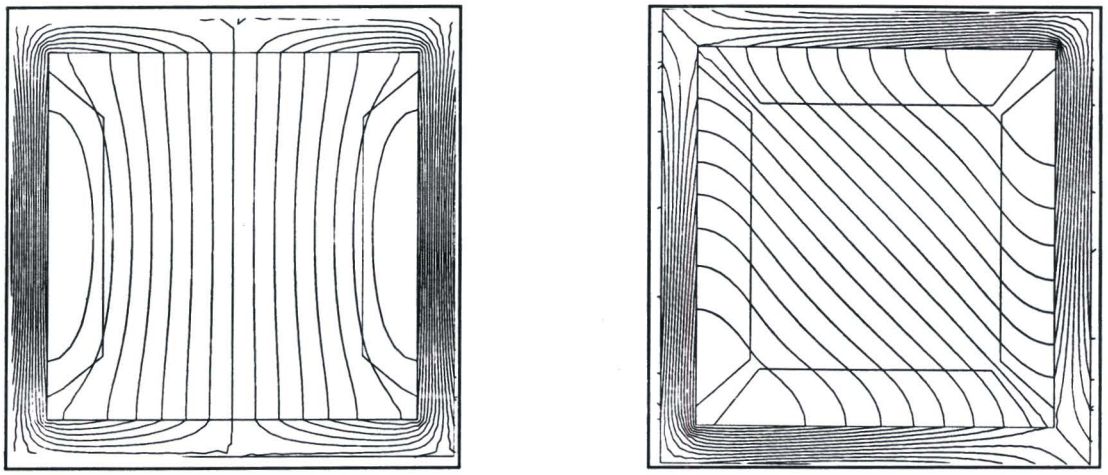

a) I_H *= 1280 A.turns* *b)* $I_H = I_V$ *= 1280 A.turns*

Fig. 5.8 Field profile in the window-frame corrector in the xy-plane for correction in the vertical direction (a) and for correction in both vertical and horizontal direction (b).

The fringe fields along the magnetic axis are extended many centimetres beyond the yoke as a consequence of the large aperture diameter (80mm) in comparison to the magnet length (50mm). In these fringe fields the electron beam is deflected. However the deflection of the beam is only determined by the field integral $\int B.dl$ and is therefore not influenced by inhomogeneities.

5.3.3 Field measurements in the window-frame corrector magnet

The induction in the corrector magnet is determined using a Hall-probe and a movable XY-table. The experimental set-up is described in appendix E. The hysteresis in the magnet is determined by measuring the induction at a fixed location, while changing the current.

The remnant induction equals $B_r \approx 4.5$ Gauss. Compared to the rms-value of the induction required for the correction - $(B_x)_{rms} \approx (B_y)_{rms} \approx 80$ G - the remnant induction is small. With software the hysteresis can be corrected for; otherwise the correction lattice will adjust the corrector settings after feedback from the beam position measurements.

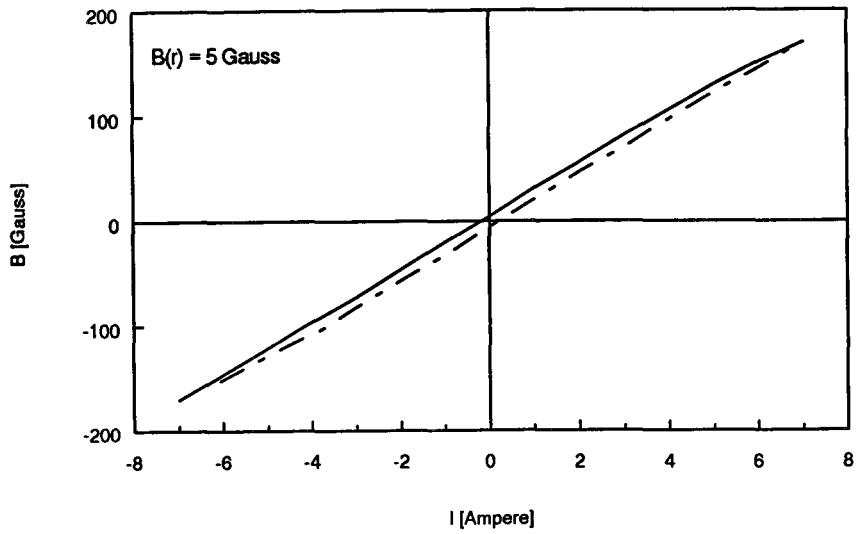

Fig 5.9 Hysteresis in the window frame corrector magnet.

The induction B_y in the sx-plane of the corrector magnet is measured and shown in fig. 5.10. In the horizontal direction the induction is constant, as expected. Along the longitudinal axis the induction is inhomogeneous. The measured induction along this axis is compared with the induction calculated in Poisson, see fig. 5.11.

The magnitude and direction of the induction in the vertical plane is within a few percent equal to the induction in the horizontal plane. The induction in the vertical direction is shown in appendix E.

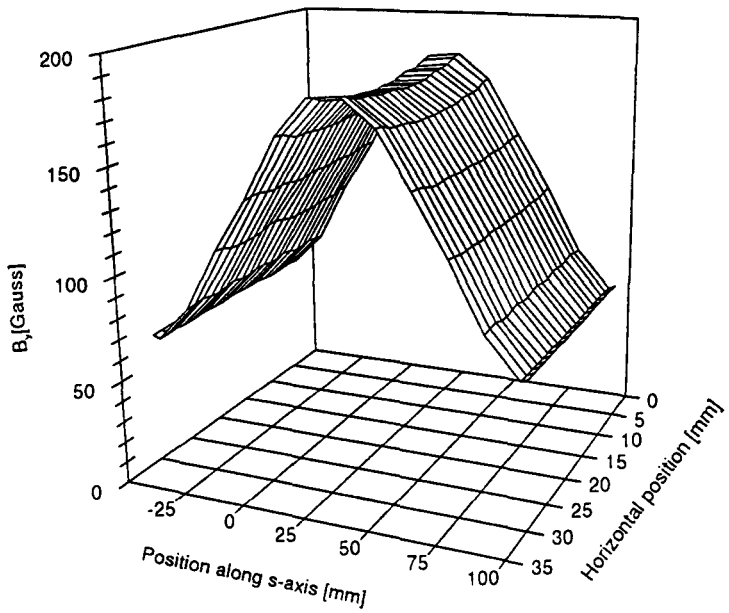

Fig. 5.10 *Measured induction in the window frame corrector magnet in the horizontal plane, NI = 1280 A.turns*

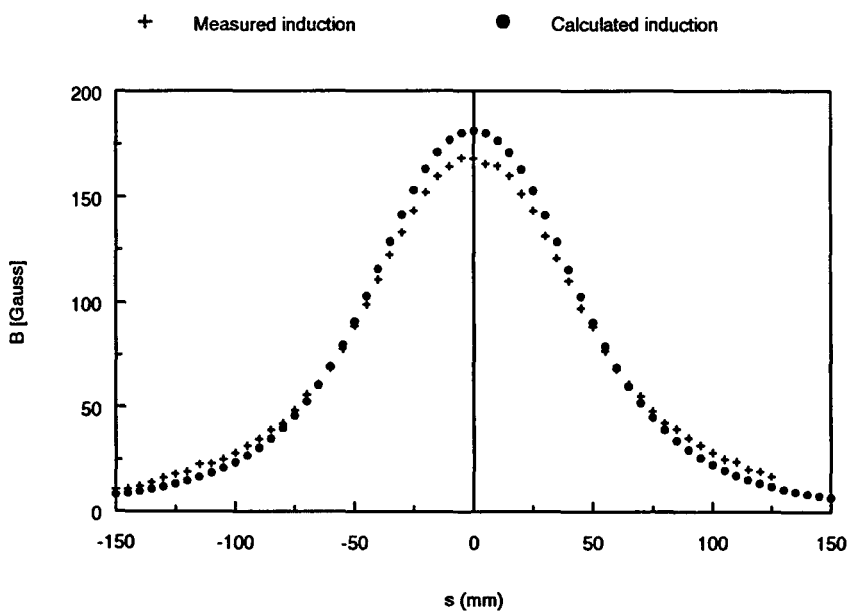

Fig. 5.11 *Comparison of the measured and calculated induction along the s-axis.*

5.4 Beam position Monitors

In this paragraph a brief study is presented on two types of beam position monitors: the striplines and the button type monitors. The basic principles of the monitors are given in §5.4.1. In the same paragraph the size of the output signals is theoretically derived. Some general parameters are estimated for the EUTERPE monitors and are given in §5.4.2. With these parameters, the expected output voltages and difference/sum signals of the monitors are calculated. The specifications of several monitors included in similar storage rings are given in the same paragraph. Finally the button monitors and striplines are compared.

5.4.1 Theory concerning the button type and stripline beam position monitors

For the successful operation of the closed orbit correction system, high resolution beam position monitors (BPM's) are required. Many different types of beam position monitors are available. The button type pickup monitor is most commonly used in electron storage rings. The monitor has the advantage of being easy to manufacture and has a very low impedance and therefore does not disturb the beam. In this paragraph the basic principles of the button type monitor are treated based on [Bea89]. The button type monitor is compared with the stripline monitor, which is treated as well.

A capacitive pick-up monitor is a small button or plate, which is placed in the vacuum-chamber. Exposed to the electric field of the beam, a mirror current will be driven into the buttons. The induced voltage in the left button V_L equals [Bea89]

$$V_L(t) = \frac{\phi_L l}{2\pi C}\frac{I_B(t)}{\beta_b c} - V_0 \qquad (5.6)$$

with ϕ_L the azimuthal extent of the left button, l the button length, C the capacitance of the button, I_B the beam current, $\beta_b c$ the electron velocity and V_o a constant. The output voltage of eq. 5.6 is just the voltage developed over a capacitance C with a current $I = \phi_L\, l.I_B\,(t)/2\pi\beta_b c$.

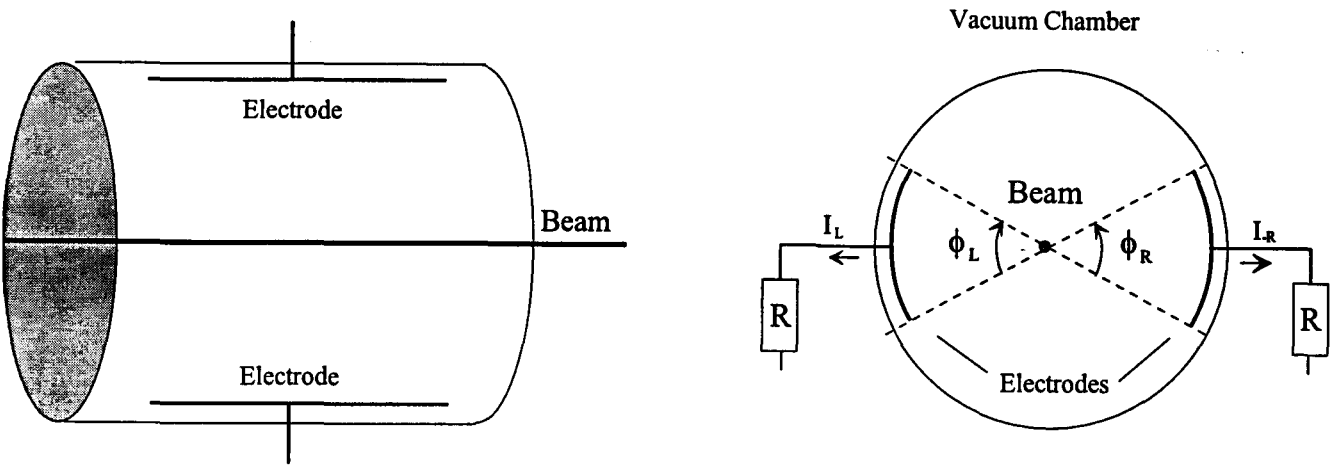

a) Side view *b) Cross section*

Fig. 5.12 Schematic view of a circular button type position monitor.

If a resistor R placed in series with the button, the output signal is differentiated in time

$$V_B(t) = Ri_s(t) = \frac{\phi l R}{2\pi\beta_b c}\frac{dI_b(t)}{dt}. \tag{5.7}$$

This principle is used in button monitors.

With the expansion of the beam current in its Fourier components the output current is found as a function of the frequency.

$$I_b(t) = \langle I_b\rangle + 2\langle I_b\rangle \sum_{m=1}^{\infty} A_m \cos(m\omega_o t), \tag{5.8}$$

with A_m the Fourier components. Combining the Fourier expansion with eq.5.7 gives

$$V(\omega) = \frac{\sqrt{2}\phi R}{\pi} \langle I_b\rangle A(\omega) \frac{\omega l}{2\beta_b c}. \tag{5.9}$$

Higher harmonics are more amplified than the components with lower frequencies. The Fourier components A_m approach 1 as long as the bunch length is shorter than the wave length of the modulation signal ($A_m \sim \exp(-m^2\omega_0^2\sigma^2/2)$ for a bunch with Gaussian distribution).

The actual beam position is measured with two striplines on opposite sides of the beam; in the plane of the striplines the beam position is calculated from the ratio of the difference and sum signals. The difference and sum signals are deduced from eq 5.9. Considering only linear terms the difference/sum signal S in a circular monitor is linear to the horizontal displacement, x, of the beam

$$S = \frac{4\sin(\phi/2)}{\phi}\frac{x}{\rho}, \tag{5.10}$$

with ρ the aperture radius of the monitor [The94].

Several other monitor techniques are known, based on the detection of the wall current, that is induced on the inner surface of the vacuum chamber by the electron beam, e.g. stripline monitors. The striplines are conductive plates isolated from the vacuum chamber. Two connectors connect the stripline to coaxial transmission lines at both ends of the plate.
The striplines serve as transmission lines for the TEM wave accompanied by the electrons. When the beam pulse approaches the upstream end of the electrode the TEM wave is split in

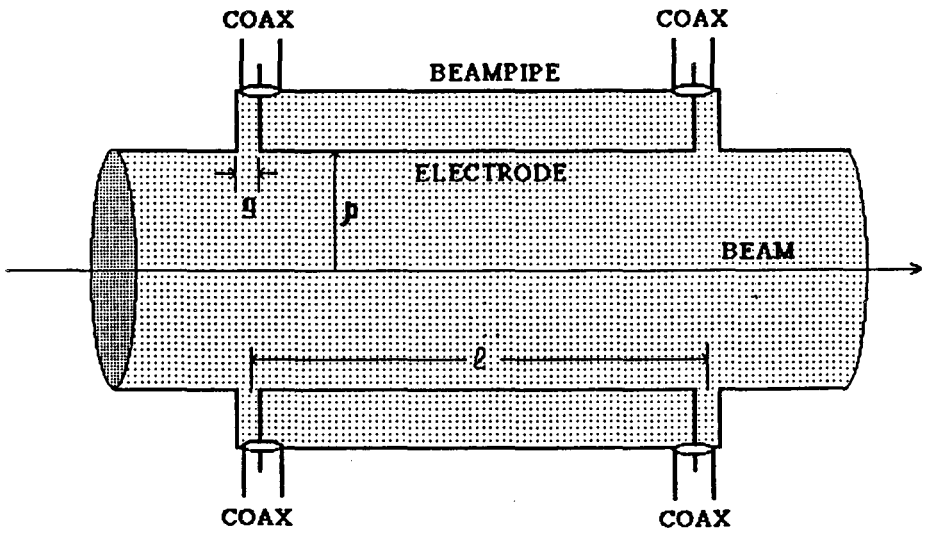

Fig. 5.13 A schematic view of a stripline beam position monitor.

two (with the right choice of its characteristic impedance). Part of the wave flows to the other end of the stripline and part is coupled into a detection device. At the other end of the stripline this wave is dissipated in the resistor. When the beam accompanied by the TEM wave approaches the downstream, the TEM is split in two again. The part of the wave flowing to the upstream end is coupled out. The output signal is a superposition of TEM waves. Due to interferention the maximum output signals are reached if the stripline is one quarter of the measured wavelength $l=\lambda/4$. The length of most striplines in operation equals a quarter wave-length of the measured harmonic, but in principle lower frequencies can be measured as well.

The response of the stripline monitor is given by

$$V(\omega) = \frac{\phi Z}{\sqrt{2}\pi} \langle I_b \rangle A(\omega) \sin\left[\frac{\omega l}{2c}\left(\frac{1}{\beta_s} + \frac{1}{\beta_b}\right)\right]. \qquad (5.11)$$

with Z the impedance of the transmission line, β_b the beam velocity and β_s the wave velocity. The output voltage of the stripline is very similar to the output voltage of the button type monitors. For Z=2R, the output signals are equal in the low frequency range. This is shown in fig. 5.12.

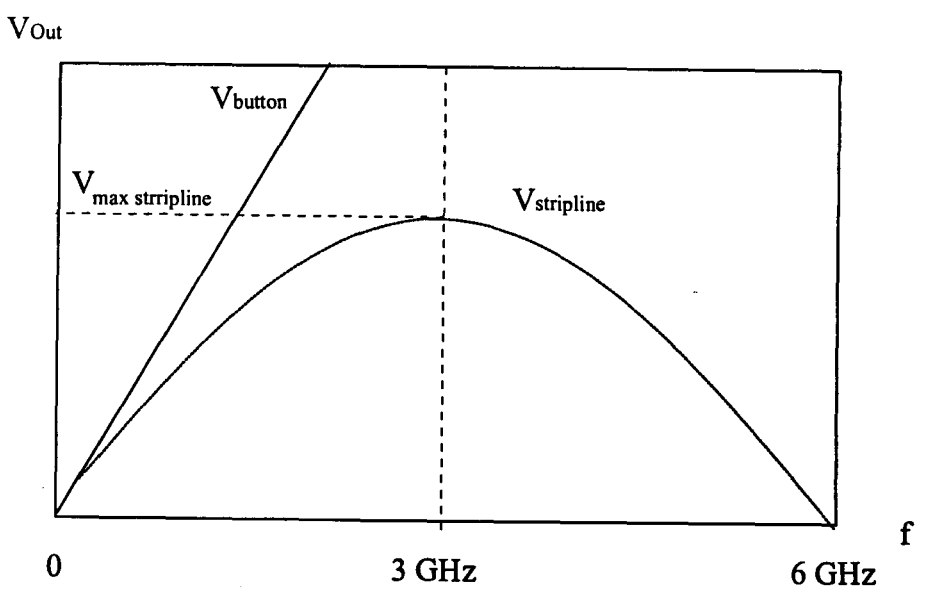

Fig. 5.14 *The output voltages of the striplines and button type monitors as a function of the frequency, with Z=2R, $\beta_s=\beta_b=1$ and l=2.5cm.*

5.4.2 Monitors for the EUTERPE ring.

In the previous paragraph it has been shown that the expected output signals of the two types of monitors are of the same order. In this paragraph the size of the output signals is estimated.

The output signals of the monitors can be calculated using the equations derived in the previous paragraph. Several parameters of the monitors are already known; therefore an estimation of the final output signals can be made.

- The position accuracy of the monitors required for the correction system is equal to σ_x, $\sigma_y \leq$ 0.1 mm for beam currents ranging from 10 mA to 200 mA.
- The aperture radius, ρ, of the monitors is determined by the inner diameter of the vacuum chamber, which is 45 mm (and gives ρ =22.5mm).
- The monitors will be circular like the vacuum chamber in order to minimise their impedance.
- The position accuracy of the monitors in one direction is best if the azimuthal angle is equal to ϕ=1 rad [The94].

With these parameters an impression of the output voltages and difference/sum signals of the monitors is obtained. The difference/sum signal for a displacement of x=0.1mm is equal to

$$S = \frac{4\sin(\phi/2)}{\phi}\frac{x}{\rho} \approx 9\%. \qquad (5.12)$$

A relatively large value. The resolution of the sum/difference signal in the storage ring in Stanford is equal to 500 ppm [Seb94].

For the estimation of the output voltage several characteristic parameters are used:

- The minimum beam current in the EUTERPE ring is : $\langle I_b \rangle$ =10mA.
- The bunch lengths σ in the EUTERPE ring range from 0.08 to 3.7 cm (see table 1.2); as a result the Fourier component A_m of the beam current approximate 1 for frequencies up to 3 Ghz.
- The velocity of 400 MeV electrons nearly equals the speed of light, which gives $\beta_b c \approx c$. The transmission of the output signals through 50 Ω-coax cables requires that the characteristic impedance is $R = 50\Omega$.
- The length l and the modulation frequency of the buttons are for the moment chosen to be equal to l=1cm and f=45 MHz (the basic frequency of the beam)

With the use of the parameters estimated above the output voltage of the monitor becomes

$$V(45\ MHz) = \frac{\sqrt{2}\phi R}{\pi} \langle I_b \rangle A(\omega) \frac{\omega l}{2\beta_b c} \approx 0.9\ mV. \qquad (5.13)$$

An output voltage, which should be high enough to be measurable. If the modulation frequency is increased higher harmonics can be measured, with f=3GHz the output voltage is ca 66 times amplified. However the signal processing in the high frequency regime is much more difficult.

The desired resolution for the beam position monitors in the EUTERPE ring (σ=0.1mm) is comparatively low in comparison to the achieved resolutions in similar storage rings [Sco94], [Gil93], [Seb94], [Smi94]. The most important parameters regarding the monitors used in Daresbury, Stanford and Los Alomos are given in table 5.9.

Table 5.9 BPM parameters in other storage rings

Storage ring	SPEAR (Stanford) (button type mon.)	SRS in Daresburry (button type mon.)	MIT South Hall ring (stripline monitors)
Energy	3 GeV	2 GeV	
f_{RF} (*) f_{meas}	358 MHz 717 Mhz	500 MHz 500 Mhz	2865 Mhz 2865 Mhz
Current range	20-100 mA	20-100 mA	1-80 mA
Resolution Absolute Acc.	10 μm 10 μm	10μm ≤100μm (rms)	0.1mm
Dynamic Range	40 dB	10 dB	unknown
Monitor size	Width 155 mm Heigth 44 mm Length 20 mm	not known	Aperture 60 mm Length 24.7mm

(*) f_{RF} is the frequency of the rf-cacity
f_{meas} is the first harmonic, which is measured in the monitors.

5.4.3 Conclusions regarding the position monitors

It is expected that a measurement accury of the beam position monitors required for the closed orbit correction can be obtained. The output voltages of the stripline and button type monitors are relatively large (in the order of mV for the measurement of a 45 MHz signal); the difference/sum signals are also large due to the relatively small aperture radius (R=25.5mm) of the vacuum chamber in the EUTERPE ring. Furthermore resolutions in the order of $\Delta x=10$ μm have been obtained with monitors in similar storage rings.

The measurement accuracies attained with the striplines and button monitors are similar at first sight. Stripline monitors are more difficult to manufacture, but have the advantage that there is some experience in the group with these monitors. Stripline monitors are used for the monitor system of the Race Track Microtron Eindhoven. However for a good comparison of the two monitor types a more extensive study of both techniques is required. Because both monitors are easily constructed, it would be very useful to manufacture test models of both monitors and test them in the 45 MHz to 3 GHz regime.

5.5 Summary

The design of the hardware regarding the closed orbit correction is for the major part finished. The design of the sextupoles and window frame corrector magnets required for the closed orbit correction has been completed. However the monitoring techniques have been only briefly studied.

Sixteen sextupoles are included in the EUTERPE ring; all sextupoles will be uniform and therefore all sextupoles can be used for both the chromaticity and the closed orbit correction. Simulations show that almost perfect dipole fields can be generated in the sextupole. The uniformity of the generated sextupole and corrector fields is several times better than the tolerances. The calculated induction has to be verified with field measurements in the prototype sextupole, which is still under construction. A simple and accurate measurement of the higher order field components is possible with a rotating coil device.

The window frame corrector magnets have been designed and a prototype magnet has been constructed at the TUE. Field measurements in the prototype corrector magnet show that the dipole field is very uniform and in perfect agreement with the simulations. The field integral $\int B.dl$ along the magnet axis is more than sufficient for a deflection of 400 MeV electrons with

$\Delta x'$=1.5mrad. Along the longitudinal axis the magnetic field is extended for many centimetres beyond the yoke. Simulations in Poisson show that the coupling fields B_x/B_y and B_y/B_x, for respectively the horizontal and vertical correction are very small.

Studies on the beam position monitors show that position resolutions of 0.1mm should be attainable with the use of stripline or button type monitors.

Chapter 6

Conclusions and recommendations

The electron orbits in the storage ring EUTERPE are distorted due to lattice imperfections. An extensive study has been made of the position and field errors of the magnetic elements, which are the most important sources of the closed orbit distortion. The position errors are mainly determined by the finite measurement precision during the alignment. The displacements due to all other error sources - e.g. due to thermal expansion - are negligible. The field errors in the elements are small.

The closed orbit distortion as a result of all possible lattice imperfections has been determined with simulations in the computer code Methodical Accelerator Design (MAD). Because the position errors are expected to have a gaussian distribution, the closed orbit distortion has been determined for multiple error-configurations.

The closed orbit distortion in the EUTERPE ring are mainly determined by the position errors of the magnetic elements. From all position errors, the closed orbit distortion is most sensitive to the displaments of the quadrupoles. This is a result of the strong dependency of the magnetic induction on the position in the quadrupoles; the sensitivity is increased due to the high values of the betatron function. The field errors in the quadrupoles affect the tunes and therefore need to further examined.

It is desired that the electron trajectory approximates the design trajectory, therefore a closed orbit correction system is needed. Furthermore closed orbit correction is required if e.g. undulators are included in the ring. The maximum distortion of the electron beam is for the uncorrected orbit of almost the same size as the inner radius of the vacuum chamber. Because the aperture of an undulator is expected to be smaller, a correction of the closed orbit distortion is required in order to prevent a beam loss in these devices.

The closed orbit distortion can be reduced with a factor 28 in the horizontal and a factor 8 in the vertical direction with the use of a correction system containing 36 monitors and 20 corrector magnets. The distortion can be further reduced with a factor 2 if the monitor errors are eliminated. The resulting distortion x_{rms} = 0.13±0.02 mm and y_{rms} = 0.13±0.02 mm is of approximately the same size as the position and read errors in the monitors.

The number of elements of the correction system has been reduced to 24 corrector magnets and 24 monitors, without a significant loss of the correction quality. The number of monitors corresponds to four monitors per betatron wavelength, which is the minimum number of monitors required to establish the amplitude and phase of the distortion.

The sextupoles will be used as corrector magnets, in order to save space in the ring. Uniform dipole fields can be produced in the sextupoles in the horizontal as well as the vertical direction with the injection of extra currents through the coils. The coupling coefficients B_x/B_y and B_y/B_x, remain smaller than 2 % in the region of interest if the coils around all poles used for the generation of the correction field. The field profiles have been calculated with the use of the program 'Poisson' and show that the generated sextupole field is very uniform as well ($\Delta k_2/k_2 \leq 1\%$, with k_2 the sextupole strength).
The magnetic field profiles have to be measured on the prototype sextupole, which at the moment is under construction. Higher order field components have to be measured, which is not possible with Hall plates. Therefore a new measurement device has to be constructed, e.g. a rotating coil device.

The dipoles can be used as horizontal corrector magnets. However the correction is deteriorated, if all dipoles and sextupoles are used for the correction. This is a consequence of the fact that some of the monitors are placed directly in between two corrector magnets. The minimization of the beam position errors results in large deflections in the two adjacent corrector magnets and a local increase of the distortion. If one of the correctors near these monitors is discarded, the correction is improved.

Additional corrector magnets have to be included in the long straight section in which no sextupoles are present. The simulations show that otherwise the distance between successive corrector magnets becomes too large.
The additional correctors are of the so-called 'window frame' type. The window frame magnets have the advantage that uniform dipole fields can be generated in two directions. Furthermore they are very easy to manufacture. The specific shape of the window frame results in a dipole field of high quality; the calculated coupling coefficients B_x/B_y remain smaller than 1% in the region of interest.The first measurements on the prototype window frame magnet show that the measured field profiles are in perfect agreement with the simulations.

The field profile in the longitudinal direction is less uniform as a result of the large aperture radius with respect to the magnet length. Care must be taken if the correctors are inserted near other elements. Magnetic materials will influence the field integral of the corrector and as a consequence the deflection of the beam.

The yokes of the window frame can be made of ordinary steel. The remnant induction in the prototype magnet is smaller than 6 G, corresponding to a deflection equal to $\Delta u' = 0.06$ mrad of a 400 MeV electron beam. Due to the feedback of the beam position with the monitors, the corrector settings will be adjusted.

6.2 Recommendations

Most of the error-configurations in the most sensitive mode of operation (the HBSB mode) the misalignments resulted in resonances of the betatron oscillations in the vertical plane. This instability can be prevented with an adjustment of the quadrupole strengths; with less vertical focusing the working point is shifted away from the semi integer resonance line.

A brief study on beam position monitors showed that a measurement precision of 0.1 mm should be obtainable. Two types of monitors are under consideration: button type and stripline monitors. Both types of monitors seem to be equally suited for the EUTERPE ring. The button type monitors have the advantage of being easier to manufacture; on the contrary, more experience in the group is present stripline monitors. Further studies have to be done to determine which type of monitors to use.

In this study the closed orbit distortion is corrected globally; the distortion at all positions is weighted equally. However, the distortion can be further reduced with local correction. It is possible that local correction is required, e.g. for the reduction of the closed orbit distortion in the bypass. Therefore the possibilities and the necessity of local correction have to be examined.

An integration of the monitors and optical elements of a subsection on a single support structure is recommended. This is expected to provide perfect alignment within such a straight section and will therefore further increase the quality of the correction system and reduce the distortion.

References

[Aut73] B. Autin, Y. Marti, *Closed orbit correction of A.G. Machines using a small number of magnets*, CERN ISR-MA/73-17, Genova Switzerland.

[Bac79] W.H. Backer, *Some aspects of the orbits in an electron storage ring used as a synchrotron radiation source*, PhD EUT (1979).

[Bes89] BESSY II, *Eine optimierte Undulator/Wiggler-Speicherring Lichtquelle fur den VUV- und XUV-Spektralbereich* - 2 Teil- Technische studie, Berlin, Juni 1989.

[Bre95] J. Bresser, *Trillingsmetingen aan een EUTERPE-dipool + onderstel*, Internal report EUT, VDF/NK 95- 8.

[Cas85] P. Bryant, S. Turner, CERN Accelerator School, *General Accelerator Physics*, CERN 85-19 (Geneva 1985).

[Cas91] S. Turner, CERN Accelerator School, *Fourth General Accelerator Physics Course*, CERN 91-04 (Geneva 1991).

[Cas94] S. Turner, CERN Accelerator School, *Fifth General Accelerator Physics Coarse*, CERN 94-01 (Geneva 1994).

[Chu93] Y. Chung, G. Decker, and K. Evans Jr, *Closed Orbit Correction Using Singular Value Decomposition of the Response Matrix*, Proc. 15th IEEE Part. Acc. Conf., Washington, D.C., (1993) 2263.

[Der94] A.T.A.M. Derksen, *Field measurements of the prototype EUTERPE dipole and related electron optical studies*, VDF/NK 94-04 (1994).

[Der94] A.T.A.M. Derksen, *Computer calculations on misalignments and field errors of dipoles and quadrupoles*, Internal report, VDF/NK 94/04, Eindhoven University of Technology.

[Dim93] R.V. Servranckx, K.L. Brown, L. Schachinger, D. Douglas, *Users guide to the program DIMAD*, SLAC Report 285 UC-28 (A) May 1985.

[Duc93] Jens J. Ducrée, *Closed Orbit Calculations for the EUTERPE Storage Ring at the University of Eindhoven*, Internal report TUE, VDF/NK 93-23 (1993).

[Dui89] W. van Duijneveldt, *Een bestudering van bundeldynamische aspecten en de gevolgen van uitlijnfouten in de bundeloptiek voor de 400 MeV/c opslagring Euterpe*, internal report EUT VDF/NK 89.

[Dui91] W. Van duijneveldt, *A Program to Minimize the Closed Orbit Distortion by Fitting Corrector Dipoles*, Internal Report NIKHEF Amsterdam (1991).

[Edw73] D.A. Edwards, L.C. Teng, *Parametrization of linear coupled motion in periodic systems*, IEEE Trans. on Nucl.Sc. 20:885, 1973.

[Kou89] J.P. Koutchouk, *Trajectory and closed orbit correction*, CERN LEP-TH/89-2 (1989) 46.

[Kuo94] C.C. Kuo, K.T. Hsu, H.P. Chang, C. Travier, G.J. Jan and C.S. Hsue, *Closed Orbit Measurement and Correction of the SRRC Storage Ring*, IEEE Proc. of the European Part. Acc. Conf, p.1018.

[MAD91] H. Grote, F.C. Iselin, *The MAD program (version 8.1), User's Reference Manual.*

[Mon85] M. Month, M. Dienes, *Physics of particle accelerators*, AIP Conference Proceedings 153, volume two.

[Mut95] P.H.A. Mutsaers, *Design and Realisation of the Eindhoven Scanning Proton Microprobe,* PhD thesis EUT, 1995.

[POI87] M.T. Wenzel, H.K. Stokes, *User's guide for the POISSON/SUPERFISH Group of Codes*, LA-UR-87-115, Los Alomos National Laboratory, New Mexico.

[Saj94] V. Sajaev, *Proposal for closed orbit correction scheme at BESSY-2*, Technical report BESSY TB Nr.187/94.

[Ste94] H.A.M. Steyaert, *De geodesie van EUTERPE - Analyse meetnetwerk en studie noodzakelijke meetmiddelen*, Internal report EUT VDF/NK 94-12.

[The94] W.H.C. Theuws, *Beam Position Monitoring and Beam Positioning in the Racetrack Microtron Eindhoven*, VDF/NK 94-39 (1994).

[Tim95] C.J. Timmermans, Private Communication, Eindhoven University of Technology.

[Tra87] C. Travier, C.C. Kuo, C.S. Hsue, *A Comparison of Three Different Orbit Correction Schemes*, SRRC/BD/IM/87-30 (1987).

[Uyt87] J.A. Uythoven, H.L.Hagedoorn, J.I.M. Botman, *Enkele bundeldynamische aspecten van het proton-electron synchrotron EUTERPE*, Internal report EUT, VDF/NK 87-29 (1987).

[Wet92] S.F.L.L. Wetzels, *De geodesie van EUTERPE - voorstudie met betrekking tot de dipolen*, Internal report EUT VDF/NK 92-25.

[Wu 91] Y.Y. Wu, *The optical design of AmPS*, PhD EUT (1991).

[Wus94] G. Wüstefeld, B. Kuske, V. Sajaev, D. Schirmer, *Optimization and Tracking Studies for the 1.7 GeV Light Source BESSY II*, IEEE Proc. of the 4th European Part. Acc. Conf., p 994.

[Xi 92] B.Xi, J.G.M. Moerel, J.I.M. Botman, *Measurement report on a prototype of the dipole magnet*, Internal report EUT VDF/NK 92-04.

[Xi 95] B. Xi, *Design studies for the Electron Storage Ring EUTERPE*, PhD EUT (1995).

Appendix A Methodical Accelerator Design

The software packet Methodical Accelerator Design (MAD) is used throughout this report for the simulations of the EUTERPE ring. In this appendix the algorithms used in the program and a short introduction to the program are given. Examples are shown of the input- and output-files for the calculation of the closed orbit distortions before and after correction in a lattice with multiple misalignments

The closed orbit distortions due to different kind of errors are determined with simulations in Methodical Accelerator Design (MAD) [MAD85]. The program was developed at CERN to design accelerator rings in 1985, but is nowadays a frequently used tool for the design of storage rings, e.g. [Saj94].

A1 Algorithms used in MAD

The program represents machine elements by transfer matrices as described in §2.2 [Wu 91], [Saj85]. The whole ring is represented by a series of matrix multiplications. The transfer matrix R between point '0' and '1' is defined as

$$Z(1) = RZ(0)$$

where Z represents the particle coordinate vector; the transpose of Z can be written as Z^T = (x, x', y, y', s, s'), where x, x', y, y', s and s' are the particle coordinates. In first-order the matrix multiplications are described by 2.3.

$$R=R(n)R(n-1)....R(2)R(1)$$

Where R are the first-order transfer matrices. However first order matrices are not sufficient to describe the machine behaviour, e.g. sextupoles can only be represented by second-order matrices. The matrix multiplication for the second-order matrices is defined as:

$$T_{ijk}\ (t) = \sum_l R_{il}(2)T_{ljk}(1) + \sum_l \sum_m T_{ilm}(2)R_{lj}(1)R_{mk}(1).$$

R(1) and R(2) are the first-order matrices between point '0' and '1', and '1' and '2' respectively; the T matrices represent the second-order matrices in these intervals. The equation truncates the matrices to second order. No individual T matrices elements are multiplied together, which would yield terms of higher order than the second. These terms can not be represented by second-order matrices.

The closed orbit distortion is deduced from the eigenvector of the transfer matrix of the whole ring is

determined. The closed orbit distortion at a particular location is found as a function of the location s with the use of the elementary transfer matrices. The tunes can be calculated by tracking electrons with small deviations from the calculated closed orbit and determining the oscillation frequency.

A2 The use of the program

Many different element types can be inserted, from normal magnets, such as dipoles, quadrupoles, etc to rf-cavities, undulators, correction elements, etc. For the simulations in this study the EUTERPE lattice has been inserted in the program. The most importent magnetic elements in the EUTERPE ring are defined; the input is listed in fig. A1.

Different kind of errors can be assigned to the elements in the lattice. All alignment errors in the EUTERPE ring have a gaussion distributions. Random numbers with a Gaussian distribution and unit standard deviation are available in the program. A particular sequence of gaussion numbers is selected with the SEED option. The misalignments are assigned to the elements with the EALIGN command (see fig. A1). The random errors assigned to the elements with fig. A1 as input is given in fig. A2.

Many ring parameters can be calculated with the 'MAD'. This study was mainly concentrated on the parameters in the Twiss-table, which are given in figure A2. The parameters given are: the closed orbit distortions x_{co} and y_{co}, the tunes ν_x and ν_y (referred to with Qx and Qy in MAD), chromaticity ξ_x and ξ_y (Qx' and Qy'in MAD), the maximum betatron amplitudes β_x and β_y, the dispersions D_x and D_y, the momentum compaction factor α, the total ring length s and the increase of the ringlengt Δs and finally the transition energy γ.

For the closed orbit correction the command CORRECT is used; the closed orbit correction settings in the corrector magnets are calculated according to the Micado-method [Aut73]. Parameters used in the statement are:

Error The desired accuracy of the correction (peak to peak error of the closed orbit)
N_{corr} The number of correctors to be used.

The description given above is certainly not complete; many other parameters can be and have been adjusted in the simulations.

********** Input file in MAD ********** *****

```
option, echo, keyword=3
assign,echo=echo.mad

TITLE, HBSB
```

```
! Test of a closed orbit correction system
! with random displacements of all dipoles, quadrupoles and sextupoles
! Comparison of 10 runs starting with seed=123...
! The correction is with lattice D with and without extra monitor/kicker in long straight section
! Epsilon = 0.01 mm, monitors displaced, with monitor read errors

!*****************        Definition of the ring        *****************

! **** Definition of the drift spaces ****
xm=0.23  ! Distance between sextupoles and monitors
xm2=0.175  ! Distance between sextupoles and the second monitors
xq=0.08  ! Distance between the first quad and the monitor

o1: drift, type=dr, l=1.000
o1a: dr, l=xm
o1b: dr, l=1.00-xm
o2: dr, l=0.450
o2a: dr, l=xm
o2b: dr, l=0.45-xm
o3: dr, l=0.600
o3a: dr, l=xm
o3b: dr, l=0.60-xm
o4: dr, l=0.100
o5: dr, l=0.165
o5a: dr, l=xq
o5b: dr, l=0.165-xq

! *** Magnet Definition (HBSB mode) ***
b: sbend, type=di, l =0.516, angle=raddeg*30, &
      e1=raddeg*15, e2=raddeg*15, hgap=0.0125, fint=0.5

q1: quadrupole, type=qu, l=0.274, k1= 4.396
q2: quadrupole, type=qu, l=0.274, k1=-4.500
q3: quadrupole, type=qu, l=0.274, k1= 7.351
q4: quadrupole, type=qu, l=0.274, k1=-1.794

s1: sextupole, type=se, l=0.05, k2= 832.932
s2: sextupole, type=se, l=0.05, k2=-1122.946


! **** definition of the correction elements, length=0 ****
m:  monitor, type=mon, l=0   ! monitor in both horizontal and vertical direction
hk: hkicker, type=ki, l=0    ! Horizontal kicker
k : kicker, type=ki,l=0   ! kicker in both horizontal and vertical direction

! **** Ring structure *****
```

```
p1: line=(q1,o5a,m,o5b,q2)
p2: line=(q3,o5a,m,o5b,q4)   ! vertical kicker in the middle of the quadrupole-doublet

          ! cell: line=(o1,p1,o3)                    ! Definition of the ring without correction
          ! cel2: line=(o2,s1,o4,p2,o4,s2,o2)
          ! super: line=(cell,b,cel2,b,-cel2,b,-cell)

cella: line=(o1,p1,o3a,m,o3b)

cel2a: line=(o2,k,s1,o4,p2,o4,s2,k,o2a,m,o2b)

! ***Definition of lattice D, with additional corrector and magnet in long straight section
super: line=(cella,b,cel2a,b,-cel2a,b,-cella,m,k)
euterpe: line=(4*super)
USE, euterpe

! ***      Calculation of the closed orbit distortions          ***
print
Twiss                                    ! Calculate Twiss parameters for the ideal lattice
EOPT, SEED=123456789                     ! start reading "random"-numbers at position 123456789
y1:=0.0001                               ! misalignment: 0.1mm or 0.1mrad
 EALIGN, type=di,qu,se &                 ! ***  all dipoles, quadrupoles and sextupoles are misaligned  ***
  dx= y1*gauss(), dy= y1*gauss(),  ds= y1*gauss(),&
  dphi= y1*gauss(),dtheta= y1*gauss(),dpsi= y1*gauss()
TWISS                                    ! Calculate Twiss-parameters for the lattice with misalignments
 EALIGN, type=mon &                      ! ***  all monitors are misaligned  ***
  dx= y1*gauss(), dy= y1*gauss(),  ds= y1*gauss(),&
  dphi= y1*gauss(),dtheta= y1*gauss(),dpsi= y1*gauss(), &
  mrex= y1*gauss(), mrey= y1*gauss()     ! ***  monitor read errors ***
eprint, type=b,mon                       ! *** print misalignment errors for verification
SELECT, OPTICS, full                     ! **** Create dataset for plot-file ****
OPTICS, filename="p2m.dr", column=s,betx,x,bety,y,dx,dy
putorbit                                 ! *** Calculate monitor-readings for the uncorrected orbit
putkick, filename="kick0"                ! *** Save zero corrector settings
CORRECT, error=0.00001,iterate=5 ,c2list ! *** Calculate the corrector settings with the MICADO method
twiss                                    ! *** Calculate Twiss-parameters after correction
getkick, filename="kick0"                ! *** Reset corrector settings to zero

! **** Second run, the same parameters are calculated for the same lattice, but with different alignment errors *
EOPT, SEED=223456789                     ! start reading "random"-numbers at position 123456789
 EALIGN, type=di,qu,se &                 ! ***  all elements are misaligned  ***
  dx= y1*gauss(), dy= y1*gauss(),  ds= y1*gauss(),&
    ....
    ....
    ....
! **** Run 3 to 10
```

Stop

Fig. A.1 Input file for MAD; calculations of the closed orbit distortion in the EUTERPE ring before and after correction for one error configuration.

```
------
HBSB                                                    "MAD" Version: 8.9/0    Run: 10/08/95
17.14.43
Linear lattice functions.    TWISS          line: EUTERPE              range: #S/#E

Delta(p)/p:     0.000000     symm: F        super:   1                                    page
 1
-------------------------------------------------------------------------------------------------------------------------------
----
     ELEMENT SEQUENCE       I              H O R I Z O N T A L              I              V E R T I C A L
pos. element occ.     dist I   betax  alfax   mux    x(co)  px(co) Dx    Dpx  I   betay  alfay   muy    y(co)  py(co) Dy
Dpy
no.  name    no.      [m]  I   [m]    [1]     [2pi]  [mm]   [.001] [m]   [1]  I   [m]    [1]     [2pi]  [mm]   [.001] [m]
[1]
-------------------------------------------------------------------------------------------------------------------------------
----
begin EUTERPE   1     0.000   23.803  0.000   0.000  0.000  0.000  0.000 0.000    0.475  0.000   0.000  0.000  0.000  0.000
0.000
end   EUTERPE   1    40.000   23.803  0.000   5.131  0.000  0.000  0.000 0.000    0.475  0.000   2.470  0.000  0.000  0.000
0.000
-------------------------------------------------------------------------------------------------------------------------------
----
total length =        40.000000          Qx          =         5.130718          Qy          =         2.469618
delta(s)     =         0.000000 mm       Qx'         =         0.006697          Qy'         =         0.213699
alfa         =         0.109009E-01      betax(max)  =        23.844893          betay(max)  =        11.120178
gamma(tr)    =         9.577861          Dx(max)     =         0.467609          Dy(max)     =         0.000000
                                         Dx(r.m.s.)  =         0.261222          Dy(r.m.s.)  =         0.000000
                                         xco(max)    =         0.000000          yco(max)    =         0.000000
                                         xco(r.m.s.) =         0.000000          yco(r.m.s.) =         0.000000
-------------------------------------------------------------------------------------------------------------------------------
HBSB                                                    "MAD" Version: 8.9/0    Run: 10/08/95
17.14.43
Linear lattice functions.    TWISS          line: EUTERPE              range: #S/#E

Delta(p)/p:     0.000000     symm: F        super:   1                                    page
 1
-------------------------------------------------------------------------------------------------------------------------------
----
     ELEMENT SEQUENCE       I              H O R I Z O N T A L              I              V E R T I C A L
pos. element occ.     dist I   betax  alfax   mux    x(co)  px(co) Dx    Dpx  I   betay  alfay   muy    y(co)  py(co) Dy
Dpy
no.  name    no.      [m]  I   [m]    [1]     [2pi]  [mm]   [.001] [m]   [1]  I   [m]    [1]     [2pi]  [mm]   [.001] [m]
[1]
-------------------------------------------------------------------------------------------------------------------------------
----
begin EUTERPE   1     0.000   27.639 -0.037   0.000 -3.435 -0.084 -0.134-0.003    0.000  0.000   0.000 -0.402 -0.733  0.001
0.013
end   EUTERPE   1    40.000   27.806 -0.054   5.127 -3.435 -0.084 -0.134-0.003    0.000  0.000   0.000 -0.402 -0.733  0.001
0.013
-------------------------------------------------------------------------------------------------------------------------------
----
total length =        40.000000          Qx          =         5.127398          Qy          =         0.000000
delta(s)     =        -0.153988 mm       Qx'         =         0.226837          Qy'         =         0.000000
alfa         =         0.107609E-01      betax(max)  =        27.806198          betay(max)  =         0.000000
gamma(tr)    =         9.639970          Dx(max)     =         0.519294          Dy(max)     =         0.175300
                                         Dx(r.m.s.)  =         0.266227          Dy(r.m.s.)  =         0.059667
                                         xco(max)    =         6.690439          yco(max)    =         4.329595
                                         xco(r.m.s.) =         1.937330          yco(r.m.s.) =         1.966563
-------------------------------------------------------------------------------------------------------------------------------
HBSB                                                    "MAD" Version: 8.9/0    Run: 10/08/95
17.14.43
Imperfections.               EPRINT         line: EUTERPE              range: #S/#E

                             symm: F        super:   1                                     page
 1
-------------------------------------------------------------------------------------------------------------------------------
----
Element sequence     Displacements in [mm]                  Rotations in [mrad]                    Field errors in
1.0E-3
pos.  element occ.   DX           DY           DS           DPHI         DTHETA       DPSI          Re(K0L)       Im(K0L)
no.   name    no.    Re(K1L)      Im(K1L)      Re(K2L)      Im(K2L)      Re(K3L)      Im(K3L)       Re(K4L)       Im(K4L)
                     Re(K5L)      Im(K5L)      Re(K6L)      Im(K6L)      Re(K7L)      Im(K7L)       etc.
-------------------------------------------------------------------------------------------------------------------------------
----
```

```
  10 B          1   0.64781E-01  -0.12988E-02   0.72286E-01   0.49999E-01  -0.25334E-01   0.66710E-01
  26 B          2  -0.88420E-01  -0.37254E-01  -0.31126E-01  -0.18270      -0.30344E-01   0.49028E-01
  42 B          3  -0.11949       0.10949E-01  -0.20702       0.10670       0.15524       0.11976
  63 B          4   0.52519E-01   0.74144E-01   0.99403E-01   0.10885       0.32891E-01  -0.85307E-01
  79 B          5  -0.63674E-02  -0.10769       0.45890E-02  -0.96416E-01  -0.46986E-01   0.75416E-01
  95 B          6  -0.77851E-01   0.53565E-01   0.11800      -0.38241E-01   0.11129      -0.72678E-01
 116 B          7  -0.25728E-01   0.35755E-01  -0.32336E-01  -0.11471E-01   0.27106E-01  -0.16042E-01
 132 B          8  -0.12230       0.95380E-01  -0.17152E-01  -0.89743E-01  -0.17639E-01   0.84012E-01
 148 B          9  -0.16131       0.10590      -0.11427      -0.42311E-01  -0.67079E-01  -0.17262
 169 B         10   0.52007E-01   0.69732E-02  -0.61075E-01  -0.74339E-01  -0.13513E-01   0.33352E-01
 185 B         11  -0.13272      -0.61990E-01  -0.70708E-01   0.10701      -0.18648       0.14235E-01
 201 B         12   0.17805E-01  -0.34584E-01   0.45354E-01  -0.10438       0.25252E-01  -0.10051E-01
------------------------------------------------------------------------------------------------------------------------
----
   4 M          1  -0.91928E-01   0.39680E-01   0.27275E-01   0.93561E-01  -0.14421       0.24770
   8 M          2  -0.10256       0.96915E-01  -0.68633E-01  -0.12116      -0.83155E-01  -0.95596E-01
  17 M          3   0.29599E-01  -0.23428      -0.16187       0.63002E-01   0.37668E-01   0.17964
  24 M          4  -0.10595       0.15275       0.18160       0.26827E-01  -0.17919E-01   0.58868E-01
  28 M          5   0.79228E-01   0.15725      -0.55595E-01   0.83241E-01  -0.57971E-01   0.53885E-01
  35 M          6   0.81567E-01   0.35956E-01  -0.92267E-01   0.11856      -0.12823       0.57057E-01
  44 M          7  -0.11714      -0.59156E-01   0.40322E-02   0.18146E-01   0.48916E-01   0.90746E-01
  48 M          8   0.15262       0.10873      -0.54545E-01  -0.81267E-01  -0.22619       0.67564E-01
  52 M          9   0.69235E-01   0.61581E-02  -0.16535       0.18279       0.76814E-02   0.13968
  57 M         10  -0.13991       0.67379E-01   0.63480E-01   0.47421E-01   0.34102E-01   0.83913E-01
  61 M         11  -0.19063      -0.79652E-01  -0.38649E-01  -0.87540E-01  -0.11894       0.14750
  70 M         12   0.83159E-01  -0.29276E-01  -0.30701E-01   0.58335E-01  -0.83881E-01  -0.24255
  77 M         13  -0.19590       0.36057E-01   0.13140E-01   0.47300E-01  -0.16766E-01  -0.12365
  81 M         14  -0.13365       0.16341E-01  -0.86702E-01   0.11131      -0.46746E-01  -0.11922E-02
  88 M         15  -0.46094E-01   0.15130       0.61560E-01  -0.48045E-01   0.21512E-01   0.16035
  97 M         16  -0.51927E-01  -0.26884E-01   0.60821E-01  -0.13967       0.16097      -0.37447E-01
 101 M         17   0.23240E-01   0.81412E-01   0.82765E-01  -0.32815E-01   0.19350       0.58425E-02
 105 M         18  -0.20654      -0.29079E-01  -0.11241E-01  -0.24746      -0.52891E-02   0.30200E-01
 110 M         19   0.29221      -0.46160E-01  -0.70521E-01   0.12304       0.66344E-01  -0.14693
 114 M         20   0.36292E-01   0.93010E-01  -0.96150E-01  -0.82926E-03   0.20641       0.78165E-01
 123 M         21  -0.46725E-01   0.93052E-01   0.10393      -0.10907       0.18743      -0.16819E-01
 130 M         22  -0.13729      -0.24463E-01   0.99535E-02   0.68478E-01  -0.67785E-01   0.85359E-01
 134 M         23  -0.14317      -0.55198E-01   0.49572E-01  -0.15739       0.11348E-01   0.22580E-02
 141 M         24   0.19999       0.24586E-01   0.13481       0.77058E-01  -0.82821E-01  -0.29127E-03
 150 M         25   0.10451      -0.63975E-01  -0.17732      -0.20480E-01   0.77178E-01   0.21776E-02
 154 M         26   0.16607       0.67685E-02  -0.22459E-01   0.10696       0.40173E-01  -0.10381
 158 M         27  -0.27461E-02   0.84410E-03   0.82356E-02   0.86418E-01  -0.24673E-01  -0.17641
 163 M         28  -0.15883       0.21775       0.27277E-01   0.22017E-01   0.20957      -0.11683
 167 M         29  -0.18861      -0.28432E-01   0.13081      -0.12942E-01   0.54099E-01   0.99963E-01
 176 M         30   0.43170E-01   0.70506E-01   0.15967       0.15086      -0.40722E-01  -0.18529
 183 M         31   0.65641E-01   0.84376E-01  -0.11034      -0.34982E-01  -0.17180       0.84269E-02
 187 M         32  -0.16504E-01   0.62193E-01  -0.98804E-01  -0.40226E-01  -0.26728E-01  -0.18489
 194 M         33   0.11109E-01   0.10519      -0.18902       0.18901E-01  -0.18270E-01  -0.25872
 203 M         34   0.15715       0.52809E-01   0.17128       0.33408E-01  -0.11524       0.11634
 207 M         35   0.11313      -0.26398E-01  -0.29406E-01   0.25479E-01   0.17850E-01  -0.12605
 211 M         36  -0.68435E-01  -0.18432E-02  -0.25366E-01   0.45790E-01  -0.10403      -0.24333
------------------------------------------------------------------------------------------------------------------------
HBSB                                                          "MAD" Version: 8.9/0     Run: 10/08/95
17.14.43
Corrector strengths (before correction) for beam line EUTERPE                                              page
 1
------------------------------------------------------------------------------------------------------------------------
----
                              horizontal                                  vertical
Correctors used:              0 (of      20)                              0 (of      20)
Maximum strengths:            0.000000 mrad at              [    0]       0.000000 mrad at              [    0]
R.m.s. strengths:             0.000000 mrad                               0.000000 mrad
------------------------------------------------------------------------------------------------------------------------
HBSB                                                          "MAD" Version: 8.9/0     Run: 10/08/95
17.14.43
Orbit and dispersion at monitors (before correction) for beam line EUTERPE                                 page
 1
------------------------------------------------------------------------------------------------------------------------
----
                              horizontal                                  vertical
Orbit monitors used:          36                                          36
Dispersion monitors use       36                                          36
Total monitors:               36                                          36
Minimum dispersion:           -0.133637 m  at M             [   36]       -0.171994 m  at M             [   16]
Maximum dispersion:            0.479969 m  at M             [   33]        0.167573 m  at M             [   20]
R.m.s. dispersion:             0.232591 m                                  0.063519 m
Minimum readings:             -3.458692 mm at M             [   36]       -4.295654 mm at M             [   20]
Maximum readings:              6.657272 mm at M             [   18]        4.338627 mm at M             [   16]
R.m.s. readings:               2.096277 mm                                 2.086537 mm
------------------------------------------------------------------------------------------------------------------------
HBSB                                                          "MAD" Version: 8.9/0     Run: 10/08/95
17.14.43
Corrector strengths (after correction) for beam line EUTERPE                                               page
 1
------------------------------------------------------------------------------------------------------------------------
----
Number  name   occur.     position      xcorr         ycorr         betx          bety          mux           muy
effect
                         [m]           [mrad]        [mrad]        [m]           [m]           [2*pi]        [2*pi]
------------------------------------------------------------------------------------------------------------------------
----
```

```
  12  K        1     3.279000    -0.069611     0.866792     2.719596     3.374594     0.445290     0.234413
  22  K        2     4.292000    -0.405492     0.293309     1.410731     4.684111     0.503618     0.288091
  30  K        3     5.708000     0.266899    -0.794009     1.410731     4.684111     0.779061     0.329313
  40  K        4     6.721000    -0.265828     1.275964     2.719596     3.374594     0.837390     0.382991
  53  K        5    10.000000    -0.029059    -0.115756    23.802882     0.475078     1.282680     0.617404
  65  K        6    13.279000    -0.114163     0.194668     2.719596     3.374594     1.727969     0.851818
  75  K        7    14.292000     0.320548     0.231220     1.410731     4.684111     1.786298     0.905496
  83  K        8    15.708000    -0.141358    -0.292890     1.410731     4.684111     2.061741     0.946718
  93  K        9    16.721000    -0.111658     0.198549     2.719596     3.374594     2.120069     1.000395
 106  K       10    20.000000     0.080543    -0.006840    23.802882     0.475078     2.565359     1.234809
 118  K       11    23.279000    -0.234284    -0.562859     2.719596     3.374594     3.010649     1.469222
 128  K       12    24.292000     0.688095     0.748729     1.410731     4.684111     3.068978     1.522900
 136  K       13    25.708000     0.288944    -0.639231     1.410731     4.684111     3.344420     1.564122
 146  K       14    26.721000    -0.386947     0.570135     2.719596     3.374594     3.402749     1.617800
 159  K       15    30.000000    -0.173593     0.143218    23.802882     0.475078     3.848039     1.852213
 171  K       16    33.279000    -0.017813    -0.422239     2.719596     3.374594     4.293328     2.086627
 181  K       17    34.292000    -0.076586     0.206041     1.410731     4.684111     4.351657     2.140304
 189  K       18    35.708000     0.262124    -0.127313     1.410731     4.684111     4.627100     2.181527
 199  K       19    36.721000     0.269658     0.209196     2.719596     3.374594     4.685428     2.235204
 212  K       20    40.000000     0.213921     0.056034    23.802882     0.475078     5.130718     2.469618
------------------------------------------------------------------------------------------------------------------

                          horizontal                                    vertical
Correctors used:          20 (of      20)                               20 (of      20)
Maximum strengths:         0.688095 mrad at K          [   12]          1.275964 mrad at K          [    4]
R.m.s. strengths:          0.269427 mrad                                0.511925 mrad
------------------------------------------------------------------------------------------------------------------
HBSB                                                                    "MAD" Version: 8.9/0     Run: 10/08/95
17.14.43
Orbit and dispersion at monitors (after correction) for beam line EUTERPE                                    page
 1
------------------------------------------------------------------------------------------------------------------

                          horizontal                                    vertical
Orbit monitors used:      36                                            36
Dispersion monitors use   36                                            36
Total monitors:           36                                            36
Minimum dispersion:       -0.015700 m  at M           [   27]          -0.048185 m  at M           [   20]
Maximum dispersion:        0.439284 m  at M           [   30]           0.061946 m  at M           [   16]
R.m.s. dispersion:         0.223102 m                                   0.026329 m
Minimum readings:         -0.182139 mm at M           [   19]          -0.339748 mm at M           [   28]
Maximum readings:          0.222737 mm at M           [   20]           0.248732 mm at M           [   29]
R.m.s. readings:           0.086945 mm                                  0.106893 mm
------------------------------------------------------------------------------------------------------------------
HBSB                                                                    "MAD" Version: 8.9/0     Run: 10/08/95
17.14.43
Linear lattice functions.    TWISS              line: EUTERPE          range: #S/#E

Delta(p)/p:    0.000000      symm: F            super:   1                                                   page
 1
------------------------------------------------------------------------------------------------------------------
----
     ELEMENT SEQUENCE       I              H O R I Z O N T A L                I              V E R T I C A L
pos.  element occ.     dist I   betax  alfax   mux    x(co)  px(co) Dx   Dpx  I   betay  alfay   muy    y(co)  py(co) Dy
Dpy
no.   name    no.      [m]  I   [m]    [1]     [2pi]  [mm]   [.001] [m]  [1]  I   [m]    [1]     [2pi]  [mm]   [.001] [m]
[1]
------------------------------------------------------------------------------------------------------------------
----
begin EUTERPE    1     0.000   24.457 -0.025   0.000  0.037 -0.053  0.005 0.001    0.423  0.033   0.000 -0.011  0.045
-0.012-0.008
end   EUTERPE    1    40.000   24.283 -0.015   5.136  0.037 -0.053  0.005 0.001    0.420  0.016   2.456 -0.011  0.045
-0.012-0.008
------------------------------------------------------------------------------------------------------------------
----
total length =        40.000000          Qx           =         5.135804          Qy           =         2.456410
delta(s)     =        -0.175215 mm       Qx'          =        -0.033278          Qy'          =        -0.078892
alfa         =         0.108364E-01      betax(max)   =        24.949443          betay(max)   =        12.439237
gamma(tr)    =         9.606323          Dx(max)      =         0.474810          Dy(max)      =         0.063311
                                         Dx(r.m.s.)   =         0.259781          Dy(r.m.s.)   =         0.025022
                                         xco(max)     =         0.343187          yco(max)     =         0.492176
                                         xco(r.m.s.)  =         0.129138          yco(r.m.s.)  =         0.154082
------------------------------------------------------------------------------------------------------------------
```

Fig. A.2 MAD Output file; calculations of the closed orbit distortion before and after correction for one error configuration.

Appendix B

Closed orbit distortions due to misalignments

The closed orbit distortions due to single and multiple misalignments have been determined with simulations in MAD. The effects of all single misalignments are given in part B1. The effects of multiple misalignments in the HLF mode are given in B2. The results are summarised in Chapter 3.

B1 Single misalignments

The effects of misalignments and other errors causing closed orbit distortion have been examined by simulating them with the program MAD. The Closed orbit distortions and the tune shifts are given in table B.1 to B.4.

Table B.1 The effects of single misalignments of the dipoles in the HBSB mode

Dipole	Displa-cement	x_{max} (mm)	x_{rms} (mm)	y_{max} (mm)	y_{rms} (mm)	$\Delta \nu_x$ $*10^{-5}$	$\Delta \nu_y$ $*10^{-5}$
1	dx	0.2	0.07	0	0	1	20
1	dy	0.002	0.0005	0.25	0.12	0.4	0.2
1	ds	0.73	0.25	0	0	2	80
1	dϕ	0.00001	0	0.008	0.004	0	0
1	dθ	0	0	0	0	0.1	3
1	dψ	0.002	0.0005	0.25	0.12	0.4	0.2
2	dx	0.09	0.03	0	0	0	0.1
2	dy	0.001	0.0004	0.21	0.1	0.4	0.1
2	ds	0.32	0.13	0	0	0.4	1
2	dϕ	0	0	0.003	0.002	0	0
2	dθ	0.00001	0	0	0	0.4	0
2	dψ	0.001	0.0004	0.21	0.1	0.4	0.2

The closed orbit distortions reach their maximum values at the long straight sections.

For the single displacements of the dipoles it is important to know how the displacement errors are defined. In MAD all displacement errors are assigned at the entrance of each element. In a dipole the electron-orbit is bent; the comoving reference frame rotates with the orbit. As a result, displacements assigned at different positions describe different misalignments.

In table B.1a the closed orbit distortions are calculated for single misalignments in the s'- and x'-directions (these are the s- and x-directions in the middle of the dipoles). In this new reference frame the influence of a single displacement in the x'-direction is nihil (compare this with the effects of a displacement dx), the influence of a displacement in the s'-direction is about 3 % bigger than for a displacement in the s-direction.
The rotational directions ϕ', θ' and ψ' in the middle of the dipoles also differ from the rotational directions ϕ, θ and ψ. The influence of the rotation of the reference frame on the closed orbit distortion is limited (a few percent for $d\psi$) and the correlation between the two reference frames complex; the single misalignments $d\phi'$, $d\theta'$ and $d\psi'$ have not been simulated.

Table B.1a *Single misalignments of the dipole with the displacements defined with respect to the middle of the dipole (mode HBSB)*

Dipole	Displa-cement	x_{max} (mm)	x_{rms} (mm)	y_{max} (mm)	y_{rms} (mm)	$\Delta \nu_x$ $*10^{-5}$	$\Delta \nu_y$ $*10^{-5}$
1	dx'	0.00007	0.00002	0	0	0	0
1	ds'	0.77	0.26	0	0	2	78
2	dx'	0.00003	0.00001	0	0	0	0
2	ds'	0.34	0.13	0	0	0.4	1

Table B.2 *The effects of single misalignments of the dipoles in the HLF mode*

Dipole	Displa-cement	x_{max} (mm)	x_{rms} (mm)	y_{max} (mm)	y_{rms} (mm)	$\Delta \nu_x$ $*10^{-5}$	$\Delta \nu_y$ $*10^{-5}$
1	dx	0.02	0.008	0	0	0.4	0.2
1	dy	0.0002	0.0001	0.22	0.12	0.2	0
1	ds	0.06	0.03	0	0	1	1
1	$d\phi$	0	0	0.004	0.002	0	0
1	$d\psi$	0.002	0.0005	0.23	0.12	0.2	0

2	dy	0.00006	0.00003	0.12	0.06	0.1	0
2	ds	0.14	0.07	0	0	0	0.1
2	dψ	0.00007	0.00004	0.12	0.06	0.1	0

B.1.2 Single misalignments of the quadrupoles

The beam parameters are calculated for the situation in which all magnetic elements are perfectly aligned, with the exception of one quadrupole, which is misaligned in one direction. The EUTERPE-ring has 4 superperiods each containing 8 quadrupoles. Because each superperiod is symmetric, there are only 4 independent quadrupoles, with different strengts.

The effects of misalignments in de x- and y-directions and rotations around the y-axis have the largest influence on the closed orbit. The influence of single displacements in the s-direction and rotations around the s-axis are nihil. In table 2 only the effects of the most important misalignments are given.

In the HBSB-mode the effects of misalignments of the first three quadrupoles on the closed orbit distortion are comparible, the effects of misalignments of the fourth quadrupole are several times smaller. In the HLF-mode the closed orbit distortion is the least sensitive to misalignments of the second quadrupole. Comparing the effects of misalignments for the two different modes, we see that the closed orbit distortions in the HLF-mode are an order of magnitude smaller than in the HBSB-mode.

Table B.3 The effects of single misalignments of the quadrupoles in the HBSB mode

Quadru - pole	Direc- tion	x_{max} (mm)	x_{rms} (mm)	y_{max} (mm)	y_{rms} (mm)	$\Delta \nu_x$ $*10^{-4}$	$\Delta \nu_y$ $*10^{-4}$
Q1	dx	3.4	1.2	0	0	25	1
Q1	dy	0.004	0.001	0.38	0.18	0.1	0.1
Q1	ds	0	0	0	0	0.1	3
Q1	dϕ	0.00008	0.00003	0.05	00.03	0	0
Q1	dθ	0.46	0.16	0	0	4	0.1
Q1	dψ	0	0	0	0	0	0
Q2	dx	2.0	0.7	0	0	27	2
Q2	dy	0.01	0.01	0.65	0.32	0.1	0.2
Q2	dϕ	0.0002	0.0001	0.09	0.04	0	0
Q2	dθ	0.25	0.09	0	0	3	0.2

Q3	dx	2.6	0.9	0	0	34	6
Q3	dy	0.007	0.002	0.48	0.24	0.1	0.2
Q3	dϕ	0.0001	0.00005	0.07	0.03	0	0
Q3	dθ	0.36	0.12	0	0	4	0.6
Q4	dx	0.46	0.16	0	0	3	1
Q4	dy	0.0007	0.0002	0.16	0.08	0.01	0.02
Q4	dϕ	0.00001	0	0.02	0.01	0	0
Q4	dθ	0.06	0.02	0	0	0.5	0.2

Table B.4 The effects of single misalignments of the quadrupoles in the HLF mode

Quadru - pole	Direc- tion	x_{max} (mm)	x_{rms} (mm)	y_{max} (mm)	y_{rms} (mm)	$\Delta \nu_x$ $*10^{-5}$	$\Delta \nu_y$ $*10^{-5}$
Q1	dx	0.17	0.08	0	0	5	2
Q1	dy	0.00008	0.00003	0.1	0.05	0.2	1
Q1	dθ	0.02	0.01	0	0	5	2
Q2	dx	0.05	0.02	0	0	0.4	1
Q2	dy	0.00001	0	0.04	0.02	0.8	0.5
Q2	dθ	0.07	0.03	0	0	0.6	0.6
Q3	dx	0.15	0.9	0	0	0.4	2.4
Q3	dy	0.0001	0.00006	0.02	0.01	0.2	0.8
Q3	dθ	0.02	0.01	0	0	0.7	0
Q4	dx	0.38	0.18	0	0	0.6	2
Q4	dy	0.0004	0.0001	0.3	0.15	5	0.6
Q4	dθ	0.05	0.02	0	0	0.3	3

B.2.1 Summary of the effects of single misalignments

The simulations show that the closed orbit is most sensitive for misalignments of the quadrupoles in the horizontal direction. The single misalignment of the first quadrupole $\Delta x = 0.1$mm results in a maximum

closed orbit distortion of x_{co} = 3 mm; the resulting closed orbit distortion is 30 times as large as the displacement. The closed orbit is also very sensitive for dipole displacements along the electron trajectory (with respect to the middle of the dipole). The main contributions to the vertical distortion come from the displacements of the quadrupoles and the dipole in the vertical direction and rotations of the quadrupoles around the y-axis and the dipoles along the s-axis.
The closed orbit in the HLF mode is sensitive for similar displacements. However the resulting distortions are about 10 times smaller in the HLF mode due to the weaker focusing.

B.2 The effects of multiple misalignments on the closed orbit

The effects of multiple misalignments of all elements in the HLF-mode are given in table B.5.
For all calculations with multple misalignments the first address read from the gaussian table in MAD is: Eopt = 123456789. All random errors are read from the table; each consequetive error read from the consequetive address. In chapter 3 the effects of multiple misalignments on the closed orbit in the HBSB mode are discussed. The maximum values of the closed orbit distortion averaged over 10 runs are given in table B.5.

Table B.5 *Effects of multiple displacements (σ=0.1mm and σ=0.1mrad) on the closed orbit distortion (mode HLF).*

Displacement	x_{max} (mm)	y_{max} (mm)
All dipoles	2 ± 0.5	1.3±0.6
All quads	12 ± 5	2.9±0.8
All sextupoles	0.012 ±0.004	0.003 ±0.001
All elements	12 ± 7	5±2

The effects of multiple misalignments in the HLF mode are given in B.6. The results in table B.5 show that the effects of multiple alignments in the HLF mode are about 2 times smaller in the vertical and about 10 times smaller in the horizontal direction than in the HBSB mode.

Table B.5 *Effects of multiple displacements (σ=0.1mm and σ=0.1mrad) on the closed orbit distortion (mode HLF).*

Displacement	x_{max} (mm)	x_{rms} (mm)	y_{max} (mm)	y_{rms} (mm)	$\Delta \nu_x$ $*10^{-2}$	$\Delta \nu_y$ $*10^{-2}$
All dipoles	0.3±0.1	0.12±0.5	1.0±0.2	0.4±0.2	0.008 ± 0.006	0.01 ± 0.01
All quads	1.0±0.5	0.5±0.2	1.3±0.4	0.5±0.2	0.04 ± 0.03	0.04 ±0.03
All sextupoles (σ=0.2mm,mrad)	0.004 ±0.002	0.002 ±0.0004	0.006 ±0.003	0.0016 ±0.0005	0.16 ±0.07	0.3 ± 0.2
All elements	1.2±0.6	0.6±0.3	1.5±0.5	0.65±0.2	0.05 ±0.02	0.2 ±0.06

Appendix C Closed orbit correction

The closed orbit distortion in the vertical direction is shown after correction. Furthermore the values of several beam parameters are compared before and after correction.

The closed orbit distortion after correction is calculated for several lattices with different error configurations. The 'random' displacements assigned to the magnetic elements are again read from the gaussian table in MAD. The first errors in the consequetive runs were read from respectively address 123456789, address 223456789, address 323456789, address 423456789, address 523456789, address 623456789, address 723456789, address 823456789, address 923456789 and address 933456789. This way the errors assigned to the magnetic elements were equal for every correction lattice.

C1 The closed orbit distortion in the vertical direction after correction

The closed orbit distortion in the HBSB mode in the vertical direction has been determined after correction with the second lattice in §4.2.1. The monitor locations in this lattice are reversed with the corrector locations with respect to the standard lattice. Although the vertical distortion is 'only' reduced with a factor 8, the difference between the distortion before and after correction is very large, see fig. C.1.

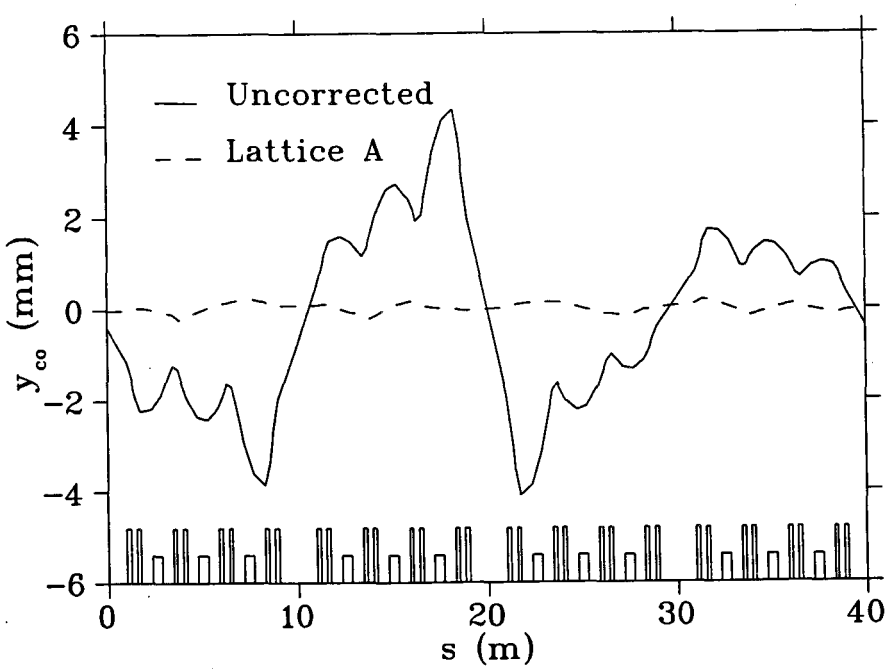

Fig. C.1 The closed orbit distortion in the vertical plane before and after correction in the HBSB mode.

C2 The effects of the closed orbit correction on other beam parameters

Many beam parameters have been calculated with the simulations (see appendix A); the values of the chromaticity, the dispersion and the betatron amplitude are compared in this paragraph for the ideal lattice and the lattice with all elements misaligned before and after correction with all sextupoles used as corrector magnets, lattice C described in §4.2.3.

The chromaticity and betatron amplitude are increased as a results of the misalignments. However the chomaticity remains small; the momentum spread of $\Delta p/p \approx 0.04\%$ under normal circumstances results in a tune shift of less than $\Delta\nu < 5.10^{-4}$, which is negligible on the total tune shift. The maximum beam width is proportional to $\beta^{-1/2}$ and is ca 10 % increased due to the misalignments; 5 % of this increase in the maximum beam width is eleminated after correction.
The change in the dispersion due to the misalignments is very small.

Table C.1 The chromaticity, dispersion and betatron amplitude in the ideal, the distorted and corrected lattice.

Parameter	Ideal lattice	All elements misaligned	Closed orbit correction with lattice D
Chromaticity ξ_x	0	0.4 ± 0.4	0.05 ± 0.04
ξ_y	0	---[1]	0.4 ± 0.2
Dispersion $(D_x)_{rms}$	0.257	0.268 ± 0.008	0.259 ± 0.003
$(D_y)_{rms}$	0	0.04 ± 0.02	0.02 ± 0.01
Betatron function $\beta_{x\,max}$ (m)	23.8	29 ± 2	25 ± 1
$\beta_{y\,max}$ (m)	11.1	---[1]	18 ± 5

Horizontal chromaticity reduced with a factor 8, Horizontal betatron amplitudes reduced with about 20 %. The dispersion is within 1% constant for the three lattices.

The dispersion function after correction is shown in fig. E.2.

[1] For 6 out of 10 error configurations the vertical betatron oscillations were unstable; the vertical betatron amplitudes and vertical chromaticity are not known for these runs and are therefore not given.

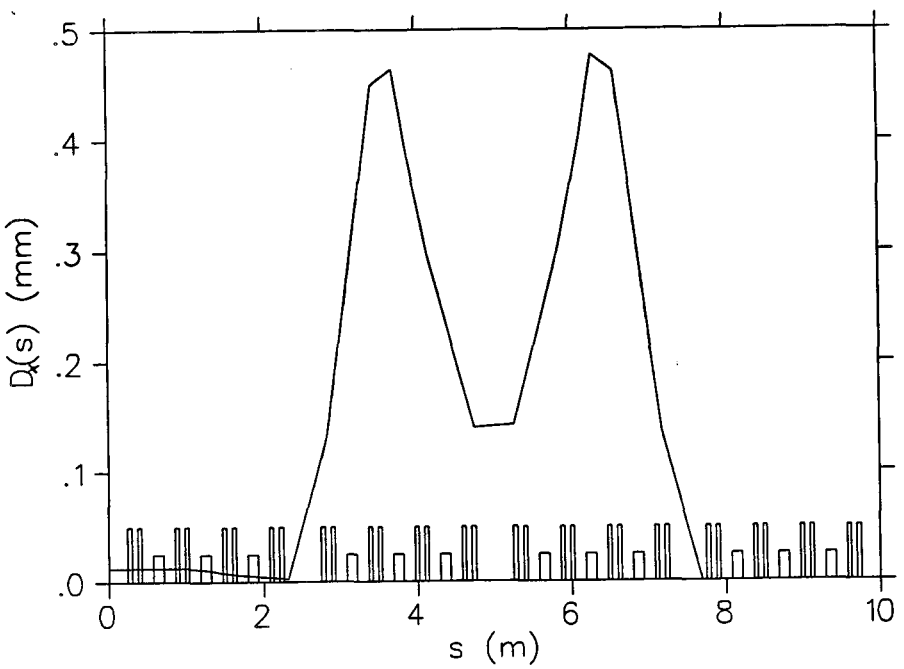

Fig. C.2 The dispersion in the HBSB mode after correction.

Appendix D Mechanical drawings of the designed sextupole and corrector magnet.

The drawings of the EUTERPE sextupole and window corrector magnet, which are constructed at the Design and Construction Facility (CTD) of the TUE, are given.

D1 The sextupole

The mechanical drawings of the prototype sextupole magnet are depicted below. Furthermore the currents through the coils of the sextupoles used as horizontal and vertical corrector are shown. Finally the inductance in the coils is calculated.

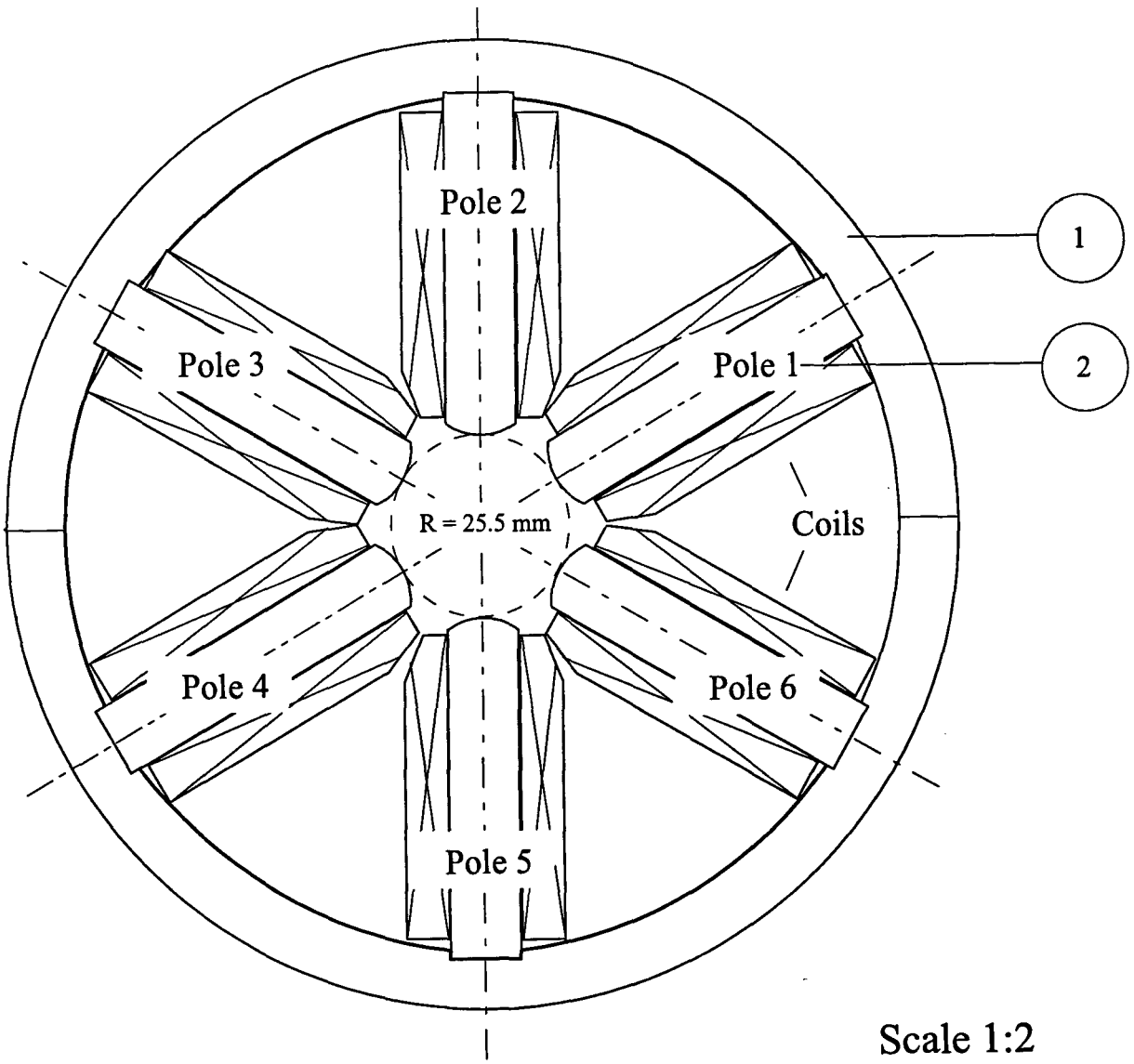

Side view sextupole

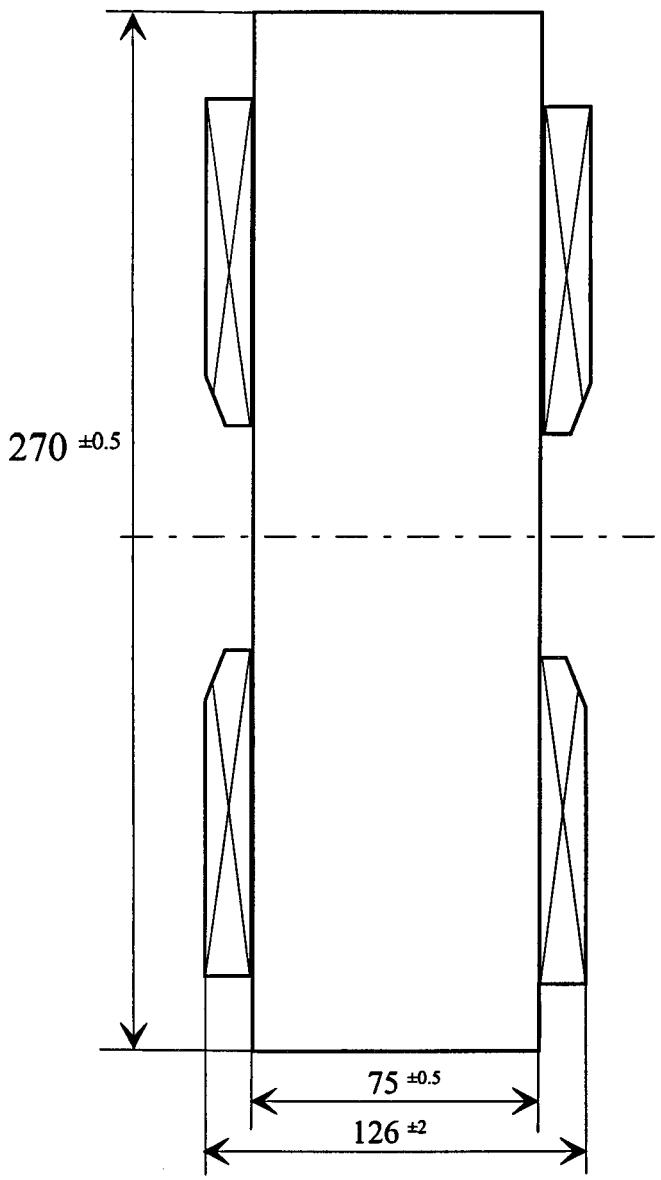

Note, for simplicity only the coils around pole 2 and 5 are drawn

1 Yoke

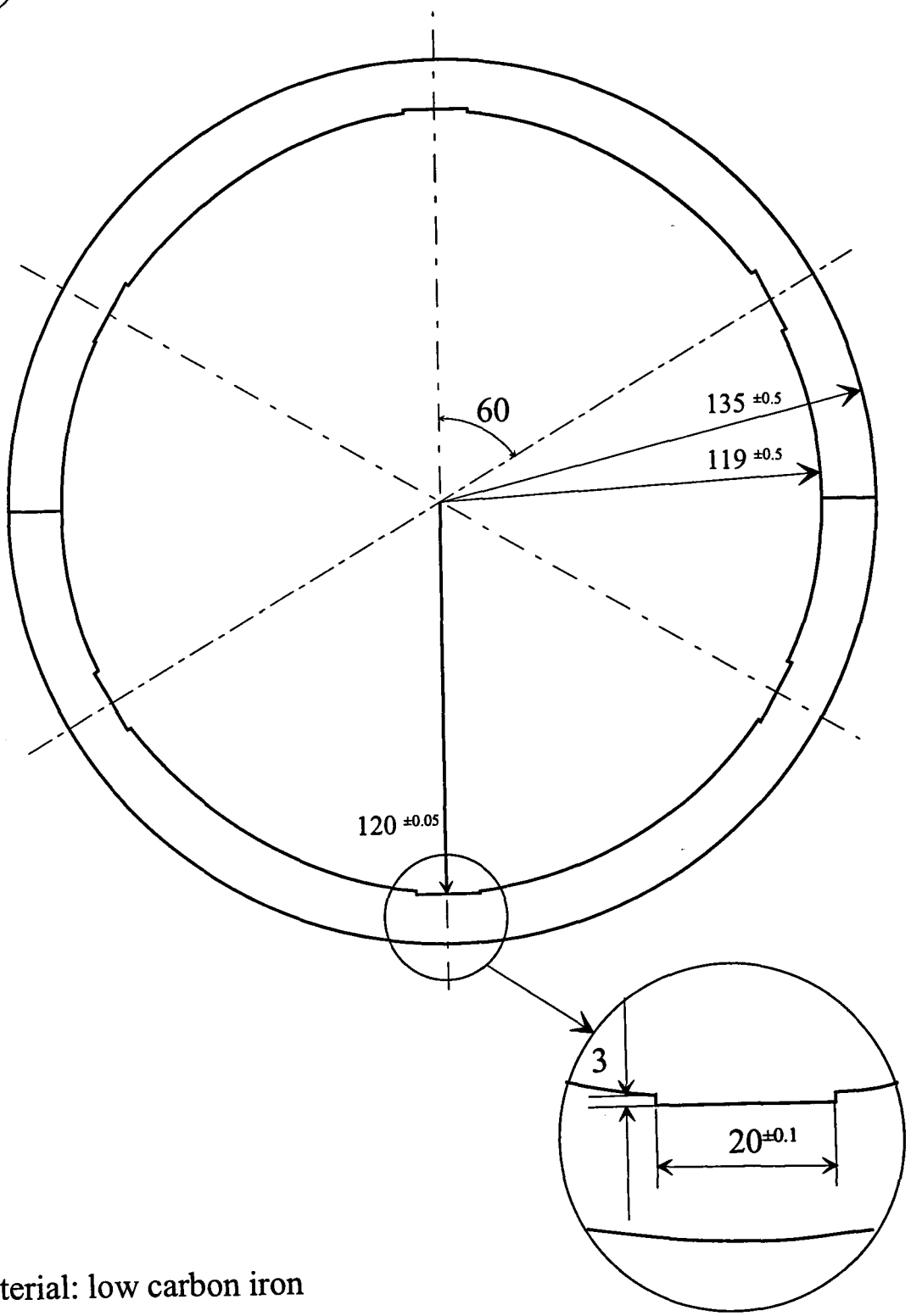

Material: low carbon iron

Scale 1:2

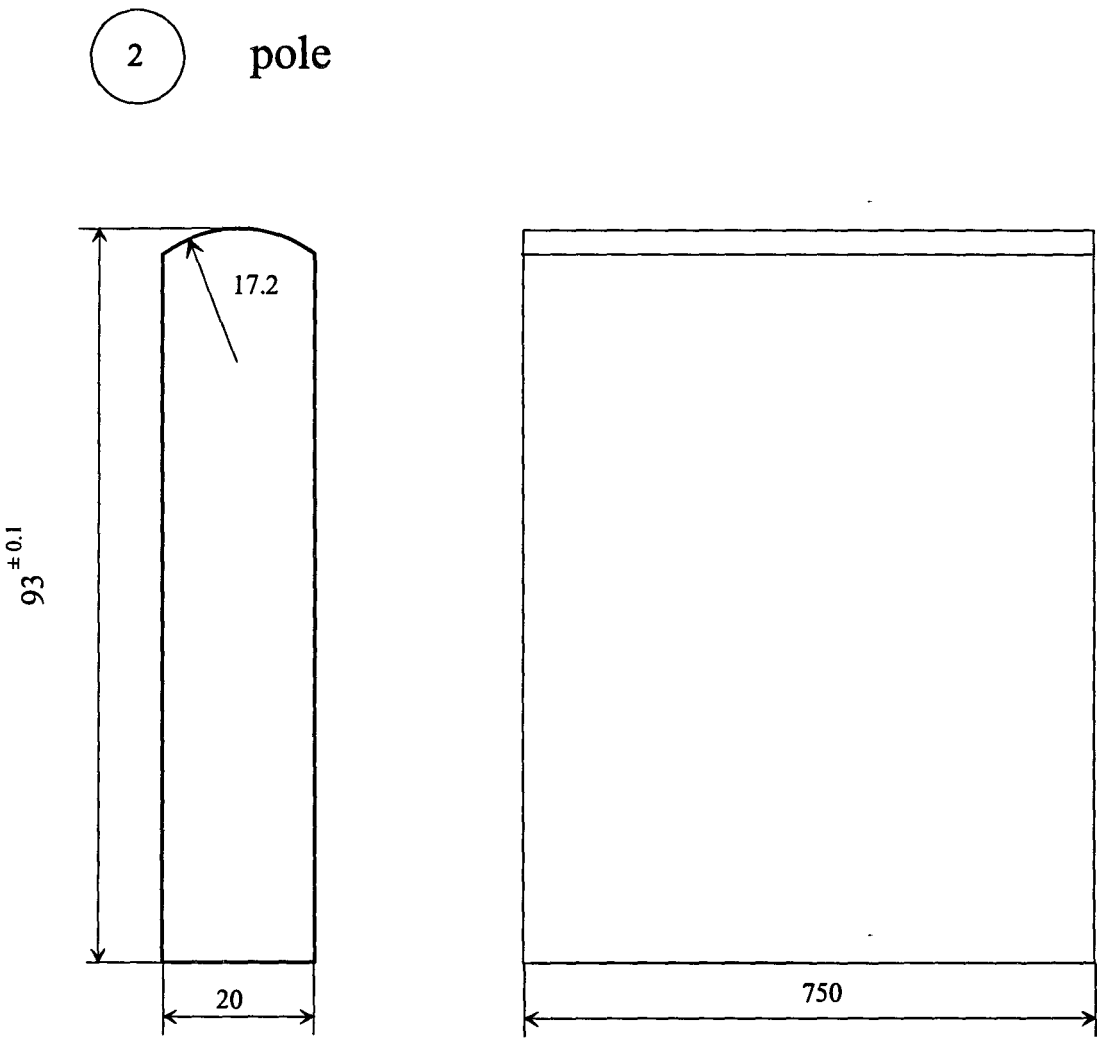
2
pole
17.2
$93^{\pm 0.1}$
20
750

Currents through the coils

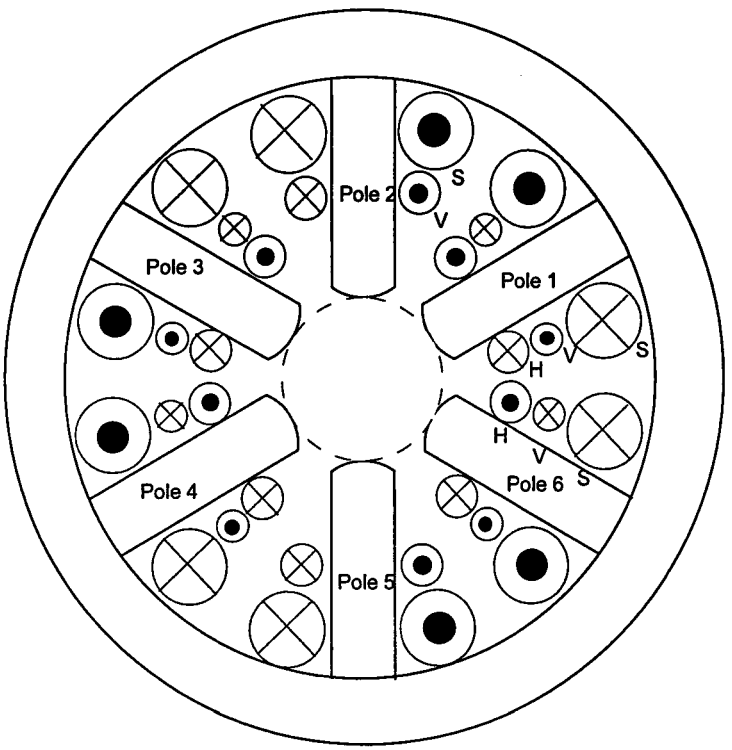

Generated fields

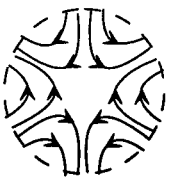

Sextupole field

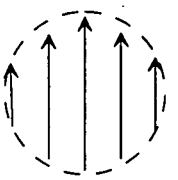

Vertical Dipole field

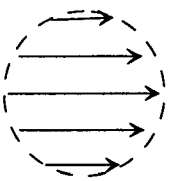

Horizontal Dipole field

The fields shown on the right are generated with the assigned currents through the coils.

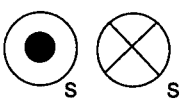

Currents for the generation of the sextupole field

Currents for the generation of the vertical dipole field

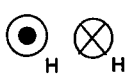

Currents for the generation of the horizontal dipole field

The figure shows that the currents throught the coils around opposite poles are always equal. However the polarity of opposite poles is reversed; if pole 1 is a magnetic N-pole, pole 4 is a S-pole.
The total currents through the coils is superposition of the required currents for the generated fields.

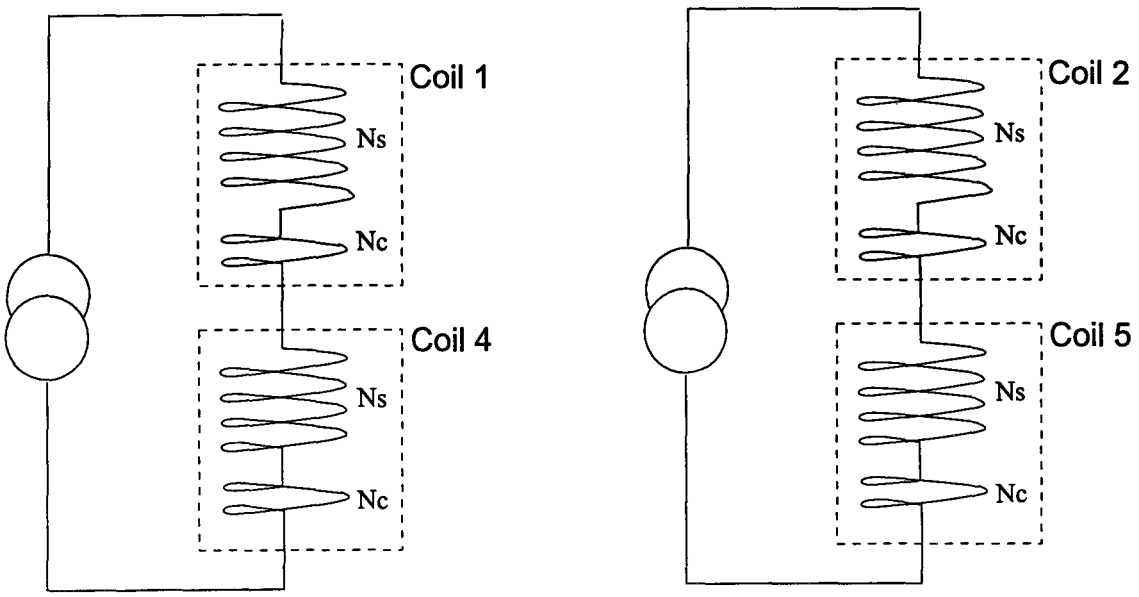

The electric circuit for the coils around pole 3 and 6 is similar.

Ns = 268 turns
Nc = 100 turns
Ntot = 368 turns,
Imax = 7 A

NI = 2576 A.turns (max)

D2 The window-frame corrector magnet

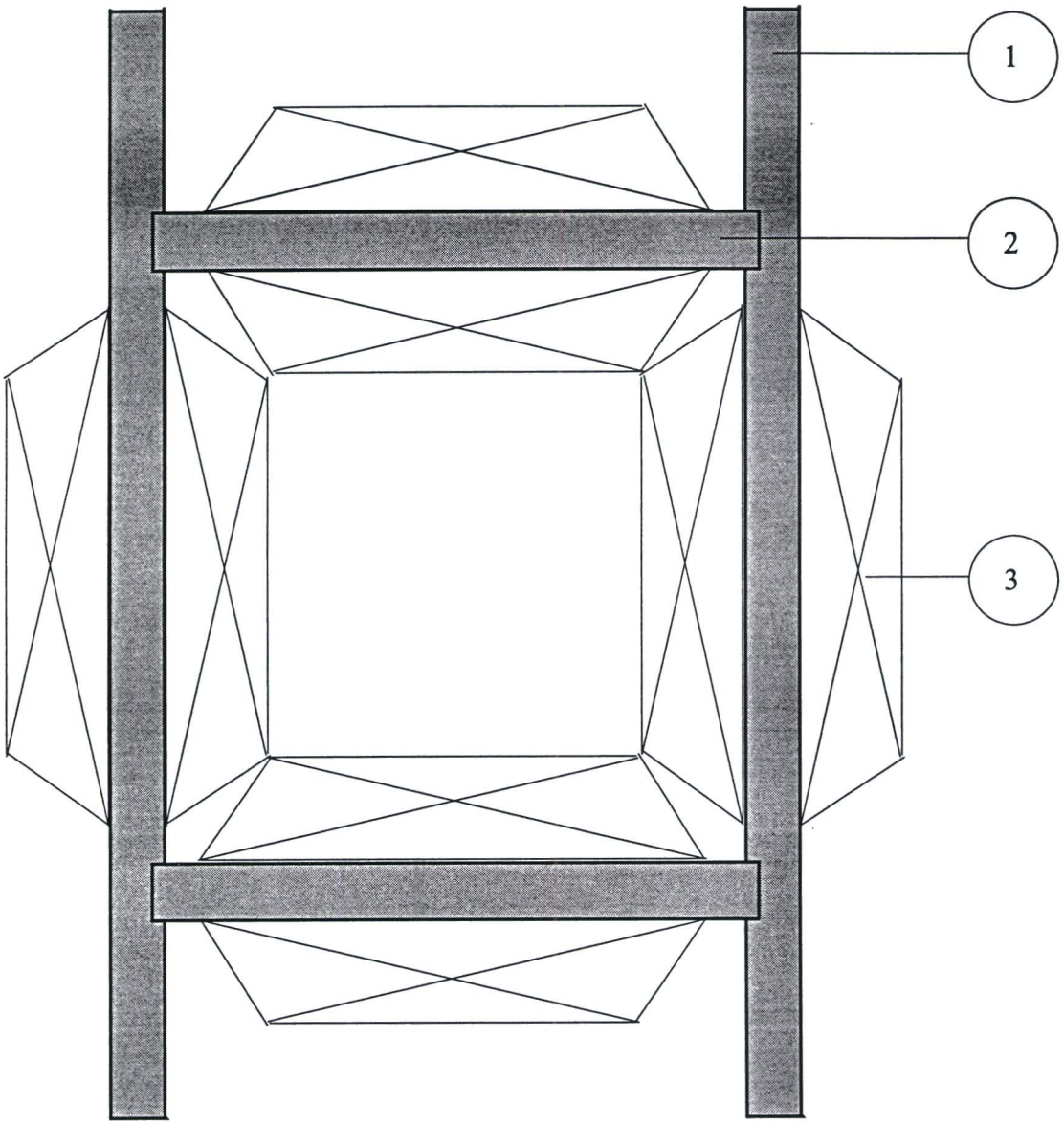

3 Coils:

182 turns 2.5x1.5 mm
NI = 1274 A.turns (max)
No cooling.

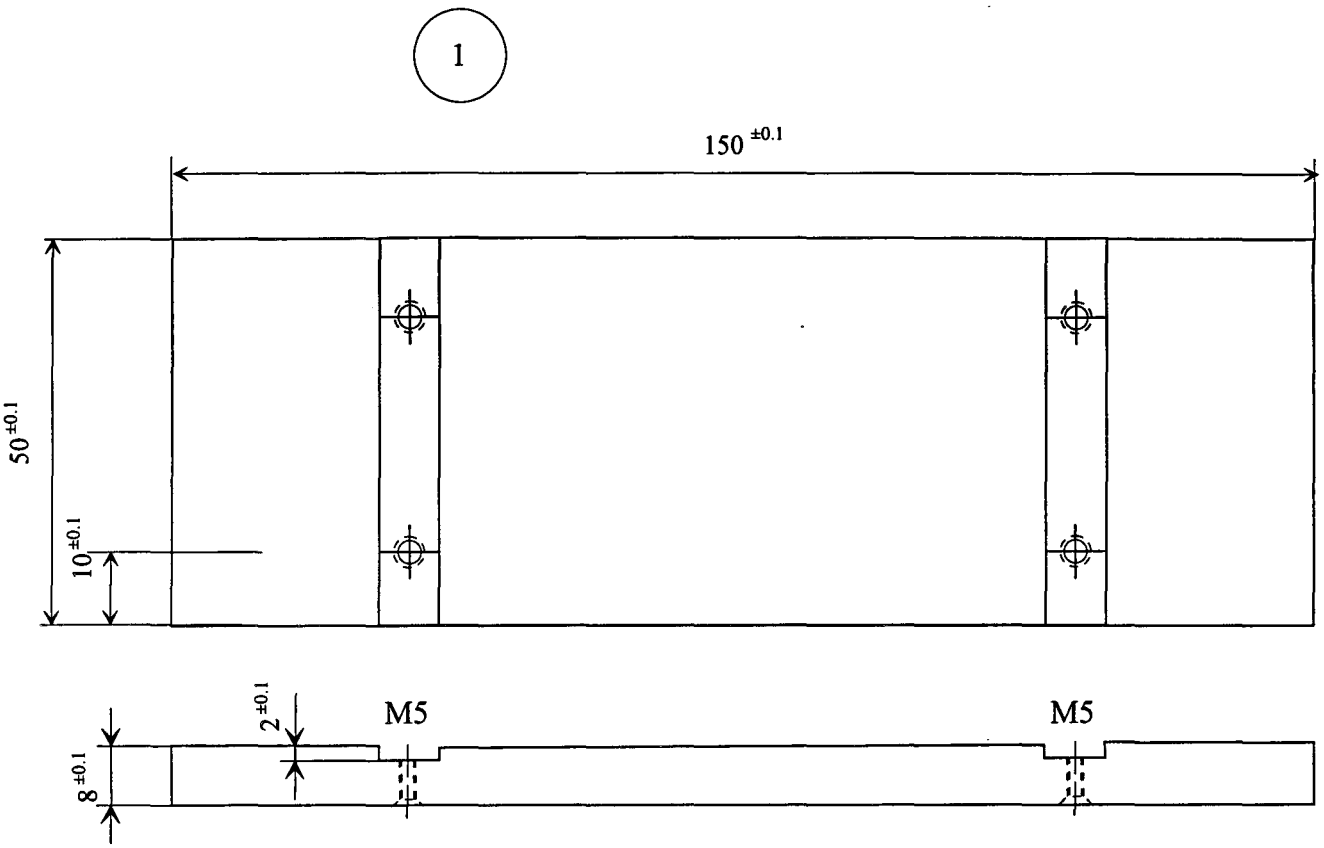

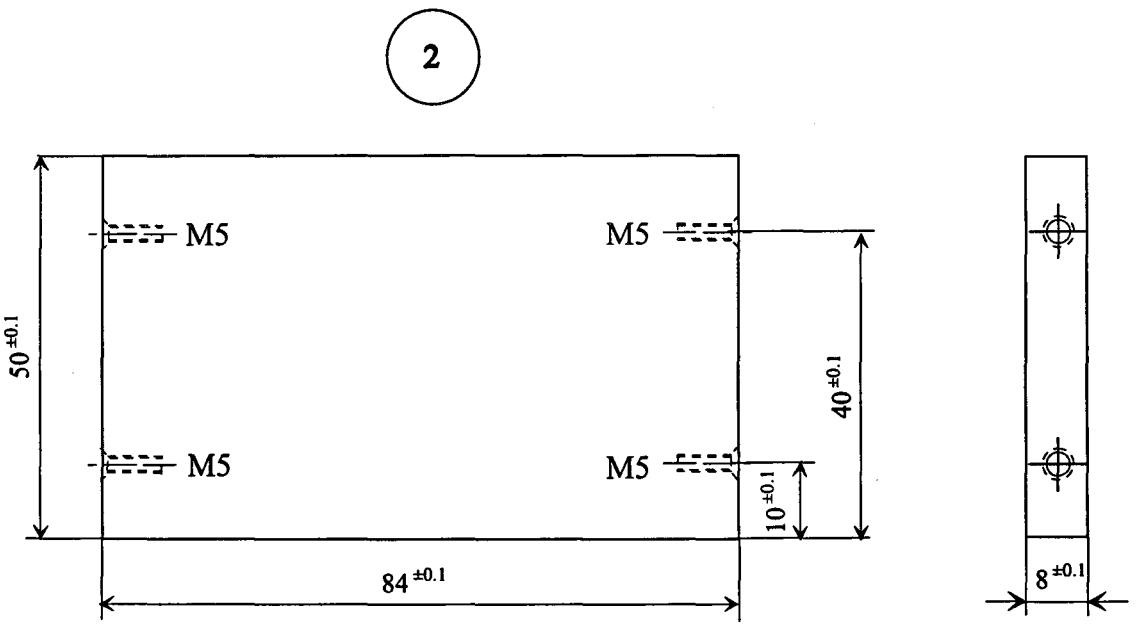

Material: Steal 35

Scale 1:1

D3 The time constant of inductance

Due to the inductance in the coils it takes a finite time to induce the sextupole field. The time constant τ of the inductance is given by [Mon85]:

$$\tau = \frac{L}{R},$$

with L the inductance of the coil and R the resistance. The inductance depends on the number of turns per circuit N, the flux ϕ and the current I through the wire according to

$$R = \rho \frac{l}{A}.$$

The resistance of the coil is dependent on the total length of the wire l, the resistance of the conduction material ρ and the conductive area A

$$L = N \frac{\phi}{I}.$$

Using these formulas the time constants of the window frame corrector magnet and the sextupole are calculated. The value of all parameters used in the calculation are given below.
The time constants are equal to τ=0.1s for the sextupole and $\tau \approx$ 1ms for the window frame corrector magnet. Both time constant are negligible in comparison to the time it takes to accelerate the electrons from 75 MeV to 400 MeV.

Specifications wire	
Material cupper	$\rho = 1.7.10^{-8}\Omega$m
Conductive area	$A = 2.5$x1.5 mm^2
Maximum current	$I_{max} = 7$A

	Sextupole	Window frame
Total number of turns through one circuit	$N = 744$	$N = 182$
Total length	$l \approx 200$ m	$l \approx 70$ m
Maximum magnetic flux	$\phi \approx 1.10^{-3}$ Tm^2	$\phi \approx 1.10^{-4}$ Tm^2
Total resistance per circuit	$R \approx 1\Omega$	$R \approx 0.3\Omega$
Inductance	$L \approx 0.1$ H	$L \approx 3$ mH
Time constant	$\tau \approx 0.1$ s	$\tau \approx 1$ms

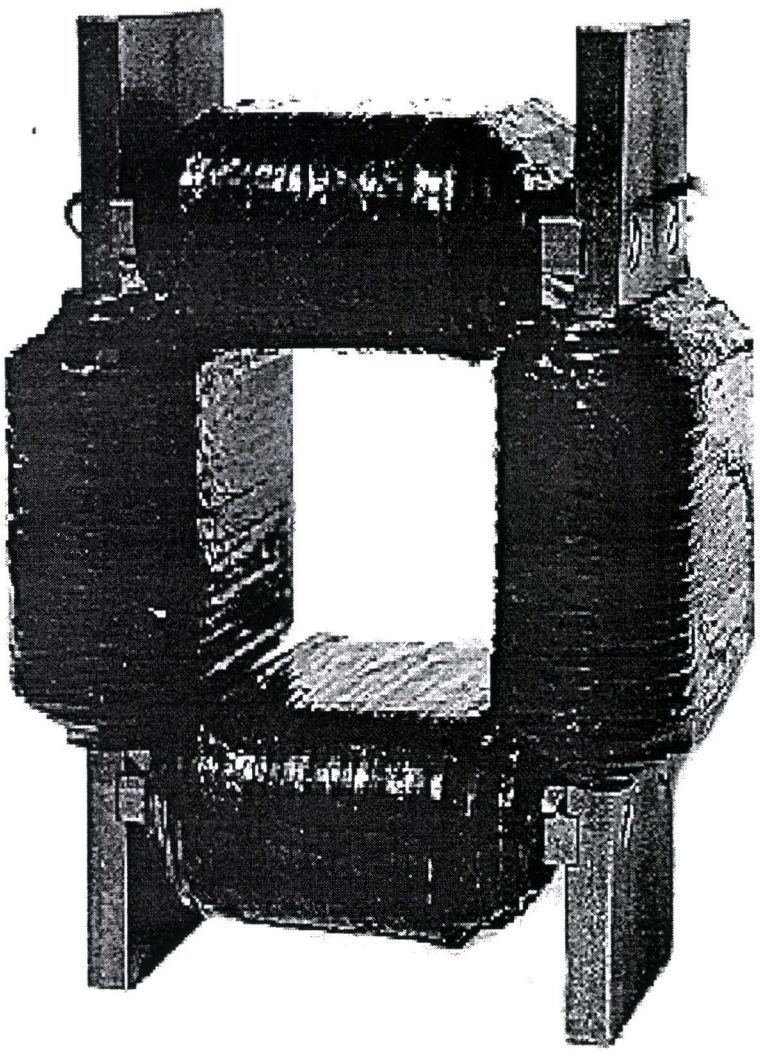

Appendix E Field measurements

The magnetic induction in the prototype window frame corrector magnet is measured using a Hall-probe (SIEMENS, model SVB613) attached to a xy-table. A step motor is used to position the X-Y table. A control/interface unit is used for the reading of the Hall voltage and the steering of the X-Y table. Some general characteristics of the measurement system are listed in table E.1 [Web94].

Table E1 Specifications of the Hall probe used for the measurements of the induction

Size	1 x 1 mm^2
Absolute position accuracy	1 mm
Relative position accuracy	0.05 mm
Stability	10^{-4}
Temp. effect of Hall probe	$< 10^{-4}/°C$

The Hall-probe has been calibrated with a Nuclear Magnetic Resonance coil in the range of $-0.25T < B < 0.25T$. With a third order polynomal the induction in the Hall probe was fitted. The residue inductions were smaller than 2G. Higher order components yield no significant reduction of the residues.

Appendix F Poisson

With the program Poisson, the field profiles in the magnets have been calculated. In this appendix the derivation of the Poisson equation is given, and the use of the program is described.

F1 Derivation of the Poisson equation

For the calculation of the magnetic induction in a static situation only two Maxwell-equations are relevant:

$$\nabla . B = 0$$
$$\text{and} \quad \nabla \times H = J, \qquad H = \frac{B}{\mu_0 \mu_r}. \tag{F.1}$$

In these equations B is the magnetic induction, H the magnetic field strength, J is the current-density, μ_0 the magnetic permeability in vacuum and μ_r the relative magnetive permeability.

If no currents are present in the region of interest, then J=0 and H can be described as the gradient of a potential ϕ: $B=\nabla\phi$. ϕ is called the magnetic scalar potential. Using this equality in the first part of formula (2.16) the Poisson equation is found:

$$\nabla^2 \phi = 0 \tag{F.2}$$

Assuming ϕ is locally constant along the magnetic axis (e.g. in a long magnet or due to symmetries) equation (2.17) is reduced to a two-dimensional problem. Solving this equation in cylindrical coordinates and throwing all singular solutions away, the equation for the potential becomes

$$\phi = \sum_{n=1}^{\infty} (J_n r^n \cos n\theta + K_n r^n \sin n\theta). \tag{F.3}$$

The induction is the derivative of the potential

$$B_r = \sum_n \left(\frac{j_n}{(n-1)!} r^{n-1} \cos n\theta + \frac{k_n}{(n-1)!} r^{n-1} \sin n\theta \right)$$
$$\text{and} \quad B_\phi = \sum_n \left(-\frac{j_n}{(n-1)!} r^{n-1} \sin n\theta + \frac{k_n}{(n-1)!} r^{n-1} \cos n\theta \right). \tag{F.4}$$

The components j_n and k_n in the equation above represent the multipole coefficients. The components with n=0 correspond to a dipole-field, the components n=1 to a quadrupole-field, etc. In general magnets are designed for the introduction of one harmonic; in that case all other harmonic components represent error-fields. The expression of field errors in harmonic components is called harmonic analysis.

The components j_n represent the skew components, which are equal to zero if the elements have a normal orientation and are perfectly aligned. The orientation of the elements is defined to be normal if the induction is perpendicular to the horizontal axis.

The cylindrical coordinates can be transformed into Cartesian coordinates [Cas94]

$$B_y + iB_x = B_0 \sum_n (b_n - ia_n)\left(\frac{x}{r_0} + i\frac{y}{r_0}\right)^{n-1} \sin n\theta). \qquad (2.20)$$

In this formule, B_0 is the strength of the main field component at r , the coefficients b_n are called the "normal" multiple coefficients, a_n are the "skew" multiple coefficients (for skewed, or rotated elements) and r_0 is a normalization radius. This is the representation used in the program Poisson.

F.2 The use of the program Poisson

The most important parameters, which have been adjusted during the use of Poisson

Table Con-values used in Poisson

Program	Con-value	Description
Lattice	con(6)	Magnetic permeability in iron, con(6)=0, permeability dependent on H con(6)=-2, permeability equal to ∞
	con(9)	Scaling factor
	con(21)-con(24)	Boundary condition for respectively the left, right, top and bottom boundary, con(21)=0 gives a Dirichlet problem
	con(46)	Symmetry

Poisson		Harmonic analysis-components.
	con(110)	Number of coefficients to be calculated
	con(111)	Number of points used
	con(112)	radius
	con(113)	circle
	con(114)	normalisation radius

Sextupole used as a vertical corrector, I=305 A.turns through the coils around pole 1, 3, 4 and 6.

```
! **** Definition of outer boundaries ****

&reg conv=0.1,nreg=17,dx=1.95,dy=2.,xmax=140,xmin=-140,ymin=-140,ymax=140,npoint=4,mat=2 &
&po r=140,theta=0 &
&po nt=2, r=140. ,theta=180 &
&po nt=2, r=140.,theta=270 &
&po nt=2, r=140.,theta=0. &

! **** Definition of inner boundaries ****

! **** First quadrant ****
&reg mat=1, npoint=20 &
&po x=0.,y=0. &
&po x=120.,y=0. &
&po nt=2.,r=120.,theta=24.74 &
&po x=30.1199,y=5.843 &
&po x=27.609,y=7.280 &
&po x=25.4869,y=8.9414 &
&po x=23.773,y=10.838 &
&po x=22.3435,y=12.9 &
&po x=21.273,y=15.169 &
&po x=20.4869,y=17.602 &
&po x=20.109, y=20.270 &
&po x=20.1199,y=23.26 &
&po x=98.1418,y=69.052 &
&po nt=2.,r=120.,theta=84.74 &
&po x=10., y=29.006 &
&po x=7.5, y=27.55 &
&po x=5., y=26.543 &
&po x=2.5, y=26.007 &
&po x=0.,y=25.8 &
&po x=0.,y=0. &
```

....

....

! **** The definiton of the Second to Fourth Quadrant are similar ****

! **** Definitions of coils and currents ****

! **** Coil around pole 1 ****
&reg mat=1, cur=305., npoint=5 &
&po x=30.1199,y=5.843 &
&po x=64.46,y=1.3 &
&po x=113.89316,y=29.42734 &
&po x=105.89,y=48.479 &
&po x=30.1199,y=5.843 &

&reg mat=1, cur=-305, npoint=5 &
&po x=20.1199,y=23.26 &
&po x=34.46,y=58.0902 &
&po x=83.823,y=83.853 &
&po x=96.7,y=66.8 &
&po x=20.1199,y=23.26 &

! **** Coil around pole 2 ****
&reg mat=1, cur=0, npoint=5 &
&po x=10., y=29.006 &
&po x=32., y=56.4 &
&po x=32., y=114 &
&po x=10., y=114 &
&po x=10., y=29.006 &

&reg mat=1, cur=0, npoint=5 &
&po x=-10., y=29.006 &
&po x=-10., y=114 &
&po x=-32., y=113 &
&po x=-32., y=56.4 &
&po x=-10., y=29.006 &

! **** Coil around pole 3 ****
&reg mat=1, cur=-305, npoint=5 &
&po x=-20.1199,y=23.26 &
&po x=-34.46,y=58.0902 &
&po x=-83.823,y=83.853 &
&po x=-96.7,y=66.8 &
&po x=-20.1199,y=23.26 &

```
&reg mat=1, cur=305., npoint=5 &
&po x=-30.1199,y=5.843 &
&po x=-105.89,y=48.479 &
&po x=-113.89316,y=29.42734 &
&po x=-64.46,y=1.3 &
&po x=-30.1199,y=5.843 &

! **** The Coils around pole 4 to 6 are not given ****
```

With the successive use of AUTOMESH,

LATTICE , assigning the con values: *6 0 *21 0 0 0 0 *46 1 s ,
and POISSON , with the use of the con values: *110 5 20 1 360 1 s
the following field coefficients are calculated.

Table for field coefficients
Normalization radius = 1.00000
(Bx - iBy) = i[sum n*(An + iBn)/r * (z/r)**(n-1)]

n	n(An)/r	n(Bn)/r	Abs(n(Cn)/r)
1	-5.9576E-03	-2.1400E+02	2.1400E+02
2	1.8715E-03	-1.2124E-03	2.2299E-03
3	-2.3717E-03	4.3609E-02	4.3674E-02
4	2.4573E-03	2.9252E-03	3.8203E-03
5	-1.9050E-03	3.5557E+00	3.5557E+00